THE
PHYSICAL REVIEW

A journal of experimental and theoretical physics established by E. L. Nichols in 1893

SECOND SERIES, VOL. 71, No. 11 JUNE 1, 1947

The Neutron Absorbing Isotopes in Gadolinium and Samarium

R. E. LAPP,[1] J. R. VANHORN,[2] AND A. J. DEMPSTER
Argonne National Laboratory, Chicago, Illinois

(Received February 20, 1947)

The large absorption for slow neutrons in samarium was found to be caused by the isotope at mass 149, and in gadolinium to the isotopes at masses 155 and 157, the cross section for 157 being about three times that for 155. Mass spectra were made with the double focusing mass spectrograph, using the spark with nickel tubes packed with oxide as electrodes. Mass spectra of normal samples were compared photometrically with those of samples in which this isotope abundance had been altered by long exposure to slow neutrons. In the altered gadolinium the abundance of mass 157 was less than 155 instead of greater, and 156 became greater than 160 rather than less. In samarium the abundance of mass 149 was reduced to be nearly as weak as 148, and mass 150 was correspondingly increased.

IT was shown in 1935 by Dunning, Pegram, Fink, and Mitchell[3] that neutron absorption in samarium and gadolinium is extremely large. It is of interest to find which isotopes in these elements are responsible for the large absorption. The isotopes have been identified by measuring the reduction in their intensity, produced by long exposure to neutrons in the Clinton Pile. The samples were prepared and exposed in the Clinton Pile by Dr. L. Borst in the form of very thin layers of oxide, 1.6 milligrams per sq. cm for the gadolinium and 1.9 milligrams per sq. cm for the samarium. With this thickness the inside of a sample receives almost the same bombardment as the outside layers.

The isotopes were photographed with a double focusing mass spectrograph,[4] using a vacuum spark and an electrode containing about 0.5 milligram of the sample. The abundance of the isotopes was deduced from photometer traces made with a Moll recording microphotometer. The intensity standards were the normal isotope abundances as discussed below.

For normal gadolinium the abundances measured by Wahl[5] give a normal photographic density curve in terms of isotope abundance as shown in Fig. 1. The curve is made from five traces of different exposures on the same plate. The points shown on the curve are plotted with the abscissae marked on the five scales below. In the normal material the mass at 157 is more abundant than the one at 155, and the mass at 160 is more abundant than the one at 156.

With the exposed gadolinium, the abundances were radically altered, and it was necessary to take the new abundance ratios shown in Fig. 2

[1] Research and Development Division, War Department General Staff, Pentagon Building 4-D-830, Washington, D. C.
[2] Physics Department, University of Illinois, Urbana, Illinois.
[3] J. R. Dunning, G. B. Pegram, G. A. Fink, and D. P. Mitchell, Phys. Rev. 48, 277 (1935).
[4] A. J. Dempster, Proc. Am. Phil. Soc. 75, 758 (1935).
[5] Wahl, Soc. Sci. Fenn. 11, 1 (1941). According to a paper by J. Mattauch and H. Ewald, Zeits. f. Physik 122, 321 (1944), the standard intensity marks were made by x-rays and a rotating sector.

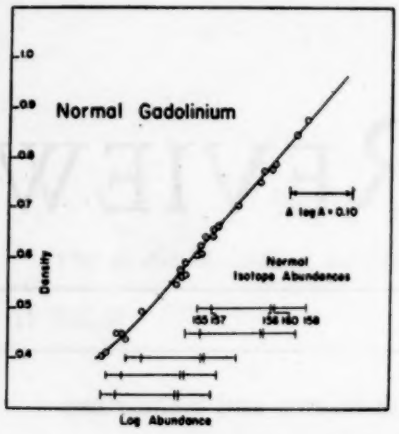

FIG. 1. Photographic density curve made from microphotometer traces of five mass spectra on one plate. The logarithmic isotope abundance ratios are given by the five scales.

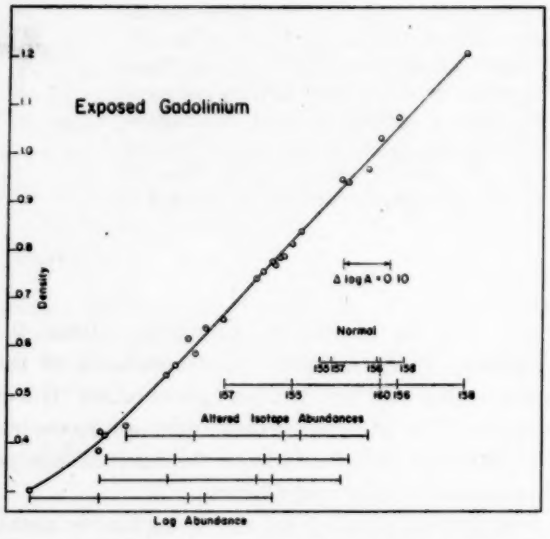

FIG. 2. Density curve plotted from microphotometer traces of five mass spectra of exposed gadolinium. The isotope abundance scales are indicated on the five lines below. One normal scale is shown for comparison.

to make the observed densities fit on the photographic density curve. The points shown on the curve are plotted with the abscissae marked on the five altered abundance scales. The normal scale is shown for comparison. The isotopes at masses 157 and 155 are reduced, and those at 158 and 156 are increased. The normal and altered abundances in percents are given in Table I.

We may conclude that the absorbing isotopes are at masses 155 and 157 with the absorbing cross section for 157 approximately 3.5 times as large as that for 155.

A sample of samarium oxide was exposed in the same way. Here there is the difficulty that the normal abundances are not accurately known,

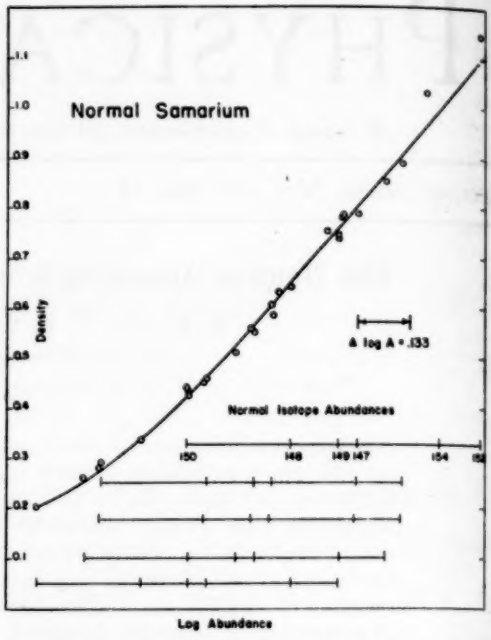

FIG. 3. Density-abundance curve drawn from microphotometer traces of five mass spectra of normal samarium. The isotope abundance scales are shown on the five lines below.

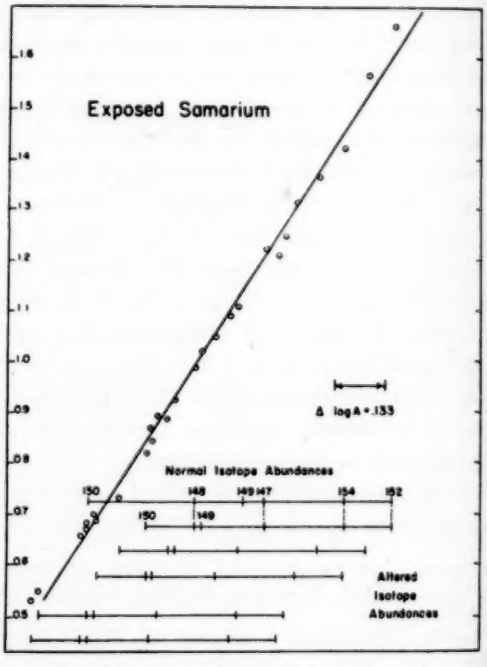

FIG. 4. Density curve of five mass spectra of samarium exposed to neutrons. The altered isotope abundance scales are given below with one normal scale for comparison.

as Dr. Aston's estimates made from incompletely resolved spectra are the only ones now available.[6] New abundances were deduced from an indirect comparison with the gadolinium, in which the densities from standard light intensities served as a reference in both cases. These new normal abundances are used in plotting the photographic density curve in Fig. 3, made from five spectra with different exposure times on one plate.

The abundances of the isotopes in the exposed sample were altered by a reduction in the isotope at mass 149 and an increase in the mass at 150. This is shown in Fig. 4 where the new abundances shown on the lines at the bottom for the five spectra are those required to make the observed densities fall on one photographic density curve. The normal abundances of Fig. 3 are shown for comparison in the top scale. Although the changes are less than in the case of gadolinium, the samarium isotope at mass 149 has become less abundant, from 12.8 to 10.0 percent, and the isotope at mass 150 has increased from 5.0 to 7.1 percent. We may conclude that the large absorption in samarium is due primarily to the isotope at mass 149.

TABLE I.

Isotope	155	156	157	158	160
Gd (normal)	15.6	20.6	16.42	23.45	20.87
Gd (altered)	13.6	22.3	9.86	30.60	20.62
Change	−2.0	+1.7	−6.6	+7.1	

The authors are indebted to Dr. L. Borst for preparing the thin deposits and exposing them in the Clinton Pile.

These observations were carried out while the authors were associated with the Metallurgical Laboratory at the University of Chicago.

[6] F. W. Aston, Proc. Roy. Soc. **A146**, 46 (1934).

PHYSICAL REVIEW VOLUME 71, NUMBER 11 JUNE 1, 1947

Note on the Nuclear Electric Quadrupole Spectrum of a Homonuclear Diatomic Molecule in a Magnetic Field*

H. M. FOLEY
Columbia University, New York, New York

(Received February 20, 1947)

It is shown that for very large values of the rotational quantum number J the energy of interaction of the electric quadrupole moments of a homonuclear diatomic molecule may be expressed as the sum of the energies of states of the single nucleus problem. This approximation becomes less accurate for any J value as the applied magnetic field is decreased.

THE effect of the nuclear electric quadrupole moment in the magnetic spectrum of a heteronuclear molecule has been given by Feld and Lamb.[1] In this work the molecule was treated as if the two nuclei were entirely independent. The calculations were actually carried out for the case of a single nucleus interacting with the molecular field.

In the case of a homonuclear molecule certain apparent complications arise due to the exchange degeneracy and to the fact that both nuclei are coupled to the molecular rotational angular momentum through the quadrupole interaction. The Hamiltonian expression for two nuclei with quadrupole moments in a magnetic field is

$$\mathcal{H}=\frac{e^2q_1Q_1}{2J(2J-1)I_1(2I_1-1)}\{3(\mathbf{I}_1\cdot\mathbf{J})^2+\tfrac{3}{2}(\mathbf{I}_1\cdot\mathbf{J})-\mathbf{I}_1^2\mathbf{J}^2\}+\frac{e^2q_2Q_2}{2J(2J-1)I_2(2I_2-1)}$$
$$\times\{3(\mathbf{I}_2\cdot\mathbf{J})^2+\tfrac{3}{2}(\mathbf{I}_2\cdot\mathbf{J})-\mathbf{I}_2^2\mathbf{J}^2\}+\mu_0g_1\mathbf{H}\cdot\mathbf{I}_1+\mu_0g_2\mathbf{H}\cdot\mathbf{I}_2+\mu_0g_J\mathbf{H}\cdot\mathbf{J}, \quad (1)$$

* Publication assisted by the Ernest Kempton Adams Fund for Physical Research of Columbia University, New York.

[1] B. T. Feld and W. E. Lamb, Phys. Rev. **67**, 15 (1945), hereinafter referred to as FL.

in which Q_1 and Q_2 are the quadrupole moments, $\mathbf{I}_1$ and $\mathbf{I}_2$ the spin vectors of the nuclei, and q_1 and q_2 are directly related to the electric field gradients at the positions of the nuclei.[1] It is assumed that the energy of interaction between the magnetic moments of the nuclei, and of the molecular rotational magnetic field with the nuclear magnetic moments, is small compared to the quadrupole energy.

For the discussion of the energy levels of a homonuclear molecule it is convenient to employ a "strong-field" representation, in which the rotational angular momentum, the spins of the individual nuclei, and the components of each of these quantities in the direction of the magnetic field are diagonal matrices. In the absence of the quadrupole interaction all states with the same value of m_J and of M_S, the component of total nuclear spin in the magnetic field direction, are degenerate.

If the wave function representing a nucleus with z component of spin given by i is α_i, then the part of the total nuclear wave function which depends on the nuclear spin coordinates may be written $\alpha_i(1)\cdot\alpha_k(2)$ where $i+k=M_S$. It is useful to alter the representation by forming the symmetric and antisymmetric combinations of these functions

$$\Gamma_{ik}^{\pm}=\frac{1}{\sqrt{2}}\{\alpha_i(1)\cdot\alpha_k(2)\pm\alpha_k(1)\alpha_i(2)\},\quad \Gamma_{ii}=\alpha_i(1)\cdot\alpha_i(2).$$

The magnetic terms in the Hamiltonian are diagonal in this representation with energy values

$$g_I M_S H_z+g_J m_J H_z.$$

The matrix elements of the quadrupole interaction for an individual nucleus have been given by Kellogg, Rabi, Ramsey, and Zacharias.[2] Non-vanishing matrix elements exist between states with the following relationships of quantum numbers

$\Delta m_S=0$	$\Delta m_J=0$
$\Delta m_S=+1$	$\Delta m_J=-1$
$\Delta m_S=-1$	$\Delta m_J=+1$
$\Delta m_S=+2$	$\Delta m_J=-2$
$\Delta m_S=-2$	$\Delta m_J=+2$

In the case of a homonuclear diatomic molecule there are no matrix elements of the two quadrupole terms between the states defined in the Γ representation having a common value of M_S. Thus if the quadrupole interaction is considered to be a small perturbation (strong-field condition), the Γ representation is the correct set of wave functions in first-order approximation. The diagonal matrix element of the quadrupole operator for a single nucleus is given by

$$F_{im_J}^{im_J}=\tfrac{1}{2}[3i^2-I_1(I_1+1)][3m_J^2-J(J+1)]. \tag{2}$$

For two identical nuclei in the Γ representation the diagonal element is

$$F_{im_J}^{im_J}+F_{km_J}^{km_J}=[\tfrac{3}{2}i^2+\tfrac{3}{2}k^2-I_1(I_1+1)][3m_J^2-J(J+1)]. \tag{3}$$

The total nuclear spin is not diagonal in the Γ_{ik} functions, that is, the wave functions in terms of which the quadrupole energy is a diagonal matrix consist of combinations of functions corresponding to different values of total nuclear spin. The first-order quadrupole energy consists simply of the sum of the energies of two individual nuclei. It will be shown below that if the rotational angular momentum is very large the eigenvalues of the magnetic and quadrupole energies may always be expressed as the sum of two eigenvalues of the individual nucleus problem.[1]

The Hamiltonian of Eq. (1) may be written as

$$\mathcal{H}=H_1(I_1JH)+H_2(I_2JH). \tag{4}$$

[2] J. M. B. Kellogg, I. I. Rabi, N. F. Ramsey, and J. R. Zacharias, Phys. Rev. **57**, 677 (1940).

(The rotational moment term is not important for the following discussion.) The matrix elements for an individual nucleus in the strong-field representation are

$$V_{Q_j}{}^{i}R_{m_J',\,m_J+i-l}^{m_J}\delta_{m_J',\,m_J+i-l}+V_{M_j}{}^{i}\delta_{i,\,j} \tag{5}$$

in which $V_{M_j}{}^{i}$ is the magnetic interaction energy (diagonal), and $V_{Q_J}{}^{i}R_{m_J',\,m_J+i-l}^{m_J}$ is the quadrupole matrix element between nuclear spin states i and j and rotational states m_J and $m_{J'}$. The energy matrix of Eq. (4) in the Γ representation is then

$$H_{nlm_J'}^{ikm_J}=V_{Q_n}{}^{i}R_{m_J',\,l}^{m_J}\delta_{k,\,l}\delta_{m_J',\,m_J+i-n}+V_{M_n}{}^{i}\delta_{i,\,n}\delta_{k,\,l}+V_{Q_l}{}^{k}\delta_{1,\,n}R_{m_J',\,m_J+k-l}^{m_J}\delta_{m_J',\,m_J+k-l}+V_{M_l}{}^{k}\delta_{k,\,l}\delta_{1,\,n}. \tag{6}$$

In this matrix non-zero elements appear only between states of equal values of M, the z component of total angular momentum. Within each sub-matrix for any value of M there are no matrix elements between states of the same M_S. In such a sub-matrix the value of the rotational magnetic quantum number has at most $4I_1+1$ values distributed in the interval $M-2I_1\leq m_J\leq M+2I_1$. If J is very large compared to I_1, the variation of the matrix elements $R_{m_J'}^{m_J}$, with m_J, with $m_J-m_{J'}$ fixed, will be small in this interval. (This will not be the case for the small fraction of states in which m_J or $J-m_J$ is comparable with I_1.) If this variation be neglected $R_{m_J'}^{m_J}$ depends only on

$$m_J-m_{J'}=n-i \quad \text{or} \quad m_J-m_{J'}=l-k$$

and the matrix element Eq. (5) may be written $V_j{}^{i}$. The homonuclear matrix element of Eq. (6) becomes

$$H_{nl}^{ik}=V_n{}^{i}\delta_{k,\,l}+V_l{}^{k}\delta_{1,\,n}. \tag{7}$$

In the matrix element $V_n{}^{i}$ the rotational matrix element $R_{m_J'}^{m_J}$ may be set equal to its average value for which m_J is equal to M.

We assume that the energy matrix of the individual nucleus problem is brought into diagonal form by a transformation matrix A. Thus $W=AVA^{-1}$ in which W is a diagonal matrix. The direct product matrix

$$\mathfrak{a}=A\times A \quad \text{or} \quad \alpha_{ik}{}^{mt}=a_i{}^{m}a_k{}^{t} \tag{8}$$

is to be applied to the complete energy matrix of Eq. (7)

$$\begin{aligned}H'^{mt}_{pq}&=\sum_{nl}\sum_{ik}\alpha_{ik}^{mt}H_{nl}^{ik}(\alpha^{-1})_{pq}^{nl}\\&=\sum_{nl}\sum_{ik}a_i{}^{m}a_k{}^{t}\{V_n{}^{i}\delta_{k,\,l}+V_l{}^{k}\delta_{in}\}(a^{-1})_p{}^{n}(a^{-1})_q{}^{l}\\&=W_p{}^{m}\delta_{t,\,q}\delta_{m,\,p}+W_q{}^{t}\delta_{m,\,p}\delta_{t,\,q}.\end{aligned} \tag{9}$$

Thus the transformation matrix $\mathfrak{a}$ diagonalizes the energy matrix, and the diagonal values are just the sums of eigenvalues of the individual nucleus problem.

It is clear that any system consisting of two (or more) parts, the energy matrix of which can be put into the form of Eq. (7), will show this same additivity of the energies of the individual parts. Thus a heteronuclear molecule of large rotational angular momentum, and with quadrupole interactions, will yield eigenvalues expressible as the sums of the energies of the individual nuclei. The inclusion of an interaction between the nuclei will of course destroy the form of the energy matrix of Eq. (7).

A weak oscillating magnetic field $\mathbf{H}'$ introduces a perturbation of the form

$$\mathcal{H}' = \mu_0 g_I \mathbf{H}' \cdot \mathbf{I}_1 + \mu_0 g_I \mathbf{H}' \cdot \mathbf{I}_2$$

leading to transitions between the levels given by Eq. (9). From the properties of the matrix $\mathfrak{a}$ it may be shown that the possible transitions are restricted to changes in the value of only one of the terms of Eq. (9), and the selection rules for these transitions are identical with those in the spectrum of a single nucleus. Subject to the approximation that the rotational angular momentum is large, we have the general rule: the magnetic nuclear spectrum of a homonuclear diatomic molecule, including electric quadrupole interaction, is identical with that of a single nucleus with the same spin. This rule is not in agreement with the recent results of Feld.[3]

The physical meaning of Eqs. (3) and (6) may be expressed quite simply. In a strong magnetic field the two spin vectors and the rotational angular momentum are decoupled and precess independently in the field. Equation (3) expresses the fact that the energies of the precessing spin vectors are additive. As the field is reduced to zero, the spin vectors are each coupled to the rotational angular momentum through the quadrupole interaction, and the three vectors form a resultant total angular momentum. If the rotational vector $\mathbf{J}$ is very large the spin vectors may be considered to be precessing about $\mathbf{J}$. In this case the rotational vector has the role of a strong applied field and the energies are additive (Eq. (6)).

The effect of a finite value of rotational angular momentum is to make important the variation of the rotational matrix elements with m_J within a group of states of fixed M. In this case the complete matrix of Eq. (6) may not be diagonalized by a transformation of the form $\mathfrak{a} = A \times A$ with eigenvalues expressed simply as sums of eigenvalues of the individual nucleus problem. The strong field first-order solution of Eq. (3), however, shows the additive property even for small values of J, and it is clear from the foregoing discussion that the deviations from additivity become more important in higher approximations. To investigate the maximum effect we proceed directly to the zero-field case. The following discussion will deal only with the quadrupole interaction in zero field. In this case we may use a representation in which F, m_F, I, J, I_1, I_2 are diagonal. F is the quantum number of total angular momentum, and m_F is its component on a fixed space axis. I is the total nuclear spin. The matrix elements of the quadrupole interaction are given for reference in the Appendix. Non-zero matrix elements exist between states differing in total spin by $\Delta I = 0 \pm 2$. For any value of $i_0 = F - J$ the states of total spin values $I \geq i_0$ must be diagonalized. The combinations of total spin wave functions in which the quadrupole perturbation is diagonal for any value of i_0, are the same as the total spin combinations in the strong field case for an identical value of M_S.

For a single nucleus, in the zero-field case, Feld and Lamb gave an expression (FL III 7) for the energy which is accurate for large J values

$$E_Q = e^2 q Q [3 i_1^2 - I_1(I_1+1)]/4 I_1(2I_1-1), \quad i_1 = F - J. \tag{10}$$

These authors also gave the exact solution of the single nucleus problem (FL III 5). The eigenvalue solution in the homonuclear problem described above may be expressed as the sum of two expressions of the type of Eq. (10) for large J values, in accordance with the general rule (Eq. (9)). For smaller J values, and particularly for large values of nuclear spin, deviations from simple additivity will occur. Investigation of several special cases indicates that these deviations are of the same magnitude as, though not identical with, the differences between the exact single nucleus solution (FL III 5) and the values given by Eq. (10). For nuclear spins as large as $I = 5$ and with $J = 20$ these deviations are important, and the simple formula of Eq. (10) will not apply accurately in either the homonuclear or heteronuclear case.

The author wishes to thank Professor I. I. Rabi for several interesting discussions of this problem.

[3] B. T. Feld, Phys. Rev. **70**, 112A (1946).

APPENDIX

The matrix elements of the quadrupole interaction in Eq. (1) in the weak-field representation in which F, m_F, I, I_1, I_2, J are diagonal are given here. The matrix elements of $(\mathbf{I}_1\cdot\mathbf{J})$ are[4]

$$(JIF|\mathbf{I}_1\cdot\mathbf{J}|JIF)=\frac{1}{2}\frac{I_1(I_1+1)-I_2(I_2+1)+I(I+1)}{2I(I+1)}\{F(F+1)-I(I+1)-J(J+1)\},$$

$$(JIF|\mathbf{I}_1\cdot\mathbf{J}|JI-1F)=\frac{1}{2}\left\{\frac{(I-I_1+I_2)(I+I_1-I_2)(I_1+I_2+I+1)(I_1+I_2-I+1)}{4I^2(2I-1)(2I+1)}\right\}^{\frac{1}{2}}$$
$$\times\{(F+I-J)(F+J-I+1)(F+I+J+1)(I+J-F)\}^{\frac{1}{2}}$$
$$=(JI-1F|\mathbf{I}_1\cdot\mathbf{J}|JIF),$$

$$(JIF|\mathbf{I}_1\cdot\mathbf{J}|JI+1F)=\frac{1}{2}\left\{\frac{(I+1-I_1+I_2)(I+1+I_1-I_2)(I_1+I_2+I+2)(I_1+I_2-I)}{4(I+1)^2(2I+1)(2I+3)}\right\}^{\frac{1}{2}}$$
$$\times\{(F+I+1-J)(F+J-I)(F+I+J+2)(I+1+J-F)\}^{\frac{1}{2}}$$
$$=(JI+1F|\mathbf{I}_1\cdot\mathbf{J}|JIF).$$

The off diagonal elements for $(\mathbf{I}_2\cdot\mathbf{J})$ are minus the corresponding elements in $(\mathbf{I}_1\cdot\mathbf{J})$.

In the homonuclear case $I_1=I_2$, and the matrix elements of the quadrupole terms of Eq. (1) are obtained by matrix multiplication:

$$(JIF|H_Q|JIF)=\frac{e^2qQ}{2J(2J-1)I_1(2I_1-1)}\left\{\tfrac{3}{8}[F(F+1)-I(I+1)-J(J+1)]^2\right.$$
$$+\frac{3}{8}\frac{(2I_1+1)^2-I^2}{4I^2-1}(F+I-J)(F+J-I+1)(F+I+J+1)(I+J-F)$$
$$+\frac{3}{8}\frac{(2I_1+1)^2-(I+1)^2}{(2I+1)(2I+3)}(F+I+1-J)(F+J-I)(F+I+J+2)(I+1+J-F)$$
$$\left.+\tfrac{3}{4}[F(F+1)-I(I+1)-J(J+1)]-2I_1(I_1+1)J(J+1)\right\},$$

$$(JIF|H_Q|JI+2F)=\frac{3e^2qQ}{2J(2J-1)I_1(2I_1-1)}\left\{\frac{(2I_1+1)^2-(I+1)^2}{4(2I+1)(2I+3)}(F+I+1-J)(F+J-I)\right.$$
$$\left.\times(F+I+J+2)(I+J+1-F)\right\}^{\frac{1}{2}}\left\{\frac{(2I_1+1)^2-(I+2)^2}{4(2I+3)(2I+5)}(F+I+2-J)\right.$$
$$\left.\times(F+J-I-1)(F+I+J+3)(I+2+J-F)\right\}^{\frac{1}{2}}$$
$$=(JI+2F|H_Q|JIF),$$

$$(JIF|H_Q|JI-2F)=\frac{3e^2qQ}{2J(2J-1)I_1(2I_1-1)}\left\{\frac{(2I_1+1)^2-I^2}{4(4I^2-1)}(F+I-J)(F+J-I+1)(F+I+J+1)\right.$$
$$\left.\times(I+J-F)\right\}^{\frac{1}{2}}\left\{\frac{(2I_1+1)^2-(I-1)^2}{4(2I-3)(2I-1)}(F+I-J-1)(F+J-I)(F+J+I)(I+J-F-1)\right\}^{\frac{1}{2}}.$$

[4] E. U. Condon and G. H. Shortley, *The Theory of Atomic Spectra* (Cambridge University Press, 1935), p. 71.

Diffraction of Neutrons by a Single Crystal

W. H. ZINN
Argonne Laboratory, University of Chicago, Chicago, Illinois
(Received February 26, 1947)

The intensity of neutrons emitted by the nuclear chain reactor has been shown to be sufficiently great to permit the observation of the Bragg reflection of neutrons by a single crystal. A single crystal monochromator has been constructed and used for the investigation of resonances. The well-known resonance in Cd has been measured and the Breit-Wigner constants determined.

INTRODUCTION

A NUMBER of experiments designed to demonstrate the diffraction of slow neutrons by crystals have been made in the years following the discovery of the neutron. Early methods of treating the interaction between the neutron and the nucleus, developed by Fermi[1] and extended by Wick,[2] anticipated difference in scattering in crystalline and disordered substances. Experimental verification was attempted by Preiswerk and von Halban[3] who measured the temperature variation in the distribution of neutrons transmitted by a polycrystalline medium, and Mitchell and Powers,[4] as well as Preiswerk,[5] presented evidence for a coherent component of a neutron beam scattered from an array of crystals.

More recently, further observations of neutron diffraction have been made in the measurements of slow neutron scattering by Whittaker and Beyer[6] and in the work of Anderson, Fermi, and L. Marshall[7] and of Rainwater and Havens[8] who observed variations with the energy of the neutron beam in the scattering of crystalline substances. The high neutron flux generated by the chain reacting pile has permitted, as reported here, a series of experiments which show the existence of an intense diffracted beam of neutrons from a single crystal, and which demonstrate that this beam is of sufficient intensity for the study of the energy dependence of neutron reactions by methods similar to those of x-ray spectrometry. The work of this paper has been reported briefly[9] and similar results have been given by Borst *et al.*[10]

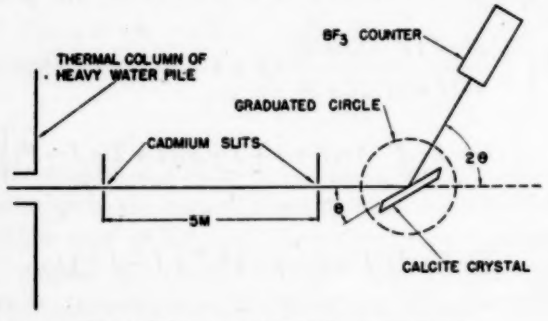

FIG. 1. First experimental arrangement.

DESCRIPTION OF APPARATUS

Neutrons diffusing from the main part of the chain reacting pile are permitted to enter a large block of graphite which acts as a slowing down column, bringing the average neutron energy to the equilibrium value for graphite at room temperature. Since the de Broglie wavelength of these neutrons is of the same order of magnitude as that of x-rays, it was possible to attempt the diffraction experiments with the customary crystals, using a spectrometer similar to that used with x-rays. As is shown schematically in Fig. 1, a collimated beam of neutrons was obtained by introducing two thick cadmium slits, 5 meters apart, in the neutron beam from the graphite thermal column of the heavy water pile. Cadmium slits sufficed here since the neu-

[1] E. Fermi, Ricerca Scient. **7**, pt. 2, 13 (1936).
[2] Wick, Physik. Zeits. **38**, 403 (1937).
[3] Von Halban and Preiswerk, Comptes rendus **203**, 73 (1936).
[4] Mitchell and Powers, Phys. Rev. **50**, 486 (1936).
[5] Preiswerk, Helv. Phys. Acta **10**, 400 (1937).
[6] Whittaker and Beyer, Phys. Rev. **55**, 1101 (1939); Beyer and Whittaker, Phys. Rev. **57**, 976 (1937).
[7] Anderson, Fermi, and L. Marshall, Phys. Rev. **70**, 102 (1946).
[8] Havens and Rainwater, Phys. Rev. **70**, 154 (1946); Rainwater and Havens, Phys. Rev. **70**, 136 (1946).
[9] W. H. Zinn, Phys. Rev. **70**, 102A (1946).
[10] L. B. Borst, A. J. Ulrich, C. L. Osborne, and B. Hasbrouck, Phys. Rev. **70**, 108A (1946); Phys. Rev. **70**, 557 (1946).

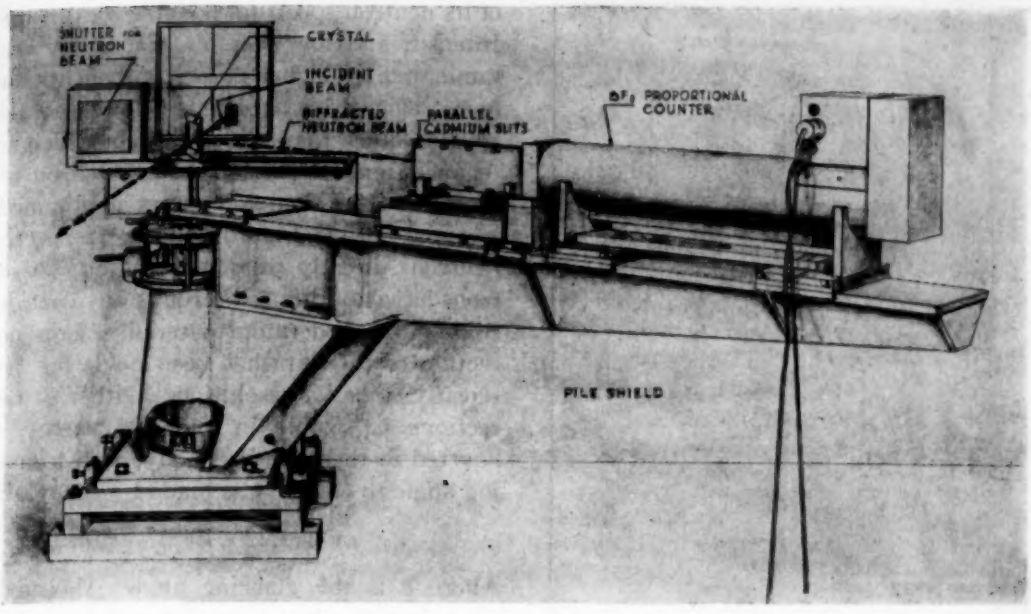

FIG. 2. The crystal spectrometer.

tron radiation from a thermal column is singularly free from fast neutrons. The collimated beam fell upon the (1, 0, 0) planes of a large single calcite crystal, and the diffracted beam was detected by means of a BF_3 proportional counter filled, for greater detection efficiency, with gas enriched in the B^{10} isotope. Only early experiments were performed at the thermal column; subsequently the apparatus was set up at a side hole of the reactor where the high energy neutron flux is much greater than at the thermal column.

The final form of the spectrometer (Fig. 2) is identical in principle with the usual x-ray instrument; however, in order to support the heavier collimators and detectors which are necessary for neutron diffraction experiments, the unit is made very massive. To improve the resolution the arm is long, having a length of 80 inches and a width of 8 inches. A 6-inch diameter crystal table is provided for mounting the crystals. The two graduated circles indicating the position of the arm and crystal table are 12 inches in diameter and are calibrated in degrees, while greater precision is attainable from readings on a cylindrical scale calibrated in quarter minutes and placed at the drive wheel. The table and arm are driven by means of large knurled wheels through a train of gears, and in use can be adjusted independently or coupled by a friction clutch. The table and arm are driven in the two to one angular ratio necessary for reflection experiments.

In order to measure with greatest efficiency the flux of diffracted neutrons, the beam was passed axially through the proportional counter. In this manner it was possible to detect nearly 100 percent of all the neutrons of the low energies. The counter was 5 cm in diameter, 60 cm long, and filled to a pressure of 40 cm of Hg with boron trifluoride. This gas was enriched about five times in the B^{10} isotope and thus transmitted but 5 percent of neutrons of kT energy. The required degree of collimation was obtained by inserting into the shield of the reactor a steel block containing a long channel. This channel was approximately $\frac{1}{2}''$ wide, $1''$ tall, and $8'$ long. The channel was directed at a part of the reactor containing heavy water and uranium. The beam collimated by this means contains neutrons ranging in energy from thermal to those of the fission spectrum itself. The intensity obtainable is a sharp function of the degree of collimation desired and the spectral region to be investigated. At the maximum of the thermal spectrum, with quite excellent reso-

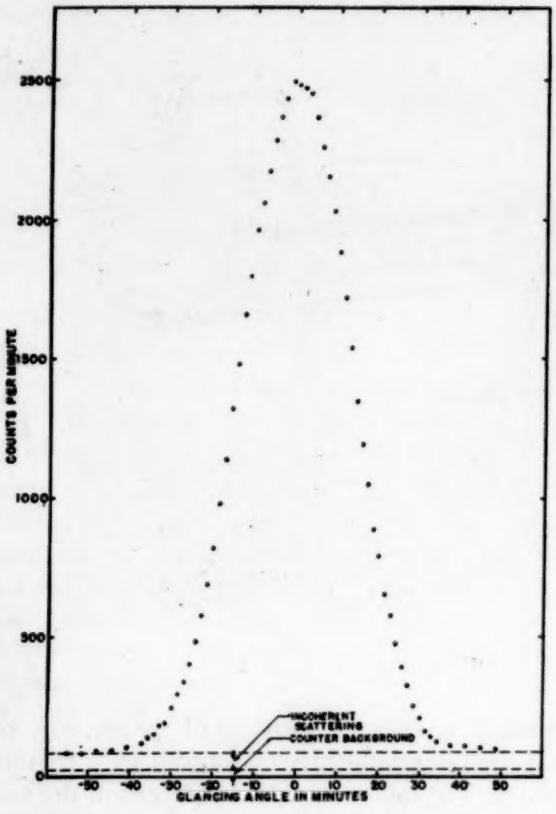

FIG. 3. Rocking curve (1, 0, 0) LiF crystal.

lution, counting rates of 5000 counts per minute can be obtained. At the suggestion of W. H. Zachariasen, roughening the crystal surfaces was tried and gives an improvement in intensity of about a factor of two. At energies in the so-called resonance region considerably smaller counting rates are obtained. A detector more sensitive to neutrons in this region is very much to be desired.

RESULTS

A typical rocking curve is shown in Fig. 3. No attempt has been made to correct these data for resolution or detector sensitivity. The detector, boron, follows a $1/v$ law for absorption, and as a result the sensitivity of the counter is not uniform over the entire range of velocities. Therefore, the rocking curve is not exactly symmetrical, showing relatively higher values on the low energy side of the diffraction peak.

Sufficient intensity of diffracted neutrons existed throughout the range of energies emitted from the thermal column to make measurement of its neutron spectrum possible by this method. Intensities at low energies, since they are contaminated by higher order components and are more efficiently detected, show considerably higher values than the real distribution in this region. Figure 4 shows the distribution of neutrons from the thermal column as obtained with a calcite crystal. Figure 5 shows the spectrum of neutrons directly from the reactor. These neutrons have not diffused through any considerable column of moderator material. Again no correction to the data has been made for detector sensitivity or for resolution. Neither of the corrections is sizable in the low energy region covered in these curves. Conversion from glancing angle to energy was made by the relation

$$\text{ev} = (2.22 \times 10^{-3})/\sin^2\theta,$$

where θ is the glancing angle. Measurements were made in the energy interval between 0.004 ev and 0.30 ev, which is in the range of glancing angles between 50° and 2°. Both spectra show a strong, approximately Maxwellian component, distorted by high order contributions on the long wave-length side of the maximum. The spectrum of neutrons from the wall of the reactor, having passed through a smaller amount of moderator, has an additional component at small glancing angles representing neutrons not yet in equilibrium with the moderator. Attempts to fit the experimental data theoretically have been made by Goldberger and Seitz[11] for various moderator temperatures and are included on the figures.

To demonstrate that the diffracted beam consists primarily of neutrons in a very small energy band, a measurement of the transmission of a Pyrex plate was made over the range 0.018 to 0.5 ev. This plate, previously standardized by means of a mechanical velocity selector, was shown to have a total cross section, because of its boron content, very close to $1/v$ in the region investigated. With the calcite crystal, measurements were made of the transmission of the plate from which effective neutron velocities were obtained by comparison with the measurements made on the mechanical velocity selector.

[11] Goldberger and Seitz, Phys. Rev. **70**, 116 (1946). A complete discussion of their method will be published shortly.

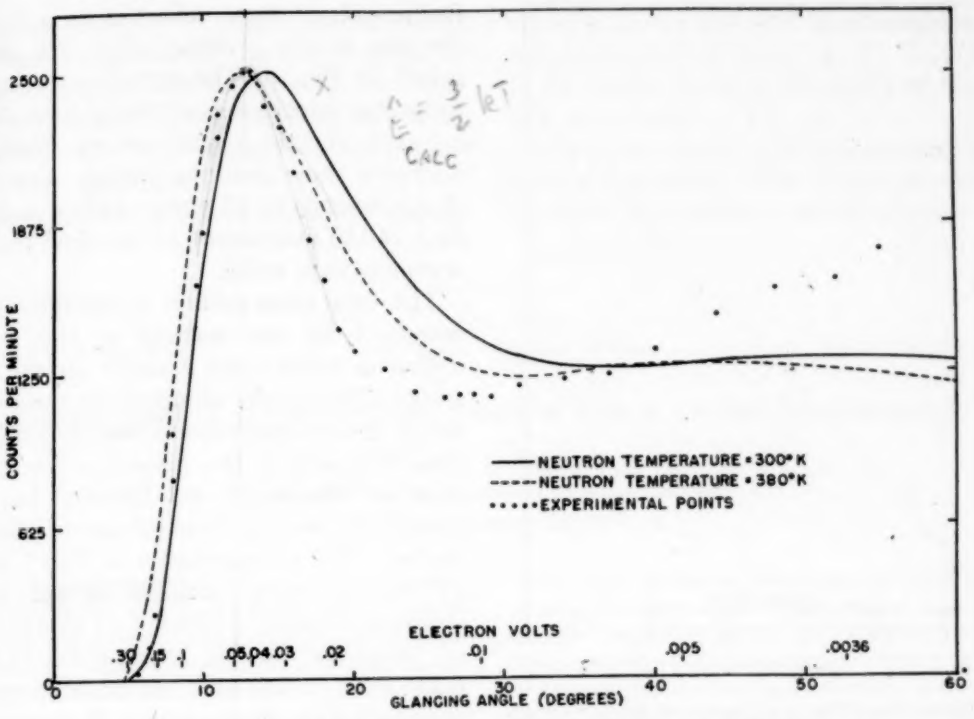

FIG. 4. Spectrum of thermal column radiation, calcite crystal. Solid line is the theoretical curve calculated by Goldberger and Seitz.

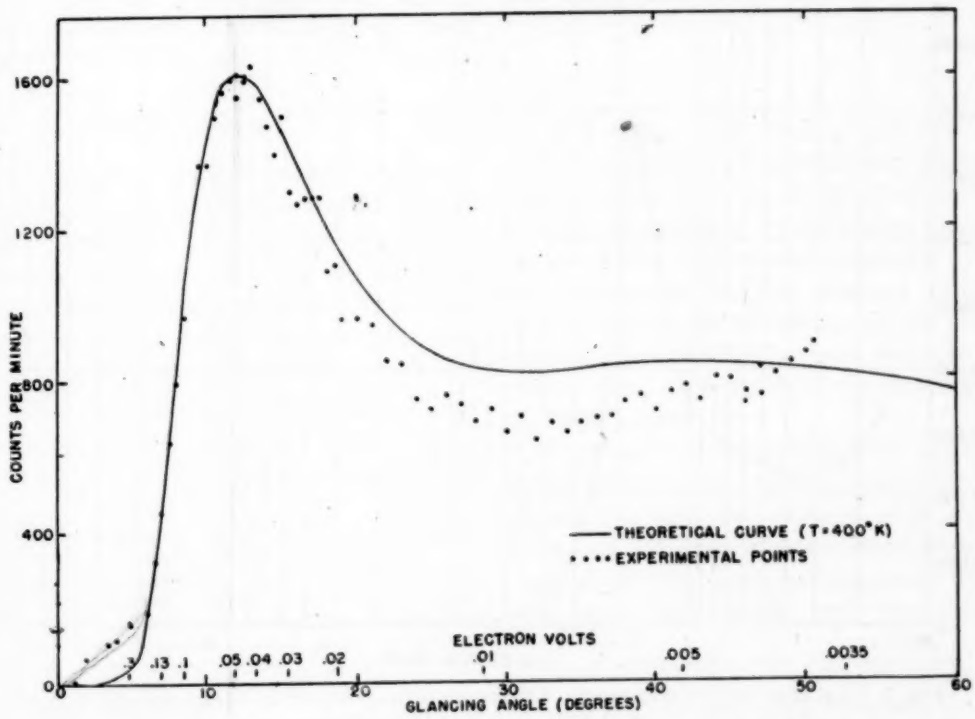

FIG. 5. Spectrum of reactor radiation, calcite crystal. Solid line is the theoretical curve calculated by Goldberger and Seitz.

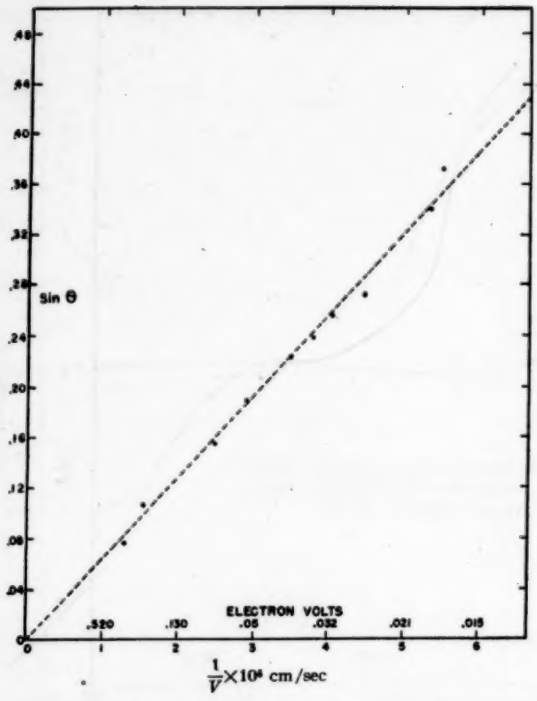

FIG. 6. Boron absorption as a function of neutron energy. The dotted curve is a plot of $(h/mv)=2d\sin\theta$. The points are experimentally determined values of $1/v$ and $\sin\theta$.

Reciprocals of these velocities as a function of the sine of the glancing angle are plotted as points in Fig. 6. The dotted curve gives the reciprocal velocity as calculated from the glancing angle and the crystal spacing. Similar measurements show that the straight line behavior shown extends to 15 volts which was the upper limit of the instrument at the time these measurements were made.

The total cross section of cadmium has been measured by the method of the modulated cyclotron beam[12] and a single strong level observed. The results obtained for cadmium with the crystal monochromator are shown in Fig. 7. The constants of the resonance are similar to those of Rainwater and Havens[8] but show a greater maximum than those of Baker and Bacher. The measurements of Fig. 7 extend to 15 electron volts, and no further resonance structure is found. A series of six foils of cadmium of thickness varying from 0.000142×10^{24} to 0.115×10^{24} atoms per square centimeter were required for the measurement. Wherever possible the range of acceptable transmissions was held

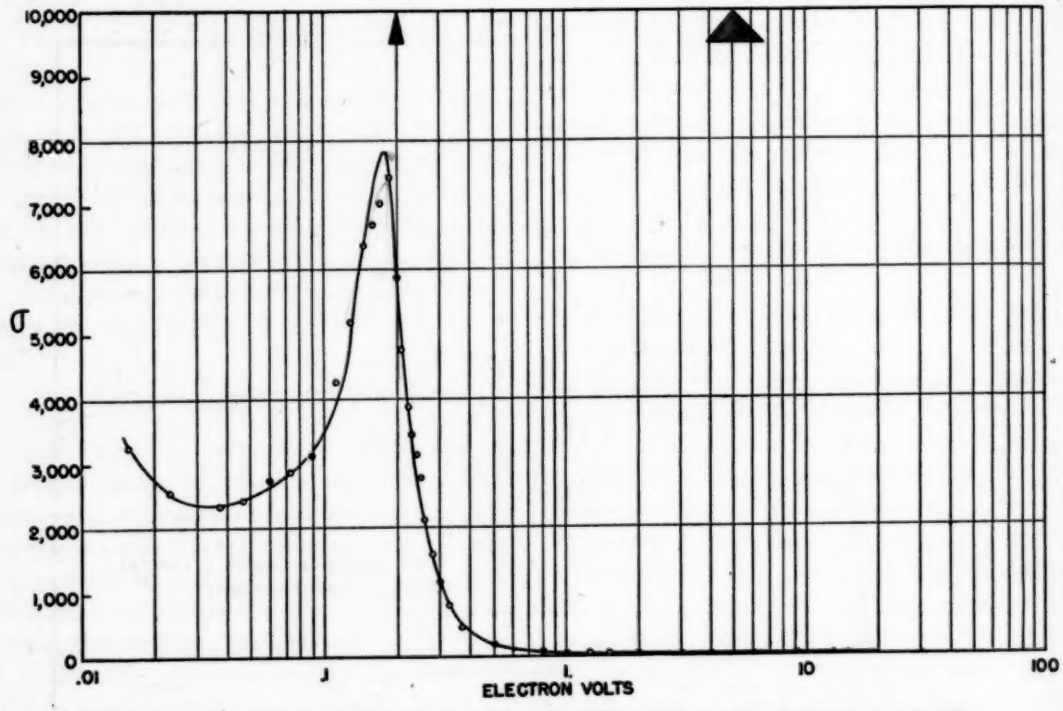

FIG. 7. Total cross section of cadmium. Solid curve is Breit-Wigner fit to experimental points. σ in units of 10^{-24} cm^2 per atom.

[12] C. P. Baker and R. F. Bacher, Phys. Rev. 59, 332 (1941).

between 0.50 and 0.75 to reduce effects of high energy beam components. The experimental results are best fitted with a curve of the Breit-Wigner function having the constants: $E_0=0.180$ ev, $\sigma_0=7800\times10^{-24}$ cm²/atom, $\Gamma=0.122$ ev, and $\sigma_s=6.0\times10^{-24}$ cm²/atom.

Acknowledgment is hereby made for the invaluable advice and skill in construction of the instrument contributed by T. J. O'Donnell, D. DiCostanzo, and J. Getzholtz of the laboratory work shop.

The initial results reported here were obtained in July–September, 1944. This work was carried out under the auspices of the Manhattan District.

PHYSICAL REVIEW VOLUME 71, NUMBER 11 JUNE 1, 1947

Measurement of Neutron Cross Sections with a Crystal Spectrometer*†

WILLIAM J. STURM**
Argonne National Laboratory, Chicago, Illinois

(Received February 26, 1947)

By use of the monoenergetic beams of neutrons diffracted from the (100) planes of lithium fluoride, survey measurements of the total neutron cross section of a series of elements have been made. The strong diffracted beams were obtained by placing a single crystal in the high flux of neutrons emitted by the heavy water moderated pile at the Argonne Laboratory. Observations on this group of elements, which includes several strongly absorbing rare earths, and elements commonly used as neutron filters and detectors, have been made in the range of energy between 0.04 and 65.0 electron volts. The method permits energy dependent cross-section measurement by activation or by transmission. However, all values reported were obtained by calculation from observed transmission data because the range of available intensities in the diffracted beam was best measured with a boron counter. Correction methods for resolution and order effects have been developed which are valid for low neutron energies. The following absorption levels have been observed: Rh, 1.28 ev; Au, 5.4 ev; Ir, 0.635, 1.35, and 6.0 ev; Gd, 0.031 ev; Sm, 0.096, 10.0, and 33.0 ev; Eu, 0.465, 3.3, 9.2, and 22.0 ev. Resonance levels at energies less than zero were found in Dy at -1.01 ev and in Eu at -0.011 ev.

I. INTRODUCTION

EARLY experiments of Szilard,[1] of Amaldi and Fermi,[2] and of Tillman and Moon[3] on the energy variation of neutron absorption cross section, indicated that not all elements showed a simple dependence of cross section upon the energy of the reacting neutron. Several techniques have subsequently been applied in an effort to study the nature of this function, because of its relation to the energy levels of the compound nucleus, in the limited region of low neutron energy. By employing filters and detectors of substances containing single strong resonance levels[1–4] it is possible to obtain an idea of the cross section of an element at the energy of the absorbing or detecting resonance. The obvious limitations of this method include the uncertainty in the knowledge of the position of the absorbing resonance level and the random nature of the distribution of the resulting data on the energy scale.

A method for determining the region of selective absorption for slow neutrons, based on the assumption that the capture cross section for boron and lithium is inversely proportional to the neutron velocity, has been suggested by Weeks, Livingston, and Bethe and by Frisch and

* Some of these results have been reported previously: Sturm and Turkel, Phys. Rev. **70**, 103 (A) (1946).

† This document is based on work performed under Contract No. W-31-log-eng-38 for the Manhattan Project and the information covered therein will appear in Division IV of the Manhattan Project Technical Series as part of the contribution of the Argonne National Laboratory.

** Now at the University of Wisconsin.

[1] Szilard, Nature **136**, 150 (1935).

[2] Amaldi and Fermi, Ricerca Scient. **1**, 310 (1936).

[3] Tillman and Moon, Proc. Roy. Soc. **A153**, 476 (1936); Nature **135**, 904 (1935).

[4] Bjerge and Wescott, Proc. Roy. Soc. **A150**, 709 (1935); Pontecorvo, Ricerca Scient. **6-7**, 145 (1935); Bethe, Rev. Mod. Phys. **9**, 113 et seq. (1937); Hanstein, Phys. Rev. **59**, 489 (1941); Horvath and Salant, Phys. Rev. **59**, 154 (1941); Feeny, Lapointe, and Rasetti, Phys. Rev. **61**, 469 (1942); Yalow and Goldhaber, Phys. Rev. **68**, 99 (1945).

Placzek.[5] According to this method, the quantitative measure of the absorption of neutrons in boron is taken as a measure of the energy of the captured neutron. Using this procedure, Goldsmith and Rasetti[6] have been able to locate with fair accuracy the position of the predominant levels in a series of strong absorbers.

A third indirect technique for observing the energy dependence of capture cross section has been employed by Powers, Fink, and Pegram[7] and others. By varying the temperature of their neutron moderator they were able to demonstrate an increase in cross section with decreasing neutron velocity for all elements tested. Since the method depends on evaluation of average cross section over a Maxwellian distribution of neutron energies having differing peak values, it cannot be expected that this type of measurement should do more than exhibit small variations in cross section due to the $1/v$ absorption in this region.

The earliest direct and continuous measurements of cross section as a function of neutron energy over a small range of energies was made possible by the rotating shutter velocity selector of Dunning, Pegram, Fink, Mitchell, and Segrè.[8] The range of this type of apparatus is limited to neutrons having energies less than 0.30 ev because of the nature of the cadmium cross section, yet with a sufficiently strong neutron source instruments of this type can be used for quite adequate measurements in this energy range.

With the modulation of the cyclotron beam by Alvarez[9] it was possible to observe the energy dependence of neutron cross section in still another manner. This technique, improved and extended by many observers,[10] has most recently been applied to the problem by Rainwater and Havens[11] who calculated the energy of the reacting neutron by measuring its time of flight over a fixed distance and evaluated many cross-section functions in this manner for energies up to 1000 ev.

The present method, utilizing the wave properties of the neutron, brings techniques analogous to those of x-ray diffraction into practice for these measurements. Using the high neutron flux made possible by the heavy water moderated uranium chain reactor, Zinn[12] has been able to demonstrate the diffraction of neutrons from a single crystal and to show the application of the phenomenon to cross section measurements. The crystal spectrometer for neutrons, unique in that it produces monoenergetic beams of low energy neutrons, provides a relatively simple tool for continuous cross-section measurement by activation or transmission for energies up to 65 ev with present collimators.

II. DESCRIPTION OF APPARATUS

The instrument used for the measurements was the heavy duty analog of an optical spectrometer described by Zinn,[12] permanently mounted in the concrete floor of the pile room in line with port number 4 of the Argonne heavy water pile. In its final, accurately centered and leveled position, tests of the angular reproducibility of the arm showed that its extreme end reproduced within 0.0005 inch repeated settings made on the dial plates of the instrument. For measurement of spectra and of cross section the table and arm could be coupled together by means of a friction clutch to drive the two elements in the two-to-one angular ratio required by these experiments.

A 61-cm long boron trifluoride counter filled to a pressure of 40 cm of mercury, operated in the proportional region and mounted with its axis parallel to the direction of the diffracted beam, served as the neutron detector in the apparatus. Use of enriched boron, consisting of the single isotope B^{10}, increased the detection efficiency for high energy neutrons approximately by a factor

[5] Weeks, Livingston, and Bethe, Phys. Rev. **49**, 471 (1936); Frisch and Placzek, Nature **137**, 357 (1936).
[6] Goldsmith and Rasetti, Phys. Rev. **50**, 328 (1936).
[7] Powers, Fink, and Pegram, Phys. Rev. **49**, 650 (A) (1936); Libby and Long, Phys. Rev. **52**, 592 (1937).
[8] Dunning, Pegram, Fink, Mitchell, and Segrè, Phys. Rev. **48**, 704 (1935). Fink, Dunning, Pegram, and Mitchell, Phys. Rev. **49**, 103 (1936); Rasetti, Segrè, Fink, Dunning, and Pegram, Phys. Rev. **49**, 104 (1936); Fink, Phys. Rev. **50**, 738 (1936).
[9] Alvarez, Phys. Rev. **54**, 235 (A) (1938); Alvarez, Phys. Rev. **54**, 609 (1938).
[10] Fertel, Gibbs, Moon, Thompson, and Wynn-Williams, Proc. Roy. Soc. **175**, 316 (1940); Baker and Bacher, Phys. Rev. **59**, 332 (1941); Manley, Haworth, and Luebke, Phys. Rev. **61**, 152 (1942); Bacher, Baker, and McDaniel, Phys. Rev. **69**, 443 (1946).
[11] Rainwater and Havens, Phys. Rev. **70**, 136 (1946) and Havens and Rainwater, Phys. Rev. **70**, 154 (1946); Rainwater, Havens, Wu, and Dunning, Phys. Rev. **71**, 65 (1947); Havens, Wu, Rainwater, and Meaker, Phys. Rev. **71**, 165 (1947); Wu, Rainwater, and Havens, Phys. Rev. **71**, 174 (1947).
[12] Zinn, Phys. Rev. **70**, 102 (A) (1946); Zinn, preceding paper.

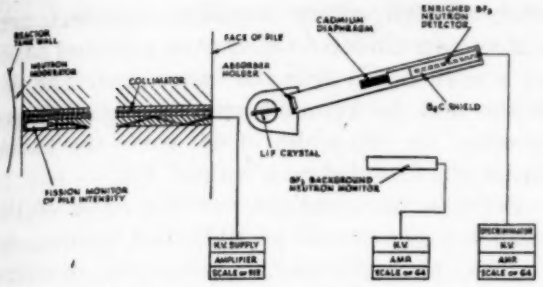

FIG. 1. Schematic diagram of apparatus for total neutron cross-section measurements.

of 5. Operated at 1500 volts above ground with electron collection on the central wire, the efficiency of detection of low energy neutrons approached 100 percent. One stage of preamplification, together with a cathode follower was mounted on the boron-cadmium shield of the counter, from which point the signal was carried by means of an 18-foot cable to an amplifier and scaler on an electronic instrument panel near the apparatus. The normal neutron background counting rate with the pile running was about 15 counts per minute, a small fraction of the 6400 counts per minute of Bragg reflected neutrons from the (100) planes of LiF in the region of the Maxwellian maximum. Counting rates in the energy region above the Maxwellian portion were [illegible]erably lower, since here the number of [illegible]ns in the spectrum as well as the detection [illegible]cy decreased.

[illegible] shown in Fig. 1, collimation of the primary neutron beam from the tank wall was achieved by inserting a 9-foot channel into the shielding of the reactor. This channel, a steel-bounded orifice with a 1.27×2.54-cm aperture, was surrounded by a mixture of paraffin, iron shot, and boric oxide to confine the path of neutrons and gamma-rays. The resultant primary neutron beam had a divergence of 32 minutes, and the diffracted beam a base width of 114 minutes. A cadmium diaphragm, consisting of a series of 12 long cadmium metal sheets spaced 3 mm apart, mounted on the spectrometer arm before the detector, served as a means of varying the divergence of the diffracted beam and the resolving power of the instrument. For the cross-section measurements, the half-width of the Bragg reflected beam of neutrons was standardized at 22 minutes.

Crystals and Absorber Mounts

Since the diffracted neutron beam for this series of experiments was obtained by reflection from the flat surface of a crystal rather than by transmission, the crystals employed were generally mounted in a long array in order to increase the strength of the diffracted beam at small glancing angles. Aside from minor variations necessitated by the differing shapes of available crystals, mounts consisted simply of a metal frame supported vertically on the spectrometer table. With this standardized type of mounting, transfer from crystal to crystal was simplified by use of a guide bar on the crystal table, since the planes of the crystal were aligned parallel to the metal frame. The mounts were usually made of aluminum with no metal in the path of the primary beam to minimize the incoherent scattering from the holder itself.

It was possible to measure the transmission, and consequently the total cross section of an element, by introducing it into the primary beam of neutrons, or by placing it in the Bragg reflected monoenergetic beam. Because the diffracted beam was considerably less intense, samples were mounted in the path of this beam to avoid irradiating them excessively. In this position also, the number of neutrons scattered by the sample was lower than if it were in the primary beam.

Except for elements available in foil form, it was necessary to add a second substance, usually sulfur or a solvent, as a support for the sample while its transmission was being measured. This, however, made it necessary to consider the effect of the binder or solvent on the transmission measured. To do this, a second sample containing the binder alone was prepared, and the number of neutrons passed through this sample was measured. The ratio of the counting rate with the bound sample in place to that with the binder alone in the beam was taken as an uncorrected measure of the transmission of the sample. A sliding holder with several apertures was used to support the two samples successively in the beam. Three apertures were provided in the holder to make possible measurement of two samples with identical supporting materials concurrently.

Monitors and Electronic Circuits

Two monitors were regularly employed with the spectrometer in the measurement of neutron cross section. The first, a monitor of the neutron intensity in the primary beam, was a fission chamber mounted near the reactor tank wall, in a removable channel adjacent to that used as a primary source for the spectrometer. The position of the monitor with respect to the tank wall could be varied so that varying pile intensities yielded the same reading on the monitor. Although the pile was automatically controlled, and did not in general fluctuate by more than 3 percent, the monitor was useful in averaging any short term fluctuations and in taking into account any long term drift of the pile. The monitor was an aluminum fission counter containing a thin foil of uranium oxide, U_3O_8, enriched some ten times in the isotope 235. This monitor, operated at 1000 volts above ground, was used as a measure of integrated incident neutron flux in timing the measurements.

A second monitor measured the variations in the intensity of neutron background which were caused by changes in neutron leakage from other points of the pile. This monitor, an unshielded boron trifluoride counter operated in the proportional region, was identical with the main detector described above, except that it was filled with normal boron trifluoride gas to a pressure of 40 cm of mercury. Since this monitor was 100 times more sensitive to change in background neutron intensity than the main detector, it increased the reliability of cross-section measurements by decreasing the uncertainty in background variation. In general the background neutron intensity in the pile room was quite small, and this monitor was used to detect only great variations in background. However, rather than correct the data for these background variations, the reading which was indicated by this monitor to be disturbed was generally repeated under more favorable conditions.

Each of the three counters, the main detector, the fission monitor, and the background counter, had associated with it a preamplifier, cathode follower, amplifier, scaler, and high voltage supply. The preamplifiers and cathode followers were mounted as near as possible to the counter, while all high voltage supplies, amplifiers, and scalers were mounted together on a control panel on a work bench near the instrument. The detector and background monitor signals were recorded on two scales of 64, while the fission signal was recorded on a scale of 512.

Between the amplifier and the scaler of the main detector circuits an additional limiting circuit has been provided,* the function of which was to eliminate large negative or positive pulses, and any small pulses with sign opposite to that of the neutron pulse. This circuit has proved useful in eliminating pulses caused by an electromagnetic disturbance in the vicinity of the spectrometer. For facility, and to assure simultaneous stopping and starting, all of the circuits were operated from a single switch. An oscilloscope was provided to watch the signal at various stages of amplification and scaling, and regular checks were made to assure the perfect functioning of the instrument. During measurements of cross section the oscilloscope constantly registered the output of the main detector.

III. ALIGNMENT

The condition for a maximum in the diffraction pattern of a space lattice is given by the familiar Bragg law,

$$n\lambda = 2d \sin\theta,$$

where d is the interplanar distance, n an[illegible] order and wave-length respectively, and θ [illegible] glancing angle. Expressed in terms of energy, the relation becomes

$$ev = kn^2/\sin^2\theta \qquad (2)$$

where k is a constant for each interplanar spacing. The problem of alignment, then, was one of determining the glancing angle θ, and thus involved centering the instrument and crystal table with respect to the primary beam, aligning the detector, and finally aligning the crystal.

Alignment of the Table, Detector, and Crystal

Two methods have been used to center the crystal spectrometer and its table with respect to the center of the primary beam. In the first, a long, snug-fitting steel bar was inserted

* This circuit was designed by Mr. Thomas Brill of this laboratory.

into the primary beam collimator and extended over the spectrometer table. With this method, by inversion of the bar to cancel out any lack of parallelism, the center line of the slot could be located within $\frac{1}{4}$ mm.

The second method used for preliminary determination of the center of the beam involved the use of photographic film. In this method a sheet of orthochromatic film was placed between two layers of cadmium metal, and this sandwich exposed to the beam of neutrons. A small hole drilled through the cadmium sheets was used to orient the film with respect to the crystal table, and the subsequent blackening of the emulsion indicated the shape and position of the neutron beam. The clear spot in the darkened area, representing the hole in the cadmium layers, served then to relate the position of the crystal table to that of the beam. This method, although less accurate than the foregoing because of the associated flux of gamma-rays which caused about 15 percent of the blackening, was useful because it showed both shape and rough position of the primary beam at any point on the arm.

After the detector had been carefully aligned parallel to the arm of the spectrometer and the table centered with respect to the beam, it was necessary to locate the angular position of the arm at which the arm was parallel with and centered in the primary beam. In order to center the detector with respect to the primary beam a curve of neutron intensity as a function of angular position of the detector was plotted. Since the primary beam consisted of a very intense flux of neutrons and gamma-rays, it was necessary to reduce its intensity so that this measurement could be made. In order to reduce the neutron intensity, a thin slab of paraffin was introduced directly into the beam, and, to eliminate entirely the effect of the gamma-rays, the gain of the amplifier was changed so that only the higher neutron pulses were counted. The zero position of the detector was then determined to be the point of intersection of two lines which represent the slopes of the two sides of the curve taken in this manner. This position could easily be determined within 2 minutes of arc, and thus contributed an uncertainty of but 1 minute of arc in the glacing angle θ.

Having determined the position at which the detector was in the center of and parallel with the direct beam, the detector was turned off this zero position by a known amount, usually 40 degrees, and the cadmium diaphragm and crystal carefully placed in position on the instrument. As the crystal approached an angle of 20 degrees with the primary beam, the diffracted maximum could be detected. Leaving the arm in its fixed position, the crystal was rotated for several degrees on either side of this maximum, and a plot of the measurement of the intensity of diffracted neutrons as function of glancing angle made. A lack of symmetry about the maximum of the observed diffraction curve arose from the fact that it was taken with a boron detector, since boron follows the well-known $1/v$ law for absorption of neutrons and is not uniformly sensitive over the entire spectrum range. These data, corrected for the $1/v$ effect, determined the peak of the diffraction maximum within two minutes of arc.

The uncertainty in the glancing angle θ, caused by uncertainties in centering of the crystal table, could be taken as negligible because the width of the beam and the width of the counter were very nearly alike and because of the precision with which this position was ascertained. Because the index of refraction of the crystal used for neutrons is not equal to unity, as has been shown for many substances, one might expect this to introduce an additional error in the measurement of the energy of the diffracted beam. However, since the value of the index of refraction is very likely of the order of 1×10^{-6}, this effect too was completely negligible. Thus the total errors were introduced in aligning the detector, and in aligning the crystal, and resulted in an uncertainty of three minutes of the glancing angle throughout the range of the instrument.

IV. CRYSTALS

Although many crystals, including mica, copper, calcium fluoride, calcite, and lithium fluo-

TABLE I. Relative reflectivity from several crystals.

Crystal	$k\times10^8$	Maximum energy (ev)	Relative reflectivity
LiF (100)	5.08	65.0	6.4
Calcite (100)	2.22	28.0	2.5
Mica (001)	0.20	2.5	9.2
Cu (100)	1.56	20.0	~5.0

ride have been used and tested for crystal spectrometry, all of the measurements of cross section as a function of energy were made with the lithium fluoride crystals. The spectrum from the side hole of the heavy water pile has been measured with several crystals, and the relative peak intensities observed with each of these crystals have been tabulated in column 4 of Table I.

As in the case of x-rays, the reflectivity of a crystal for neutrons can be increased by increasing the mosaic structure of the surface. A single crystal of LiF(100) has been carried through several steps, each involving a change in the surface of the crystal. The relative reflectivity from these surfaces is shown in Table II. In each case the rocking curve was 22 ± 1 minutes in half-width, and since this value was determined by the collimating geometry, no quantitative conclusion with regard the change in mosaic structure could be made from these data. However, obviously the roughened crystal, with its higher reflectivity, is best for use in spectrometer measurements with this type of collimation. Since the range of energies covered by the spectrometer is a function of the interplanar spacing of the crystal used, a consideration which must be weighed in selecting a crystal for spectrometer use is the value of d. As is obvious from Eqs. (1) and (2), the highest energy which can be reached by any crystal as a function of its lattice spacing varies as the square of the reciprocal of the lattice spacing. Column 3 of Table I shows the maximum energy which can be reached using these crystals, assuming that the collimation is such as to permit the utilization of diffracted beams whose incident glancing angle is 30 min.

Calcite and Lithium Fluoride

All early measurements on the thermal column, and some of the first measurements at the side port of the Argonne heavy water pile, were made with a calcite crystal. This crystal, however, because of its lattice perfection, showed a lower reflectivity than many of the other crystals tried. Since, in addition, it is quite a hard crystal and increased mosaic structure cannot easily be introduced, this crystal was used only for preliminary work.

TABLE II. Variation of reflectivity with crystal surface. LiF (100).

Surface	Reflectivity
Smooth cleavage face	1.00
Surface ground	1.65
Surface polished	2.34
Surface roughened with coarse abrasive	2.36

The simple cubic crystal, lithium fluoride, was the crystal selected for most of the work reported in this paper. Because of the small size of the unit cell, and because of the consequent small interplanar spacing in this crystal, the range of energies available for this series of neutron spectrometer studies extended up to 65 ev. These crystals, quite easily available, had the additional advantage that their mosaic structure could be increased simply by the various techniques discussed above.

The 100 planes of this crystal were used for all of the measurements of cross sections reported here. The unit cell dimension for LiF is 4.01 angstroms, and the interplanar spacing is 2.005 angstroms. With this crystal, the range of useful energy lay between 0.04 ev and 65.0 ev, a factor of 1.6×10^3 in energy. The low energy limit was set by choosing that energy characterized by the presence of less than 5 percent second and higher order components in the Bragg-reflected beam, as determined by a series of experiments of the type to be described; in the case of the high energy extreme, the limit was fixed by the smallest useful glancing angle which could be achieved with reasonable collimation, in this case 30 minutes. The LiF crystals used, a bank of small individual crystals mounted in an aluminum holder to form a long array, consisted of 5 small crystals whose individual dimensions were $3.7\times2.7\times.2$ cm. The planes of each of the individual crystals were aligned within 1 minute of arc.

V. SPECTRUM OF THE SOURCE

Two ports of the Argonne heavy water chain reacting pile were used for all of the measurements. The first, the thermal column, interposed a thickness of carbon between the source and the spectrometer rendering the greater part of the neutrons thermal. Their distribution, roughly Maxwellian, was such as to provide a useful

source of neutrons in the energy range below 0.2 ev. The second port, a side hole of the same reactor, interposed little moderator between the source and the spectrometer, and while a strong Maxwellian component was present in this beam because of the moderator inside the reactor, this beam contained, in addition, a fairly strong component of higher energy neutrons which rendered the extension of the range of the instrument to 65.0 ev possible.

The Maxwellian Region

Attempts to explain the results observed in the measurements of spectra from the thermal column and side hole of the reactor, have been made by Seitz and Goldberger.** The form of the equation relating the crystal reflectivity R with the glancing angle θ, for detection by a $1/v$ absorber as developed by them is

$$R_n = C|a_n| nK_1 \csc^3\theta \exp\left[-\alpha_n^2 \csc^2\theta\right]. \quad (3)$$

In this equation n is the order of the reflection, C is an arbitrary constant, and

$$K_1 = 2\pi/d_h$$
$$a_n = \sum_j \pm[\sigma_s^j(b)]^{\frac{1}{2}} \exp\left[2\pi i(h_1x_j + h_2y_j + h_3z_j)n\right]$$

$$\alpha_n^2 = \frac{h(2\pi/d_h)^2}{8mk_0T} n^2,$$

in which d_h is the interplanar distance, m is mass of the neutron, $\sigma_s^j(b)$ is the scattering cross section of the j'th atom in the unit cell, k_0 is Boltzmann's constant, and T is the average neutron temperature.

The fit of this expression for $T = 400°K$ to the experimental points in the Maxwellian region is shown plotted as a solid line in the curve of Fig. 2. The distribution at higher energies, when corrected for detector efficiency, resolution, and amount of beam intercepted, corresponds to the expected $1/E$ function.

VI. ORDER EFFECTS

A study of the intensities of neutron diffraction in the various orders by a series of crystals has recently been made by Fermi and Marshall.[13] Their results show that the relative amounts of first and higher order Bragg reflection varies greatly from crystal to crystal and from plane to plane, depending on the scattering cross sections and the phase of neutron scattering by the target nuclei. Thus the choice of a crystal for cross-section measurements determines the useful range over which data can be taken with diffracted beams uncontaminated by higher order components.

From Eq. (2) we see that for a constant glancing angle, θ, the energies of the first and second order have a ratio 1 to 4 in energy. A series of experiments were performed to evaluate approximately the fractional composition of the beam quantitatively to determine the useful range of the spectrometer for measurements of cross section.

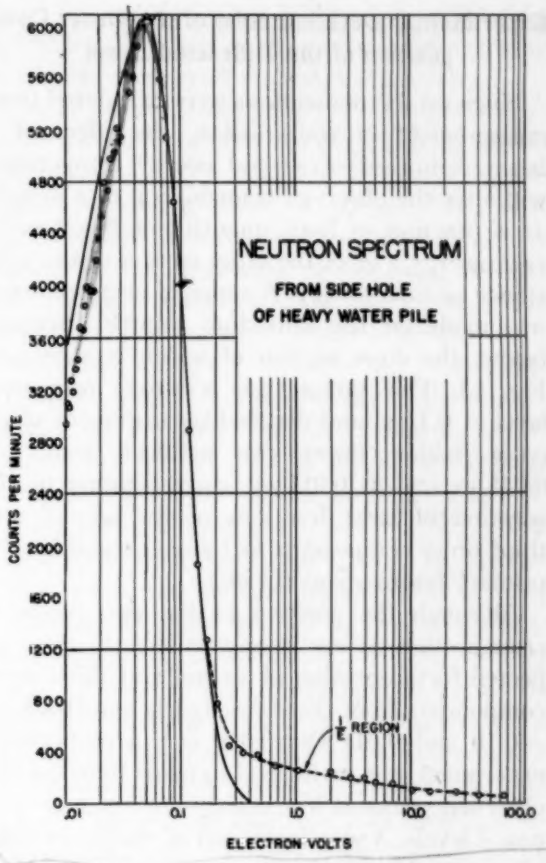

FIG. 2. Spectrum of reactor as measured with LiF(100) crystals. The solid line represents the theoretical Maxwellian distribution for $T = 400°K$.

** M. L. Goldberger and F. Seitz, Phys. Rev. 71, 294 (1947).

[13] Fermi and L. Marshall, Phys. Rev. 70, 103 (A) (1946).

Experimental Determination of the Order Composition of the Diffracted Beam

Since total cross sections were calculated from measurement of transmission, the effect of a beam composed of several energy components will alter the observed transmission of a sample as a function of both quantity of flux having each energy and of the cross section of the substance at each energy. A series of measurements was made on the samarium sample discussed below, the cross section of which is shown in Fig. 13. This sample has a strong resonance level at 0.1 ev, and detailed measurement of its cross section shows two artificial peaks at 0.025 ev and at 0.011 ev, corresponding to absorption of large fractions of the second and third order components at these energies by the primary resonance at 0.1 ev.

Although the position of the two peaks in cross section at low energy is exactly that expected for absorption of second and third-order components from the diffracted beam ($0.025\times4=0.10$ and $0.011\times9=0.099$ ev), a preliminary experiment was performed to show that the two observed peaks at low energy are not real resonance levels. A very large part of the 0.1-ev component of the primary neutron beam at 0.025 ev was removed by filtering this beam through a second samarium solution, the transmission of which, for the high order component was about 0.10. A measurement of the transmission of the first solution was made with and without the filter in place. Without the filter the transmission was 0.441, with the filter the transmission measured 0.814, indicating a lower absorption because the strongly absorbed 0.1-ev component was minimized in this filtered beam.

In order to get a quantitative estimate of the amount of second-order component in the beam diffracted by LiF(100) at 0.025 ev, a measurement of a standardized thin film of boron was made at this energy. The boron layer was a plate of Pyrex, the transmission of which had been previously measured in a mechanical velocity selector in which order effects were absent. Measured in this way, the transmissions of this plate for the first-order (0.025 ev) component was 0.441 and for the second-order (0.1 ev) component was 0.663. A measurement on the crystal spectrometer yielded a transmission of 0.490, intermediate between the values for the first and second orders alone.

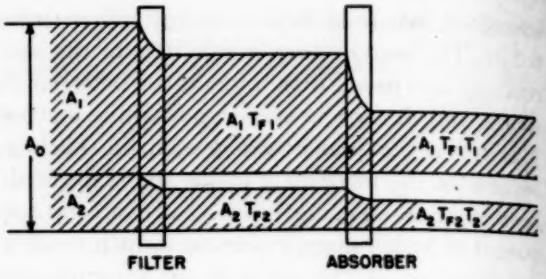

FIG. 3.

It is clear that in this measurement with a beam of several energy components impinging on an absorber of energy-dependent cross section, if A_n is the fractional order component, and T_n is the transmission of the absorber for the energy of the order n, then

$$A_0T_0=A_1T_1+A_2T_2+A_3T_3\cdots \quad (4)$$

where T_0 is the observed transmission and A_0 is the total flux and is equal to one. Since there are but two orders of significance at this angle, substitution of the transmission values given above and combining with the knowledge that

$$A_0=A_1+A_2=1, \quad (5)$$

showed that, for first order equal to 0.025 ev, the fraction of first and second-order components was: $A_1=0.78$; $A_2=0.22$.

A second evaluation of the composition of the diffracted beam at the same energy was made by altering the composition of the beam as in the case above, with a filter having known absorption for the two energy components. The filter for this measurement was a second and thicker samarium sample, having very low transmission for the second-order (0.10 ev) energy component, thus lessening the fractional absorption of this strongly absorbable component at 0.025 ev by the sample. A schematic representation of the transmission of this series of absorbers is shown in Fig. 3. The primary beam of intensity A_0 is considered to be divided into its first and second-order components A_1 and A_2, and the lessening of their intensities is shown schematically in the figure. The observed transmission of the samarium absorber in the filtered beam is

given by

$$T_0=\frac{T_1A_1T_{f1}+T_2A_2T_{f2}}{A_1T_{f1}+A_2T_{f2}} \qquad (6)$$

where T_n = the transmission of the absorber for neutrons of the energy of the order n, T_{fn} = transmission of the filter for neutrons of the energy of the order n, A_n = the intensity of the order n. Values of T_n and T_{fn} were obtained by calculation from the quantity of absorber in each cell and from the cross section shown in the Breit-Wigner curve plotted in Fig. 13. The values thus obtained were: $T_{f1}=0.374$, $T_{f2}=0.090$, $T_0=0.593$, $T_1=0.613$ and $T_2=0.280$. Again combining these by use of Eq. (5) we calculate that $A_1=0.78$ and $A_2=0.22$.

As a third method of evaluation of the ratio of order components at 0.025 ev, a filter measurement, similar to the last one was made. In this case the filter used was the same standardized Pyrex plate of the earlier measurement, and the principle the same as that of the previous experiment. Values of T_n were calculated from Fig. 13 and those of T_{fn} from the standardization mentioned earlier. The values used in Eq. (6) were: $T_{f1}=0.441$, $T_{f2}=0.663$, $T_1=0.436$, $T_2=0.294$, and $T_0=0.400$. The calculated fractions of first and second order in this case were: $A_1=0.79$ and $A_2=0.21$. The average value of the first-order component of the reflected beam, 78 percent, agrees quite well with the theoretical value at this energy calculated from Eq. (3).

The theoretical order intensity curve calculated from Eq. (3) which was used for all cross-section corrections is shown in Fig. 4.

Reduction of the Effect of Higher Order Components

In an effort to remove the effect of high order components in the diffracted beam at large glancing angles several techniques were used. Since the total cross sections for neutron reactions in this energy region in general show a decreasing cross section with increasing neutron velocity, cross sections in the region of hundredths of electron volts were measured using samples with transmissions somewhat greater than 0.5. In this manner, since the transmission of the higher energy components of the reflected beam is generally much higher than that of the first order, the effect of the second-order neutrons on the observed cross section is minimized.

Other means of reducing the effects of higher order components involved reduction of the intensity of these components in the primary beam. This was accomplished by use of filters with resonance levels at the energy of the second and higher order components, or by using the primary neutron beam of lower mean energy and minimal $1/E$ component which is emitted from the thermal column. Attempts were made also to remove neutrons of the energy of the second, fourth, etc., orders, by introducing a second (mica) crystal in advance of the lithium fluoride in the primary beam at the angle necessary to diffract these components from the beam. These efforts were unsuccessful, since, aside from reflectivity considerations, the imperfection of even a mica crystal is not as great as was the geometrically determined divergence of the primary beam. These methods of beam purification were considered necessary only for the measurements made at energies less than 0.04 ev, below which energy the diffracted beam contained less than 95 percent first-order neutrons. The small correction necessary at energies lower than 0.08 ev was applied to the observed data at the end of the cross-section measurement by use of relations (4) and (5). Since no order correction was made to data taken at energies above 0.08 ev, this correction was applied only to the few points

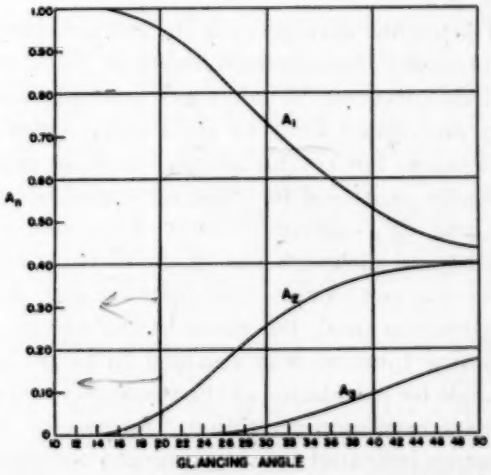

FIG. 4. Fractional order composition of diffracted beam as a function of glancing angle.

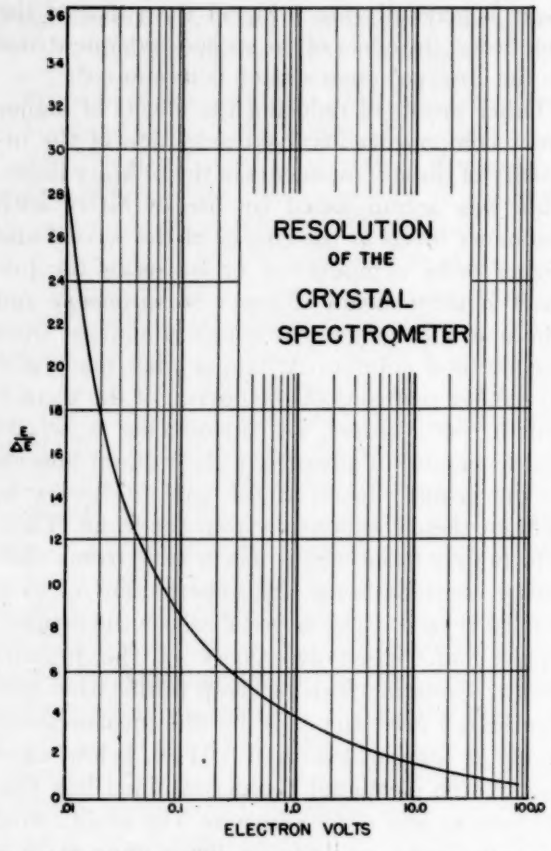

FIG. 5. Resolution of the neutron spectrometer calculated from the width of the rocking curve.

measured at very low energies, and had little effect on the final results.

VII. RESOLUTION

The angular divergence of the diffracted beam, as obtained from measurements of the crystal rocking curve, can be taken as a first approximation and upper limit to the energy spread of that beam. The crystal rocking curve, as experimentally measured for glancing angles between 45° and 3½°, showed uniform shape and half-width; and although the shape of the rocking curve was not exactly triangular because of the $1/v$ detector used, the shape of the energy distribution function was assumed to be an ideal triangle for calculation of the resolution function and for resolution correction. The base of these triangles indicated an energy spread corresponding to the base of the rocking curve, 44 minutes, for energies up to 1.4 ev, and the corresponding values of $E/\delta E$ vary between 28 at 0.01 ev and somewhat less than 1 at 65.0 ev. (See Fig. 5.)

The spectrometer resolution as a function of neutron energy varies as $1/d$, the extent of the useful energy range varies as $1/d^2$. Thus the cleavage (100) face of LiF because of its small d, provided a wide range of energies of sufficiently well-resolved monoenergetic neutrons for cross-section measurements. In practice, the resolving power of the instrument was determined by the minimum width of collimating slits which provided ample diffracted intensity at high energies. This width, 1.25 cm, could have been made smaller at low energies where the intensity was higher, but this was not considered necessary, as the resolution was more than ample with the wide slit in this region, and under these conditions the intensity was considerably increased.

The base width of the rocking curve was not constant for energies greater than 1.4 ev with LiF(100), since for glancing angles less than 3° 28′ and energies greater than 1.4 ev, the 18-cm bank of crystals was not sufficiently long to intercept the entire primary beam. As a consequence, the Bragg-reflected beam at these small glancing angles is less divergent and the width of the rocking curve smaller, varying from 44′ base width for a 3° 28′ glancing angle to 19′ at 30′ glancing angle. This resulted in an improvement in resolution and a loss of intensity in the high energy region. The triangles shown on the curves of cross section indicate the idealized shape of the final intensity-energy distribution of the diffracted neutron beam at the energy of the apex.

Resolution Correction

It was possible to correct the transmission measurements in the energy region below 0.2 ev for the slight distortion in the nature of this curve caused by the finite resolution.[14] To do this, we note (see Fig. 6) that the measured transmission, Φ, is given by

$$\Phi=\frac{\int_{E'-\gamma}^{E'+\gamma} f(|E-E'|)\phi(E)N(E)dE}{\int_{E'-\gamma}^{E'+\gamma} f(|E-E'|)N(E)dE} \tag{7}$$

[14] M. Goldberger, unpublished work.

where $f(|E-E'|)$ is the resolution function, $\phi(E)$ is the true transmission at energy E, and $N(E)$ is the incident flux distribution over the energy interval. Assuming that $N(E)$ in the region of interest is very nearly constant, we can substitute in the simplified expression the triangular resolution function (Fig. 6)

$$f(|E-E'|)=(\delta/\gamma)\{(|E-E'|)+\gamma\} \quad (8)$$

we obtain

$$\gamma^2\Phi(E')=\int_{E'-\gamma}^{E'}E\phi(E)dE-\int_{E'}^{E'+\gamma}E\phi(E)dE+\int_{E'}^{E'+\gamma}(E'+\gamma)\phi(E)dE-\int_{E'-\gamma}^{E'}(E'-\gamma)\phi(E)dE.$$

Expanding the right side of the equation about $\gamma=0$,

$$\Phi(E')=\phi(E')+\frac{\gamma^2}{12}\phi''(E')+\frac{\gamma^4}{360}\phi''''(E'). \quad (9)$$

To express ϕ, the true transmission, in terms of operations on Φ, the measured transmission, we neglect in the first approximation the term involving the fourth derivative. Solving the simplified last equation for ϕ, we find

$$\phi(E)=\sum_{K=0}^{\infty}\frac{(-1)^k\Phi^{(2k)}(E)}{\alpha^{2k}}$$

in which $(2k)$ refers to the $2k$th derivative, and $\alpha=[12/\gamma^2]^{\frac{1}{2}}$, whence to this degree of approximation,

$$\phi(E)=\Phi(E)-(\gamma^2/12)\Phi''(E). \quad (10)$$

By perturbation theory, taking into account the term in the fourth derivative,

$$\phi(E)=\Phi(E)-(\gamma^2/12)\Phi''(E)-(\gamma^4/360)\Phi''''(E), \quad (11)$$

the final form of the relation, valid where γ is small relative to the half-width of the resonance level.

VIII. MEASUREMENT OF TOTAL NEUTRON CROSS SECTIONS

Cross sections can be measured by transmission or by activation in the monoenergetic diffracted neutron beam of the crystal spectrometer. Because, however, the intensity of the Bragg beam does not exceed 30,000 neutrons per minute. Activation measurements are thus limited by the low neutron flux to elements with large cross sections and short periods, and that only in the energy range of high flux near the peak of the Maxwellian distribution. Results reported here were made by measuring transmissions of a small sample of the absorbing substance by means of a boron counter.

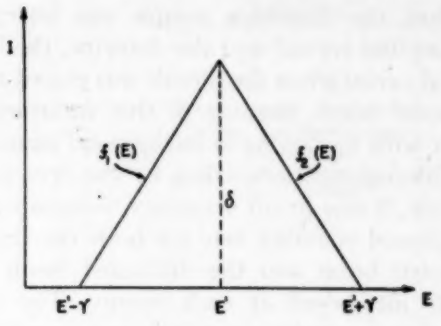

FIG. 6.

Total cross sections are calculated from the measured transmission, T, from the relation

$$T=e^{-\sigma N}, \quad (12)$$

in which σ is the total neutron cross section in square centimeters per atom and N is the surface density of atoms in the sample. Solving for σ, we have

$$\sigma=(1/N)\ln(1/T) \quad (13)$$

which is the form of the relation used for the calculation of σ. The value of N was obtained by simple assay of the foil, powder, or solution containing the element of interest, and T was obtained from the measurement of the intensity of the diffracted beam with and without the sample in place. In general, the thickness of the sample was made such that its transmission was somewhat over 0.5 for reasons indicated above. It was not necessary to apply a correction to the transmission data for beam hardening because of the fact that the diffracted beam consisted almost entirely of neutrons of a single energy.

It was, however, necessary to correct both the numerator and denominator of the transmission measurement for a background of neutrons incoherently scattered by the crystal. Since, in

addition, the absorbing sample was interposed between the crystal and the detector, the background varied when the sample was placed in the diffracted beam. Because of this variation, together with variations in background caused by the differing positions taken by the crystal and detector, it was found necessary to measure this background counting rate for both the directly diffracted beam and the diffracted beam with sample interposed at each energy. The background measurements were taken by turning the crystal one degree off the Bragg maximum, an angle at which only the incoherently scattered neutrons reached the detector. The transmission of the sample was then calculated from the four measurements according to the relation

$$T=(R_1-r_1)/(R_2-r_2) \qquad (14)$$

in which R_1 is the counting rate of the beam transmitted through the sample, R_2 the counting rate of the open diffracted beam, and r_1 and r_2 the background rates with and without the sample interposed.

Samples

Samples for cross-section measurement were prepared in one of four ways. For rhodium, gold, and iridium varying thicknesses of metal foils of these substances were used. Part of a preliminary boron curve was taken with pellets of amorphous boron powder pressed into the form of cylindrical disks of varying thicknesses and one inch in diameter. A third method, involving the use of a sulfur binder in the pressed pellets, was used for samples with high total cross sections (part of the iridium curve), where it was impossible to get samples sufficiently thin otherwise. Transmission measurements in these cases involved the use of very fine powders of the substance, and necessitated the use of a second blank pellet of sulfur of weight equal to that of the sulfur binder in the first disk.

The method most frequently used was a solution method, which was used particularly for the rare earths gadolinium, samarium, europium, and dysprosium, where cross sections were usually high and samples were small. For this purpose two very precisely ground quartz cells, 1 inch in diameter and 1 centimeter thick were employed. The nitrate of the rare earth was prepared, a proper amount dissolved in a known amount of heavy water and this solution added to one cell. Heavy water was used as the solvent in order to avoid the loss in beam intensity due to the strong scattering of hydrogen-containing solvents. To the heavy water in the second cell was added a sufficient amount of DNO_3 to equal the effect of the nitrate ion in the rare earth cell. Measurements were made then as in the case of the sulfur bound pellets.

Evaluation of Approximate Theoretical Constants for the Resonance Levels

Although the experimental data are not sufficiently precise to make very definite assignments to the constants in the Breit-Wigner relation, and thus cannot be considered either a test of the theory or the last word on the exact shape of the cross-section curves, it was considered of interest to evaluate the constants of the theoretical expression which best fitted the experimental curves. The form of the Breit-Wigner one-level equation for the energy dependence of the cross section is

$$\sigma E^{\frac{1}{2}}=\frac{\sigma_0 E_0^{\frac{1}{2}}}{1+[(E-E_0)/\frac{1}{2}\Gamma]^2}$$

in which E_0 is the energy of the resonance level, Γ is the width of the level at half-maximum, σ_0 is the cross section at the resonance maximum. The values of σ_0, E_0 and Γ can be assigned from the observed data, and are included in the discussion of cross sections below where their values can be considered to approximate the correct values because of the quality of the experimental data.

In general, the observed data taken at neutron energies less than one electron volt, when corrected for the effect of higher orders and resolution as discussed above, were considered sufficiently precise to justify evaluation of these constants. Data at higher energies are seriously disturbed by lack of resolution, and although the energy of the peak is probably accurate, the measured widths of the levels are in general much too broad, while the peaks are for the same reasons very much flattened.

IX. RESULTS

The total, absorption plus scattering cross sections for neutron reaction have been measured

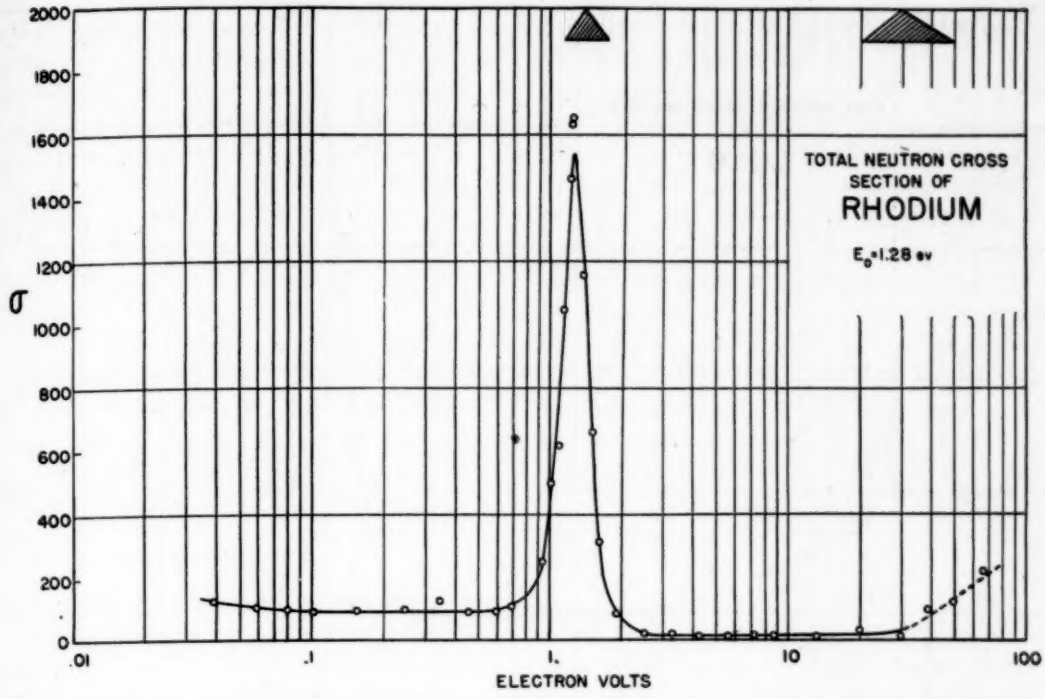

FIG. 7. Total cross section of rhodium. The cross section, σ, is given in units of 10^{-24} cm²/atom (barns).

of a series of well-known strong absorbers, detectors, and rare earths using the method discussed. All the cross sections reported have been calculated from measurements of the transmission of a sample of the substance over the range of energy indicated. Although isolated measurements of the activation cross sections have been made on the same instrument, notably in the case of indium, dysprosium, and europium, these results were not nearly as complete nor as accurate.

In the cross-section curves shown in Figs. 7 to 16 corrections to the observed data have been made for the variations in background caused by change in the amount of scattering as discussed above. In addition, these data are corrected for resolution and for order composition in the ranges of low energy where the methods of correction discussed are valid. An assay of the chemical composition of each sample was made, and corrections for the energy dependent effects of highly absorbing impurities upon the measured transmission at each energy were made. In the range of energies higher than 1.0 ev, only background and impurity corrections were applied and the cross-section values in the maxima are lower limits only. The effect of the poorer resolution at these energies also widened these peaks, and the half-widths taken from the curves are maximum values. None of the cross sections have been reduced to isotopic cross sections or cross sections of the absorbing isotope, but all have been reported as cross sections per average atom. Data taken at energies greater than 30 ev, where the detector was very near to the primary beam, can be considered to give only an indication of the nature of the cross-section function in this region.

Rhodium

Attempts to evaluate the energy-dependent variations in the cross section of rhodium have been made using the boron method[6] and by varying the mean energy of the reaction neutron source by changing the moderator temperature.[7] Further, self and resonance absorption techniques have been used to obtain the width and relative position of the resonance level.[15–18] By

[15] H. H. Goldsmith and F. Rasetti, Phys. Rev. 50, 328 (1936).
[16] H. Feeney, C. Lapointe, and F. Rasetti, Phys. Rev. 61, 469 (1942).

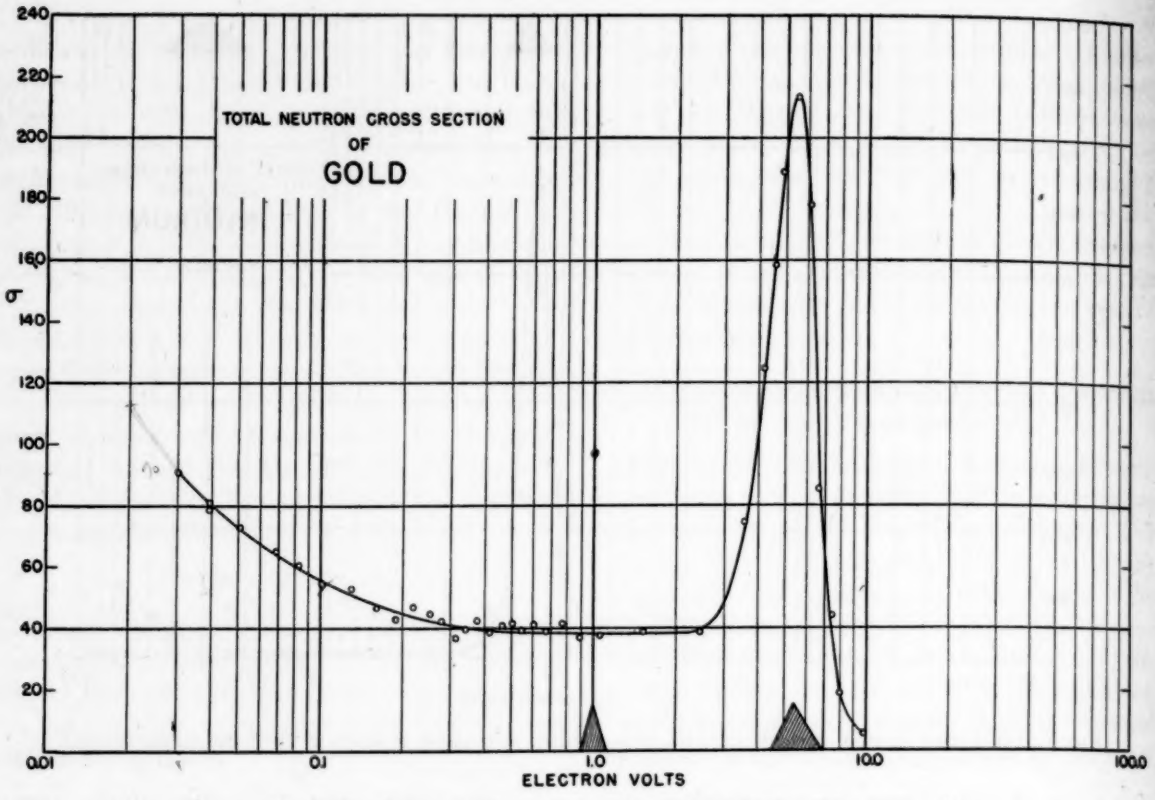

FIG. 8. Total cross section of gold, σ in units of 10^{-24} cm²/atom.

use of a series of six metal foils of the element augmented by an assortment of sulfur-bound pellets of the finely powdered element, it has been possible to measure this cross section in the continuous energy range from 0.04 ev to 65 ev with the crystal spectrometer (Fig 7).

It has been possible to place the resonance peak, the existence of which was predicted by the self-absorption and activation measurements, at 1.28 ev. However, because of the insufficient resolution of the spectrometer in this region, the observed maximum in the cross section represents only a lower limit, and since, for the same reason, the measured width is not correct, no attempt was made to evaluate theoretical constants. At the high energy end of the curve evidence is indicated for some increase in cross section at energy greater than 30 ev.

Combining this result for the energy of the level with a cyclotron measurement of the position of indium level (1.44 ev) recently made by Havens and Rainwater,[11] we find the value of 0.16 ev for the energy difference between the peaks. This is in very good agreement with the results of Hornbostel, Goldsmith, and Manley who by mutual absorption methods found $|E_{0\text{In}}-E_{0\text{Rh}}|$ $=0.15$ ev.

Gold

Two gold plates, which alone and in combination provided three thicknesses of absorber for the various cross-section regions, were used for the measurements. The surface densities of these samples, 1.674 g/cm², 2.898 g/cm² and 4.572 g/cm², made it possible to measure the cross section of gold in the region between 0.04 and 8.0 ev. The variation (Fig. 8) below 2.5 ev is very nearly as $1/v$, and the cross section at kT was found to be 99.3×10^{-24} cm²/atom, in close agreement with other measurements of the cross section at this energy.

[17] J. H. Manley, H. H. Goldsmith, and J. Schwinger, Phys. Rev. **55**, 39 (1939).
[18] J. Hornbostel, H. H. Goldsmith, and J. H. Manley, Phys. Rev. **58**, 18 (1940).
[18a] See also spectrometer measurements of L. B. Borst, A. J. Ulrich, C. L. Osborn, and B. Hasbrouck, Phys. Rev. **70**, 557 (1946); Phys. Rev. **70**, 108 (A) (1946).

Earlier measurements of the position of the resonance level by absorption methods[16] and by modulated cyclotron beam[11] placed it at 2.6 ev and 4.8 ev, respectively. Crystal data indicate the position of the level to be at 5.4 ev. The more detailed recent studies using the time-of-flight technique, however, indicate this value to be somewhat high. The resolving power of the crystal, very nearly the same as that of Rainwater and Havens' earlier apparatus in this region, results in agreement with regard to the apparent width and height of the level as measured by the two methods. ($\Gamma_{\text{apparent}}=2.48$ ev, cyclotron, $=2.50$ ev, crystal; $\sigma_{0\text{apparent}}=198\times10^{-24}$ cm²/atom, cyclotron, $=211\times10^{-24}$ cm²/atom, crystal.)

Iridium

Early measurements which Amaldi and Fermi made of the absorption of cadmium-filtered neutrons showed strong A group neutron absorption by iridium (~5 ev), and later evidence from boron absorption data of resonance absorption in iridium was obtained by Goldsmith and Rasetti,[6] and the energy of this level was placed by them at 1.16 ev.

Spectrometer measurements (Fig. 9) of the total cross section of iridium, at energies up to 8.0 ev, show three absorption resonances, one at 0.635 ev, a second at 1.35 ev, and the third at 6.0 ev. Samples used were foils of the metal 1.09, 2.22, and 3.29 g/cm². Although the resolution of the instrument is not sufficient to make very precise the determination of the theoretical constants, approximate values have been assigned for the two low energy peaks. The two sets of constants for the one-level expression when added together account very well for the observed points. The two sets are: (1) $E_0=0.635$ ev, $\sigma_0(E_0)^{\frac{1}{2}}=425$, $\Gamma=0.250$ ev; (2) $E_0=1.35$ ev, $\sigma_0(E_0)^{\frac{1}{2}}=710$, $\Gamma=0.36$ ev.

Gadolinium

The rare earth, gadolinium, long known to have a very large cross section for kT neutrons[6,19] was measured in heavy water solution. Three concentrations of the nitrate were needed to cover the various energy ranges measured,

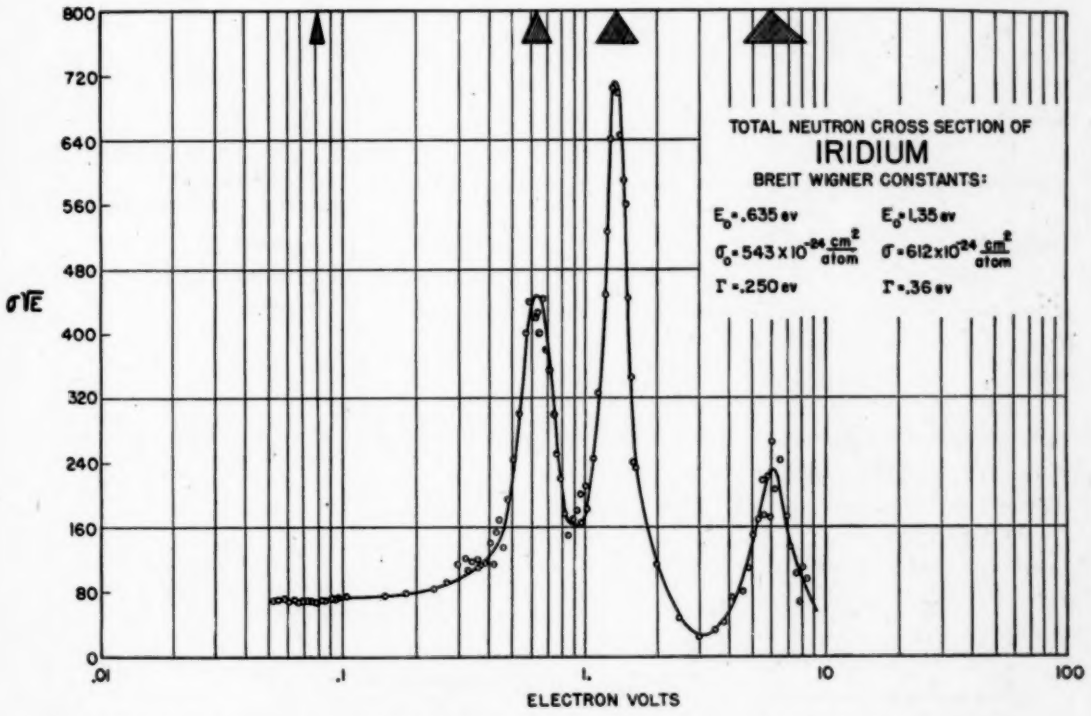

FIG. 9. Total cross section of iridium. Cross-section values are multiplied by $E^{\frac{1}{2}}$ to show the $1/v$ region as a horizontal line.

[19] W. Stupp, Ann. d. Physik **43**, 630 (1943).

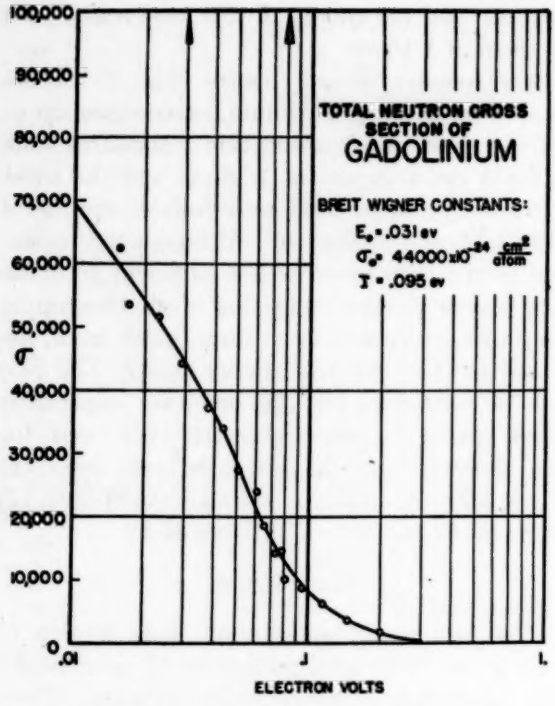

FIG. 10. Total cross section of gadolinium, σ in units of 10^{-24} cm²/atom.

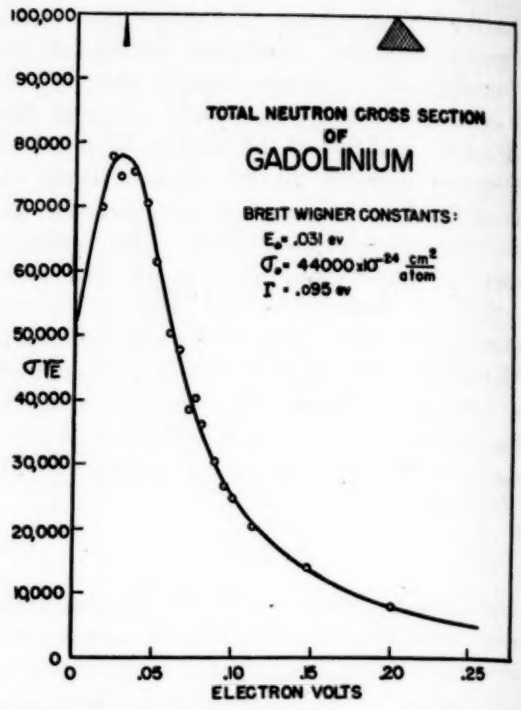

FIG. 11. $\sigma E^{\frac{1}{2}} \times 10$ plot of gadolinium data showing resonance level symmetrical about E_o.

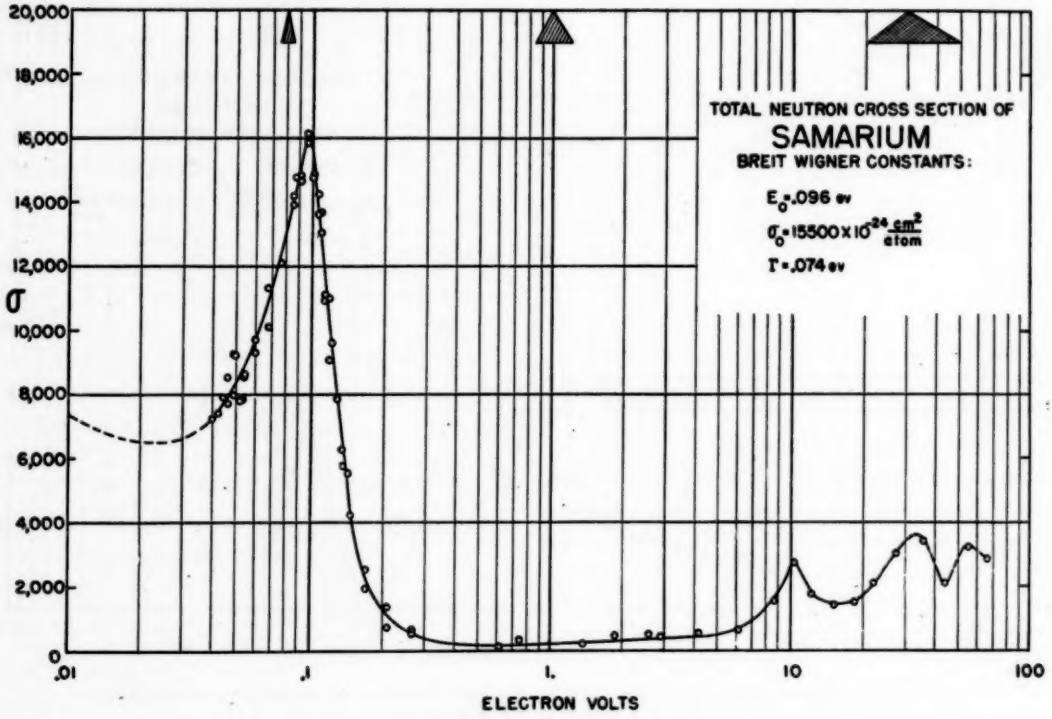

FIG. 12. Total cross section of samarium, σ in units of 10^{-24} cm²/atom.

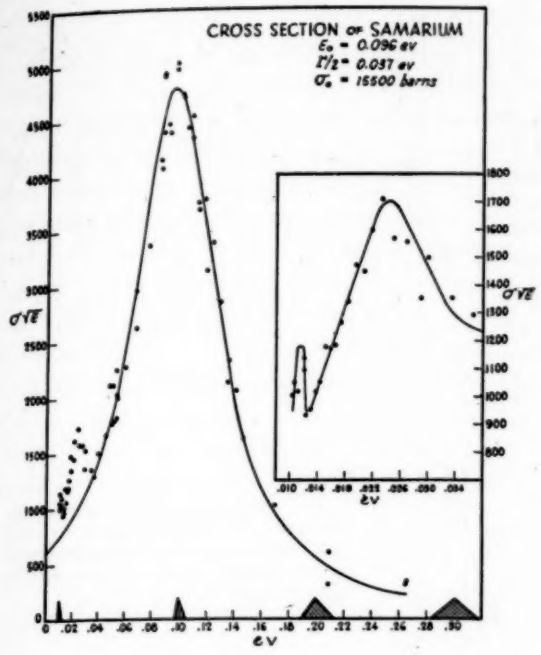

FIG. 13. Samarium cross section for low neutron energies. Two false peaks (shown on expanded scale in insert) correspond to absorption of second and third-order neutrons by the strong resonance level at 0.096 ev.

0.0108, 0.00624, and 0.000867-g gadolinium nitrate per square centimeter. The cross section (Fig. 10) was found to rise rapidly and continuously as the energy of the reacting neutrons decreased, and the rate of rise was greater than that expected for a $1/v$ absorber. Plotting the data in a different manner (Fig. 11) serves to show the resonance level which is superimposed on a strong $1/v$ component of the total cross section. Since in this case, with $\sigma(E)^{\frac{1}{2}}$ and E as the ordinate and abscissa, respectively, a $1/v$ absorber appears as a horizontal straight line, the resonance level is shown as a symmetrical peak superimposed upon it. Thus the level in this element is shown to be at very nearly thermal energy which accounts for its very large kT cross section. The Breit-Wigner constants for these data are: $\sigma_0 = 44{,}000 \times 10^{-24}$ cm²/atom, $E_0 = 0.031$ ev, $\Gamma = 0.095$ ev.

Samarium

Measurement of the total cross section of samarium made in the energy range between

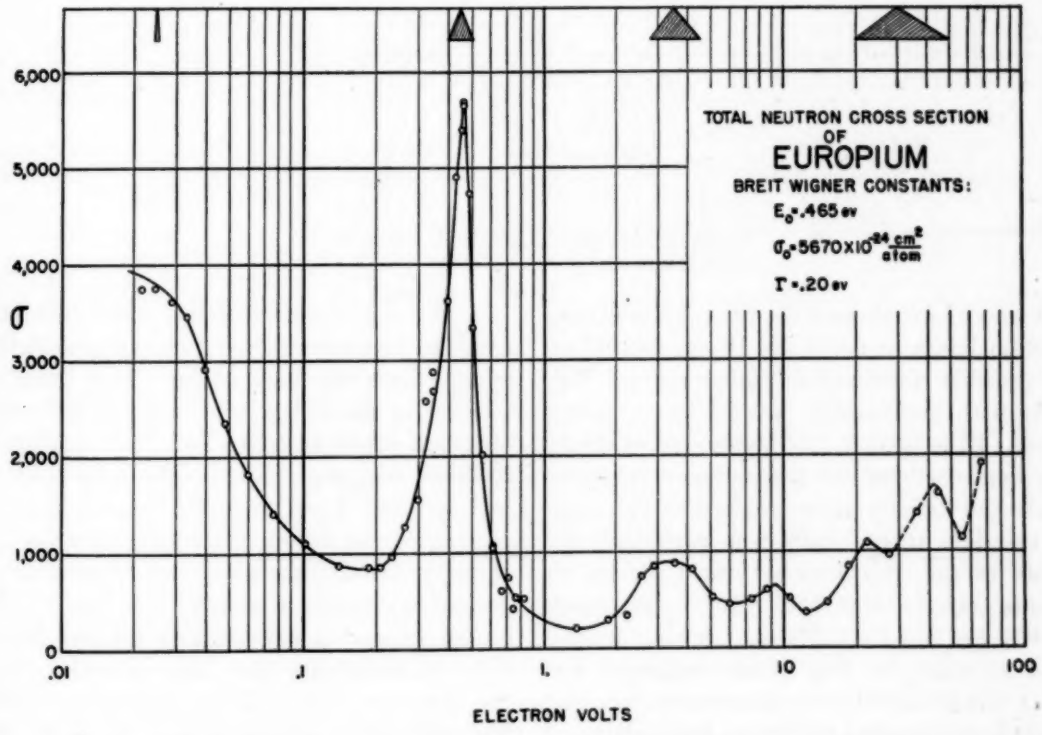

FIG. 14. Total cross section of europium. Slope of curve between 0.035 and 0.10 ev steeper than $1/v$.

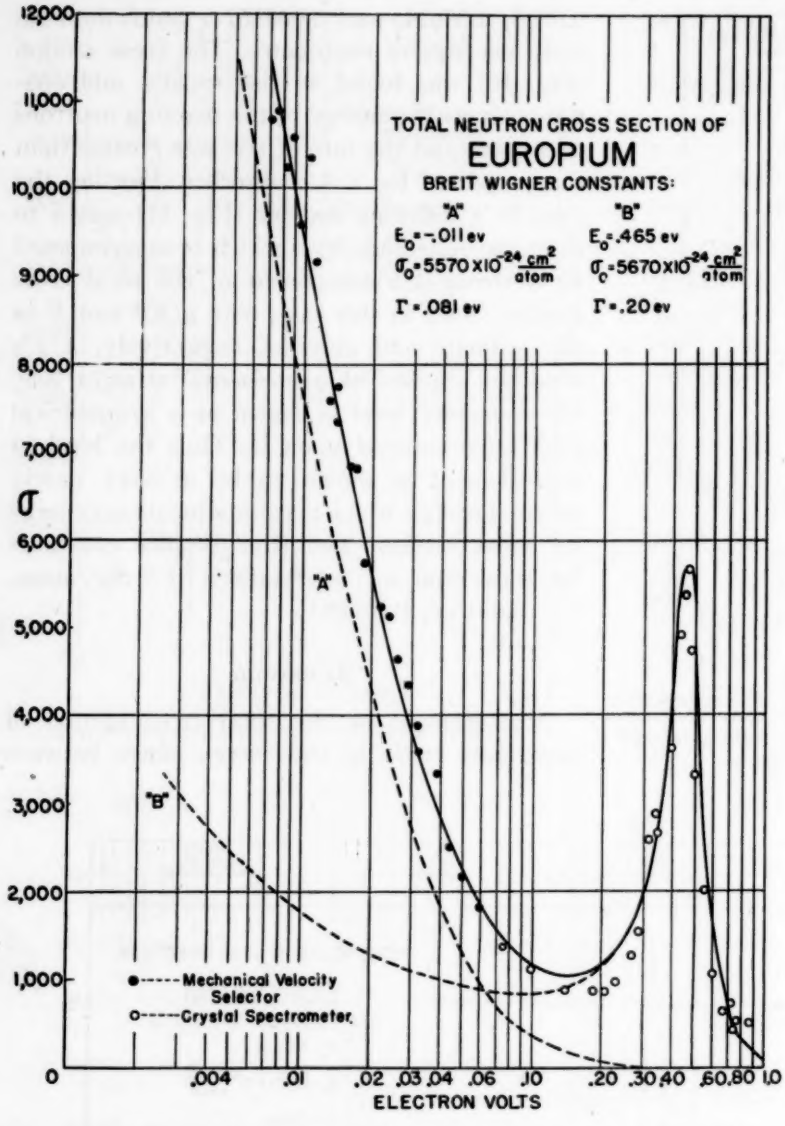

FIG. 15. Extension of europium cross-section measurements to very low energy region showing presence of resonance level at very nearly zero energy.

0.04 ev and 65 ev, showed the presence of strong absorption levels at 0.096 ev, 10 ev, and 33 ev and a possible resonance at higher energy (Fig. 12). As with gadolinium, several heavy water solutions of the nitrate and blank cells of dilute DNO_3 were used for the transmission measurements in the various energy regions. An attempt to fit the data theoretically was made only for the case of the resonance at lowest energy, its constants being: $\sigma_0 = 15500 \times 10^{-24}$ cm^2/atom, $E_0 = 0.096$ ev, and $\Gamma = 0.074$ ev. Previous indication of structure in this cross section at low energies was obtained from absorption data and showed the existence of the lowest level, although no definite energy value could be assigned.[19]

A plot of the uncorrected cross-section data at energies less than 0.04 ev shows strikingly the effect which the high energy, high order components in the diffracted beam can have on the observed cross section. The true resonance at 0.096 ev reappears as two false subsidiary maxima at 0.096/4 ev, when the second-order component of the beam is strongly absorbed, and again at 0.096/9 ev when the third-order component is strongly absorbed. The data are shown on an expanded energy scale in the insert of Fig. 13, indicating that these energies are just the expected values for the absorption of second and third-order components of the beam by the primary resonance at 0.096 ev.

Europium

Measurements of the transmission of a sample of very pure europium were made with the crystal spectrometer using the solvent method. Nitrates containing deuteryl water of crystallization were prepared and dissolved in heavy water, preparing thus samples containing 7.42×10^{20} and 2.16×10^{20} atoms Eu per square centimeter. A survey of this element for neutron energies (Fig. 14) to 65 ev, showed the presence of resonance levels at 0.465 ev, 3.3 ev, 9.2 ev, and 22 ev, and possible levels at higher energy. Since in this case the maximum cross section observed in the peak of the resonance at 0.465 ev represents only a lower limit, assignment of a value to σ_0 is necessarily low. The constants best fitting the observed points are: $\sigma_0=5670\times10^{-24}$ cm^2/atom, $E_0=0.465$ ev, $\Gamma=0.20$ ev. The 3.3-ev level is probably due to capture by Eu^{151} which Goldhaber[30] has shown from boron absorption measurements to have a level at about 4 ev. From self-absorption measurements this level shows evidence of being somewhat wider than the usual levels measured, and appears here to have characteristics not inconsistent with this point of view. It is, however, not possible to distinguish, by present spectrometer measurements at this energy between a wide resonance and a group of narrow ones with close spacing.

Crystal spectrometer measurements shows a rise in the cross section at energies less than 0.15 ev at a rate greater than that expected for a $1/v$ absorber. It was considered that this region, although outside the range of the crystal spectrometer, merited special emphasis. As a consequence, measurements of cross section in the energy range between 0.007 and 0.2 ev were made with a mechanical velocity selector which had this range.*** This instrument, the rotary shutter of which periodically releases bursts of polychromatic neutrons and by suitable delay mechanism counts them electronically at measured intervals after the release, was able to meas-

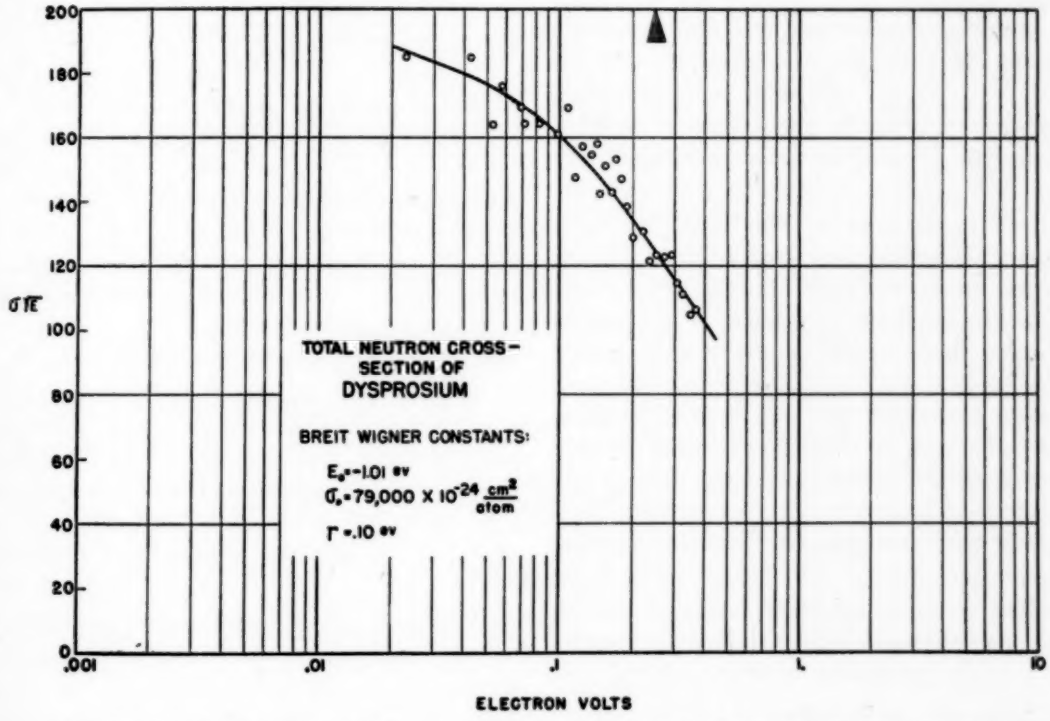

FIG. 16. Total cross section of dysprosium, cross-section values multiplied by $E^{\frac{1}{2}}$. Negative slope indicates resonance level at energy less than zero.

[30] M. Goldhaber, personal communication.

*** The assistance of G. Arnold, H. Kanner, and R. Nobles in making these measurements with the mechanical velocity selector is gratefully acknowledged.

ure transmission as a function of neutron energy. These data at low energy, combined with those from the crystal are shown plotted in Fig. 15. The constants of this low energy level were found to be: $\sigma_0 = 5570 \times 10^{-24}$ cm²/atom; $E_0 = -0.011$ ev; $\Gamma = 0.081$ ev.

Dysprosium

Although the limited supply of dysprosium available at the time of the measurements shortened the energy range covered by the data for this element, sufficient evidence was obtained to indicate the existence of a neutron resonance in the cross-section curve. As with the other rare earths, quartz cells of the nitrate dissolved in D_2O were used for the transmission measurements, the surface density of sample used here being 5.87×10^{20} atoms of dysprosium/cm².

The $\sigma(E)^{\frac{1}{2}}$ curve of these data (Fig. 16) shows a continuously rising function with decreasing energy, which, by its slope, indicates a resonance level at energy less than zero. The cross section at kT neutron energy was found to be 1180×10^{-24} cm² atom, a value considerably higher than an earlier measurement[21] of 870×10^{-24} cm²/atom at this energy. The constants assigned to the theoretical curve are of necessity highly uncertain because the only experimental data it is possible to obtain in this case is far from the peak of the level and represents but one wing of the resonance. The constants assigned to fit the data, assuming a half-width of 0.10 ev, are: $-E_0 = 1.01$ ev, $\sigma_0 = 79{,}000 \times 10^{-24}$ cm²/atom, $\Gamma = 0.10$ ev.

The writer wishes to acknowledge his indebtedness to Dr. Walter H. Zinn for his valuable suggestions and advice throughout the course of this investigation and to Mr. Solomon H. Turkel for his interest and assistance in many aspects of the work.

---

[21] L. Meitner, Arkiv. Mat. Astr. Fys. **27A**, 3 (1941).

Diffraction Pattern of a Circular Aperture at Short Distances

C. L. ANDREWS
Research Laboratory, General Electric Company, Schenectady, New York
(Received January 6, 1947)

The diffraction pattern of electromagnetic waves was studied at distances from zero to five wave-lengths from a circular aperture. Microwaves of 12.8-cm wave-length were employed. The aperture was an iris diaphragm that could be varied between one and six wave-lengths in diameter. The beam was incident normally upon the plane of the aperture from a 4 ft parabolic reflector 24 feet away. The sharpest diffraction patterns were in the plane of the aperture. Measurements were made of the intensity of radiation in the electric and magnetic planes through the axis. Individual plots were made of intensities along the diameter and along lines parallel to the diameter at steps of quarter wave-lengths from the diameter. Measurements were also made of the intensities at fixed points along the axis as the diameter of the iris was varied from one to six wave-lengths. It was observed that Fresnel zone theory could be employed as a rule of thumb in predicting the intensity along the axis even in the illogical case of predicting the intensity at the center of the aperture. Checks were made against Kirchhoff's theory.

INTRODUCTION

THE wartime development of tools and techniques for the production of continuous microwaves has provided a supplement to the study of diffraction of x-rays and light.

The study of the diffraction of electromagnetic waves by apertures has been of four kinds:

1. Fraunhofer diffraction for which the source and the field to be studied are both effectively an infinite distance from the aperture.

2. Fresnel diffraction for which the source and field to be studied are at large distances from the aperture compared to a wave-length but at small enough distances to require consideration of the effect of phase difference between secondary wavelets from the different points in the aperture, even when the source and field to be considered are on a normal to the screen.[1]

3. Diffraction by apertures of small dimensions compared to a wave-length.[2]

4. Diffraction by apertures of the order of a wave-length in diameter observed in and near the aperture.

When the second and third types of diffraction are treated theoretically, approximations can be made in the solution of Maxwell's equations or in Kirchhoff's semi-empirical equation. The theory of the fourth type of diffraction must be general and may, when developed, add to the understanding of the other two.

Most theoretical determinations of diffraction patterns since the time of Fresnel have been based on the simple but necessarily blind assumption that the field over the surface of the aperture is identical with that of the unperturbed incident wave.

When a sufficiency of precise experimental data has been taken of fields in and near the aperture, a sound theory of diffraction may be built on the basis of experimentally known boundary conditions and Maxwell's equations. Bethe has suggested[2] that it may be possible to determine the boundary conditions by rigorous theory such as he applied to small holes. However, the generalization of his method of determination of the boundary conditions appears so difficult that it would not be too unsportsmanlike to make experimental observations first.

At present the only self-consistent theory of diffraction of electromagnetic waves[3] is that for the case in which the boundary surface is a perfect reflector. The condition of perfect reflectivity is closely approximated for microwaves incident upon a metal surface.

APPARATUS

The diffraction pattern of electromagnetic waves was studied at distances from zero to five

[1] S. A. Shelkunoff, *Electromagnetic Waves* (D. Van Nostrand Company, Inc., New York, 1943), p. 365.
[2] H. A. Bethe, Phys. Rev. 66, 163 (1944).
[3] B. Baker and E. Copson, *Huygens Principle* (Oxford University Press, 1939), p. 152.

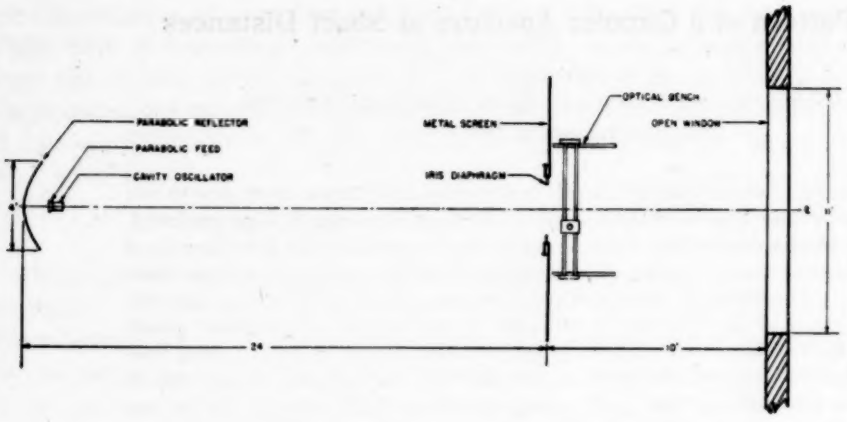

FIG. 1. Arrangement of apparatus for the study of diffraction by a circular aperture at short distances from the aperture.

wave-lengths behind a circular aperture. Figure 1 is a sketch of the horizontal cross section of the arrangement. Microwaves of 12.8 cm were employed. The oscillator was two coaxial, coupled, resonant cavities with a General Electric disk-seal 2C39 triode as an integral part of the cavities. The parabolic reflector, four feet in diameter, was fed by a small paraboloid, with a focal length of a quarter wave and diameter of one and one-half wave-lengths, having a dipole at its principal focus. The three-foot iris diaphragm was mounted in a 6 ft. by 6 ft. sheet iron "barn door" which could be rolled to one side when the undisturbed intensity was to be measured. To supplement the sheet iron screen, a wire-mesh screen was mounted around it making the total screen 12 ft. by 12 ft. The top of the optical bench was 18 in. below the bottom of the iris. A vertical wooden dowel 3 ft. long supported the receiving dipole antenna so that it could be moved in a horizontal plane through the axis of the diaphragm.

As shown in Fig. 2, the dipole was at the end of a 2-ft. coaxial line of silver tubing in the other end of which was mounted a silicon crystal detector. A quarter-wave choke, coaxial with the silver tubing, was mounted behind the dipole. A shielded line extended from the detector to a 50-microammeter outside the field. The combined crystal and meter were calibrated with a wave-guide attenuator. The rectified current through the crystal was proportional to the square of the potential across it and, therefore, to the received power and to the intensity of the radiation in the region of the dipole.

Both the dipole of the transmitter and of the receiver could be rotated to the vertical or horizontal plane. When they were vertical, the diffraction pattern in the *H* or "magnetic plane" could be measured. When they were horizontal, the pattern in the *E* or "electric plane" could be measured.

To prevent reflections, the iris was set before the center of an open window 11 ft. wide and 8 ft. high. The intensity at the edges of the window and along the floor, ceiling and walls was negligible. Standing waves were observed, of course, between the transmitter and screen. Care had to be taken that the opening and closing of the iris did not react on the oscillator to change its output. It was found that when the antenna was coupled sufficiently loosely to the oscillator, the plate current of the tube remained constant as the iris was opened and closed.

RESULTS

In the following set of graphs, all distances are expressed in wave-lengths. The intensities are relative to the intensity of the undisturbed beam when the iris and screen were removed from the region.

Figures 3a, b, c, d, and e show the intensities in the plane of the iris along the diameter in the

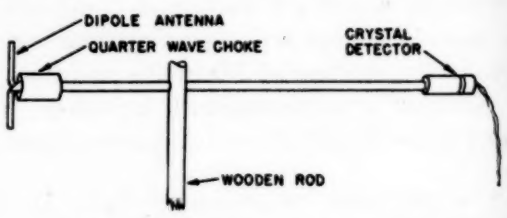

FIG. 2. Probe for exploring the field.

H plane when the diaphragm was one, two, three, four, and five wave-lengths in diameter. Figures 3a′, b′, c′, d′, and e′ were of intensities along the diameter in the *E* plane for the same sizes of diameter. To one accustomed to employing Fresnel's zone theory or Kirchhoff's theorem in optics, with the assumption of constant intensity over the aperture, it was startling to find that the sharpest diffraction pattern in the whole field was in the plane of the aperture. Measurements were made of the intensity beyond the edge of the iris. In these cases, the antenna was kept at a distance of about two millimeters from the surface of the leaves of the iris. In the *E* plane the beam was broader than in the *H* plane. Moreover, it was noted that the intensity in the *E* plane was not symmetrical with respect to the center. This was possibly caused by the fact that contact resistance between leaves of the iris diaphragm was variable so that the surface currents were not the same on the two sides.

Figures 4a, b, c, d, e, and 4a′, b′, c′, d′, and e′ are for a diaphragm one wave-length in diameter, and give the intensities in the *H* and *E* planes, respectively, along lines parallel to the plane of the iris, at various distances *f* from the iris as shown.

Figure 5 gives a similar set of graphs of the diffraction pattern of an aperture two wave-lengths in diameter. Curves *a* through *k*, and *a′* through *k′*, give the intensities in the *H* and *E* planes, respectively, taken along lines parallel to a diameter and at distances *f* from the iris as indicated on each graph.

Figure 6 similarly shows the diffraction pattern of an aperture three wave-lengths in diameter. Following down the column of graphs the peaks of intensity could be seen receding and rising. To make it simpler to visualize the intensities in the *H* plane, the three-dimensional graph, of Fig. 7 was plotted. The broken lines are lines of constant intensity over the surface. The dis-

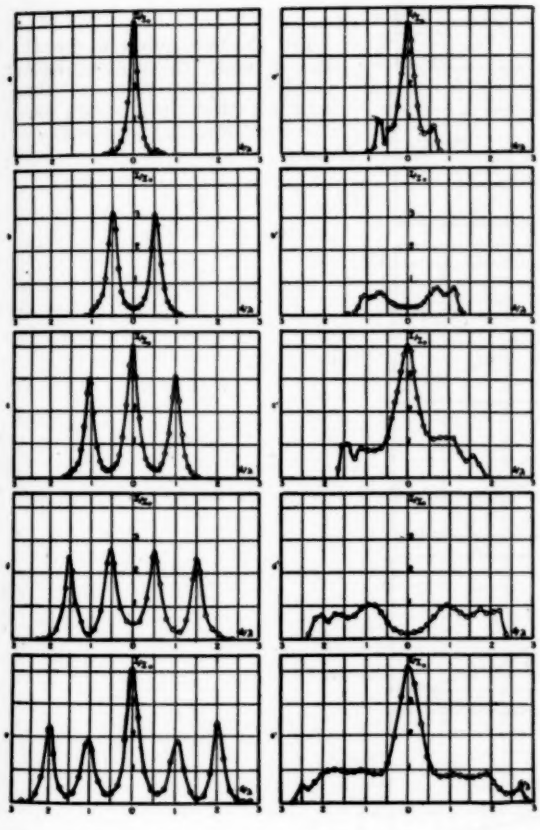

FIG. 3. Intensities along the diameters of the aperture in the *H* and *E* planes for diameter of from one to five wave-lengths.

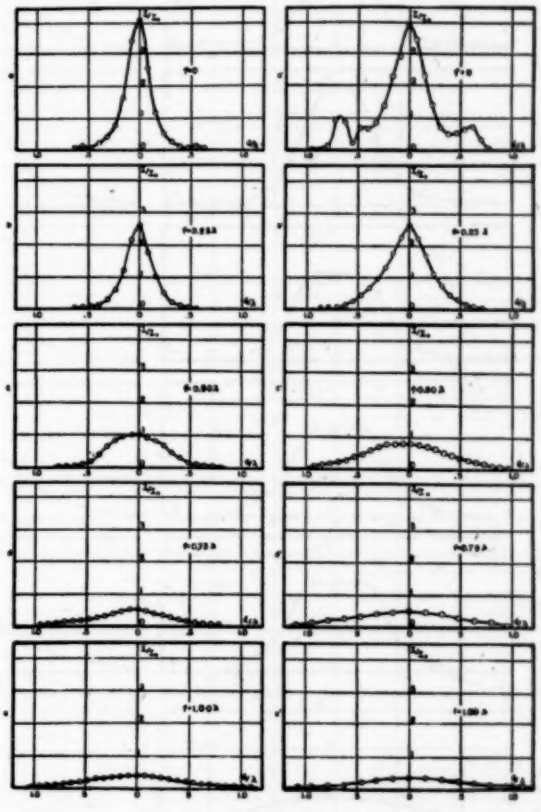

FIG. 4. Intensities in the *H* and *E* planes taken along lines parallel to the plane of the aperture when the aperture was one wave-length in diameter.

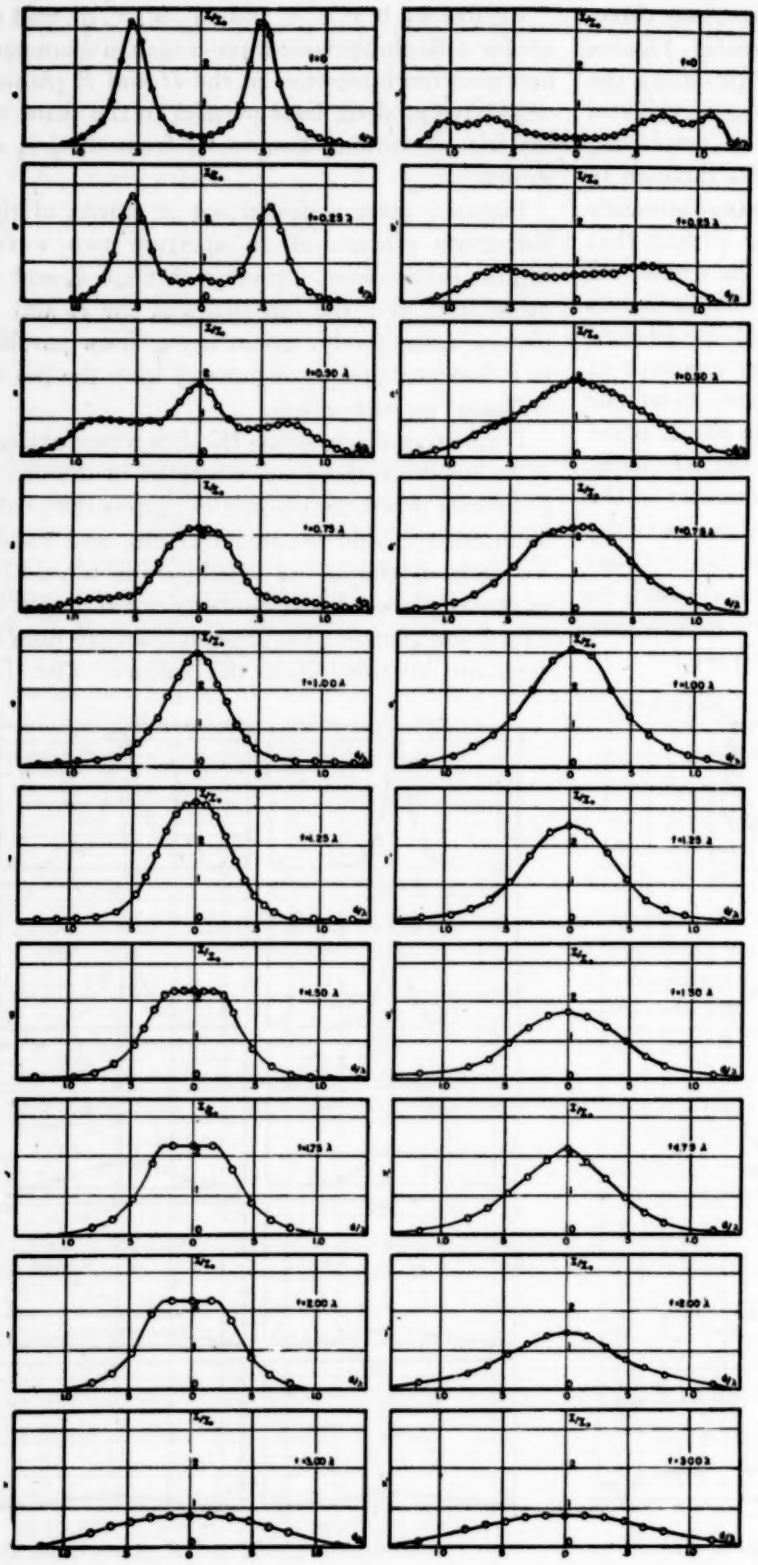

FIG. 5. Intensities in the *H* and *E* planes taken along lines parallel to the plane of the aperture when the aperture was two wave-lengths in diameter.

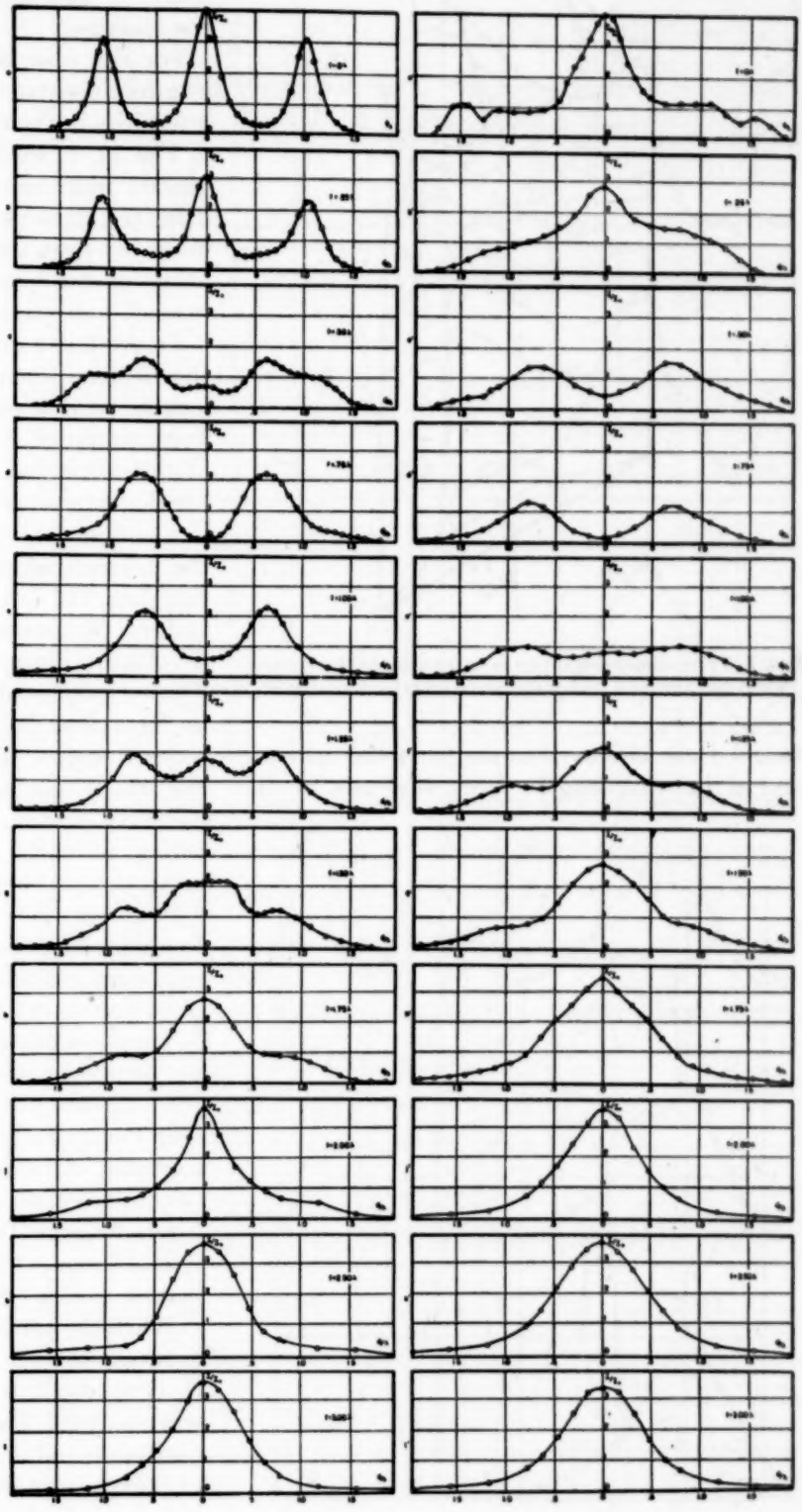

FIG. 6. Intensities in the *H* and *E* planes taken along lines parallel to the plane of the aperture when the aperture was three wave-lengths in diameter.

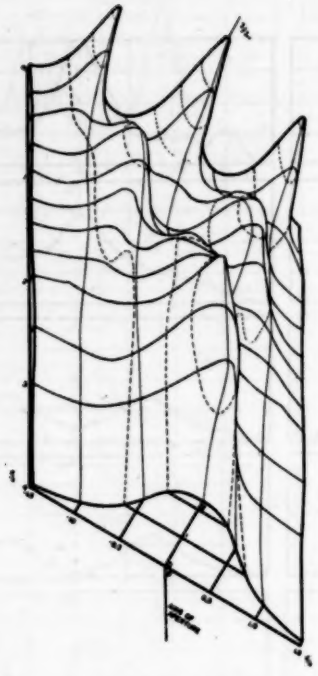

FIG. 7. Three-dimensional plot of intensities in the H plane when the aperture was three wave-lengths in diameter.

tances f are in wave-lengths from the aperture and d in wave-lengths from the axis of the aperture. This plot was shown for the width of the aperture.

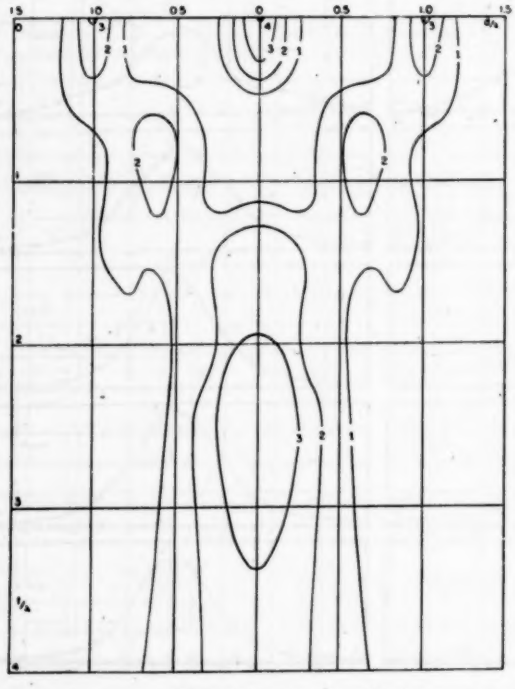

FIG. 8. Contour of intensities in the H plane when the aperture was three wave-lengths in diameter.

For the case of a diaphragm of four wave-lengths diameter, the only data taken were of intensities in the plane of the iris and are shown in Fig. 3d. It would be seen that as the iris was opened from one up to four wave-lengths in diameter, an array of peaks in intensity would move out from the plane of an iris being like an array of ten pins when the diameter of iris reached four wave-lengths.

Figure 8 is a contour map of the intensity in the H plane when the aperture was three wave-lengths in diameter. Figures 7 and 8 and the first column of Fig. 6 gave a complete picture of the diffraction pattern in the H plane when the diameter of iris was three wave-lengths.

A simple case to treat theoretically is that of the intensity along the axis of the aperture. In this case, the intensity is independent of polarization. Moreover the experimental results can be checked more readily with existing theory. Twelve graphs of the intensity at fixed points on the axis at distances f from the aperture were plotted against the diameter of the aperture of the iris. These are shown in Fig. 9, with the distances f indicated in the upper right-hand corner of each graph. The positions of the maxima and minima checked approximately with the predictions on the basis of elementary Fresnel's zone theory. For each distance f the minimum intensities corresponded to apertures of an even number of Fresnel's zones.

These results, as have been previously noted, are surprising when it is noted that in Fresnel's zone theory it is assumed that the intensity over the aperture is constant. From Fig. 3, it is seen that the sharpest diffraction pattern of the circular aperture is in the plane of the aperture. Fresnel's zone theory thus becomes merely a rule of thumb that gives results in close approximation to experiment.

When the zone theory is applied to the ridiculous case of $f=0$, the zone boundaries are circles of radii equal to an integral number of half-wave-lengths. The diameters of the aperture for maximum and minimum intensities at the center of the aperture were correctly predicted. Fresnel did not intend that his theory, which assumed constant intensity in the aperture, would be

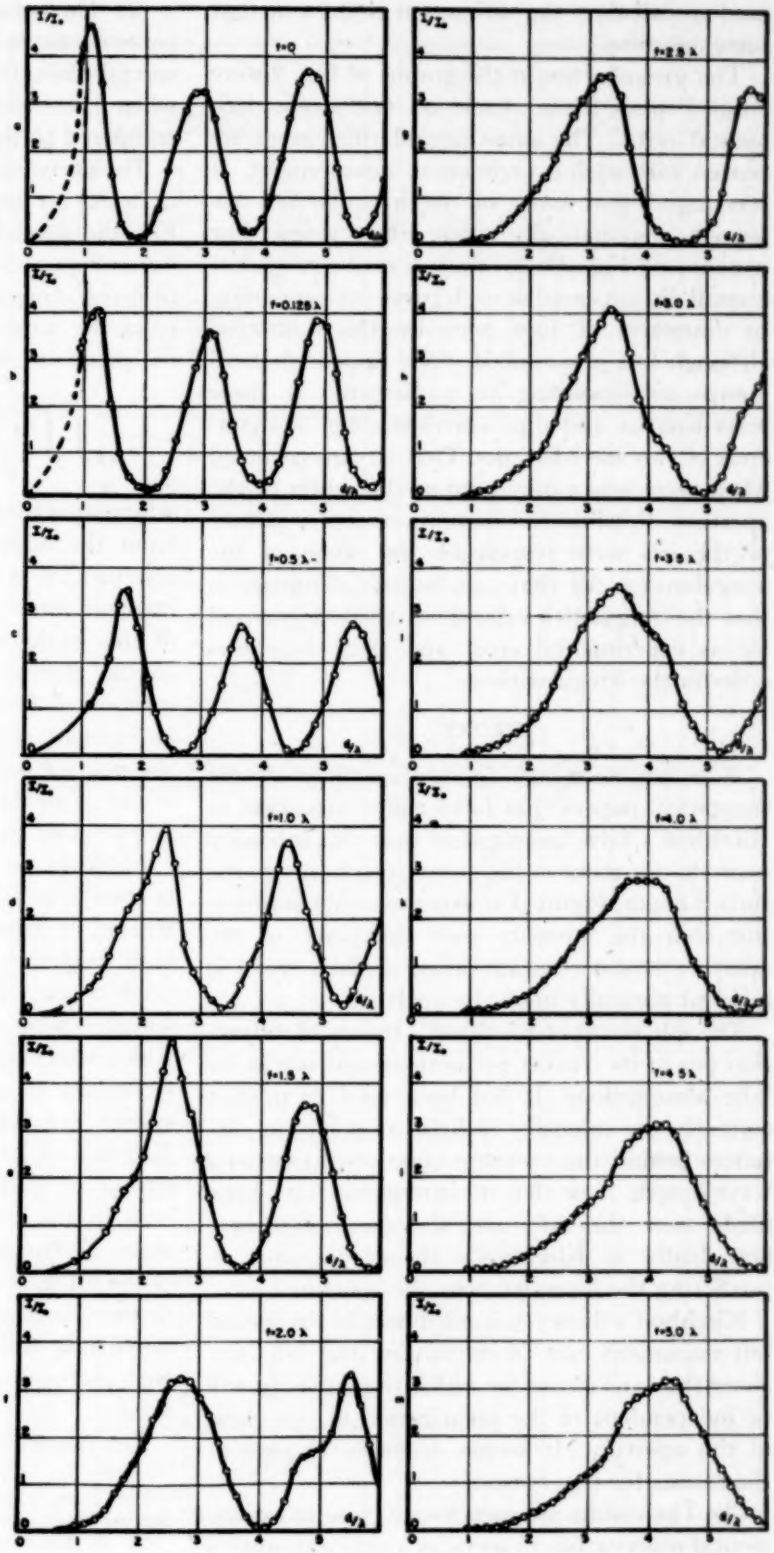

FIG. 9. Intensities at fixed points on the axis of the aperture at distances f from the aperture plotted against diameter of the aperture.

used to calculate the diffraction pattern in that same aperture.

The irregularities in the graphs of Fig. 9 were studied to see if they could be results of experimental error. The same irregularities were repeated with each experimental measurement. It was noted that some of the irregularities appeared systematically along the curves. For instance, in Figs. 9h to 9m, it was observed that a small dip appeared in each curve corresponding to diameters of four wave-lengths. Likewise, although less pronounced, there appeared small humps corresponding to a diameter of three wave-lengths and dips corresponding to diameters of two wave-lengths. That is, dips occurred when there was a minimum at the center of the aperture. Possibly the currents over the surface of the iris were responsible for some of the irregularities. All that can be said definitely is that the irregularities could not all be accounted for as experimental error and that there was order in the irregularities.

THEORY

It is not necessary to mention here all the theoretical papers that have called attention to Kirchhoff's false assumption that the intensity over the aperture is the intensity of the undisturbed beam. Figure 3 is experimental confirmation that the intensity over the plane of the aperture is not constant when a plane wave is incident normally upon the aperture.

The sole virtue of Kirchhoff's theory of diffraction lies in its correct predictions and not in its false assumptions. It has been used to predict correctly the intensity of light at points at distances behind the aperture large compared to a wave-length. Now that measurements have been made near the aperture, the question arises, how badly is Kirchhoff's theory in error in predicting the intensity near the aperture?

Kirchhoff's theory is applied here to the special but important case of calculating the intensity along the axis, a case for which the intensity will be independent of the polarization in the plane of the aperture. It seems desirable to present the results for two reasons:

(1) The results are sufficiently close to experimental observation to serve as a stop gap until a rigid theory is evolved.

(2) The solution of Kirchhoff's theory for the general case is found to be simpler than for the special case in which approximation is made when the distance from the aperture is large compared to the wave-length.

The derivation of Kirchhoff's theorem is found in books on optics[4] and electromagnetic theory.[5] For the special case of a plane wave incident normally upon an aperture, the problem is that of integrating the effects of Huygens' wavelets, from the unperturbed wave in the aperture, at the point at which the amplitude is to be found.

$$u_P=\frac{u_0}{4\pi}\int\int\left\{\frac{2\pi}{\lambda}\frac{e^{-i\phi}}{\rho}(1+\cos\theta)-i\frac{e^{-i\phi}}{\rho^2}\cos\theta\right\}d\sigma, \quad (1)$$

where u_P is the amplitude at the point P resulting from the added effects from all points in the aperture, u_0 is the amplitude of the undisturbed incident wave at the aperture, $d\sigma$ is an element of area in the aperture, ρ is the distance from P to the element $d\sigma$, ϕ is the phase lag of the component from $d\sigma$ behind the component from an element at the base of a perpendicular from the point P to the plane of the aperture, and θ is the angle between the incident beam and a line from $d\sigma$ to the point P.

In books on physical optics, the second term is always omitted since $\rho\gg\lambda$ in all of the cases treated in light. However, in the study of ultra-high frequency radio waves, useful applications occur when ρ is of the same order as the wave-length. Note the direction factor $(1+\cos\theta)$, which was discovered by Kirchhoff. A Huygens' secondary wavelet is not uniform over the whole sphere but has a maximum amplitude in the direction of propagation of the wave that generated it, half maximum at right angles and zero in the direction opposite to the primary wave. A Huygens' wavelet for the second term of the integral has zero amplitude at right angles to the direction of the primary wave and equal amplitude and opposite phase in the directions with and opposite to the direction of the primary wave.

Let the study be restricted to the determina-

[4] M. Born, *Optik* (Verlagsbuchhandlung Julius Springer, Berlin, 1933), pp. 147–151.

[5] J. A. Stratton, *Electromagnetic Theory* (McGraw-Hill Book Company, Inc., New York, 1941), pp. 424–428, 460–464.

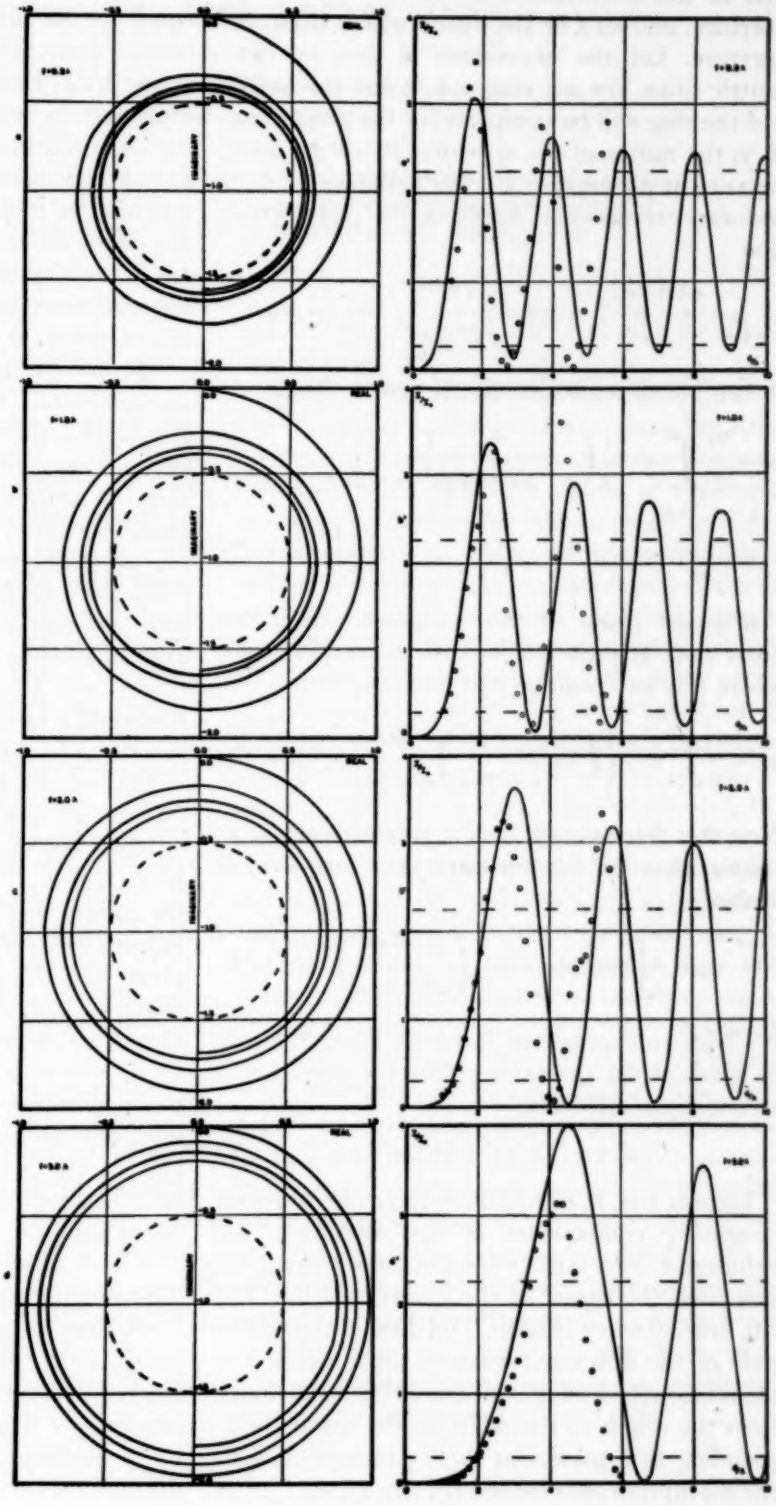

FIG. 10. (a, b, c, d) Spirals, calculated from Kirchhoff's theory, for the determination of amplitudes at fixed points on the axis as the diameter is increased. (a′, b′, c′, d′) Intensities, calculated from Kirchhoff's theory, at fixed points on the axis plotted against diameter and compared with experimental data.

tion of the disturbances along the axis of the aperture, and let f be the distance of P from the aperture. Let the increments of area be concentric rings. For any ring, ρ, ϕ, θ, and the radius r of the ring will be constants for the given ring. R_a is the radius of the aperture. It will be most convenient to express all the variables ρ, θ, r, and $d\sigma$ in terms of ϕ. Applying the transformation

$$\rho=\frac{\phi\lambda+2\pi f}{2\pi},\quad \cos\theta=\frac{2\pi f}{\phi\lambda+2\pi f},\quad d\sigma=\lambda\rho d\phi$$

to Eq. (1) after combining the cosine terms,

$$u_P=\frac{u_0}{2}\int_0^\beta e^{-i\phi}\left\{\left(\frac{1}{\lambda}-\frac{i}{\phi\lambda+2\pi f}\right)\frac{2\pi f}{\phi\lambda+2\pi f}+\frac{1}{\lambda}\right\}\lambda d\phi. \quad (2)$$

β is the phase of the component from the outer ring. Express f in wave-lengths. Let $f=n\lambda$ where n is any positive real number. Thus

$$u_P=\frac{u_0}{2}\int_0^\beta e^{-i\phi}\left\{\left(1-\frac{i}{\phi+2\pi n}\right)\frac{2\pi n}{\phi+2\pi n}+1\right\}d\phi. \quad (3)$$

Note that this solution for the general equation is simpler than the solution when the second term is omitted.

$$u_P=u_0\left[(\sin\beta+i\cos\beta)\left(\frac{\beta+4\pi n}{2\beta+4\pi n}\right)-i\right]. \quad (4)$$

We wish to express the intensity along the axis in terms of the diameter of the aperture. Let d be the diameter. Then

$$d/\lambda=[(\beta/\pi)^2+4n\beta/\pi]^{\frac{1}{2}}. \quad (5)$$

Figures 10a, b, c, and d are plots of real *versus* imaginary components of the amplitude for values of β from 0 to 7π for distances f along the axis from the center of the aperture of 0.5, 1.0, 2.0, and 5.0 wave-lengths. The ratio of the amplitude of the diffracted wave to the amplitude of the undisturbed wave is measured by the distance from the origin to the point on the spiral corresponding to a particular β. The broken circle is the asymptote approached by the spiral.

The square of the ratio of the amplitudes is equal to the ratio of the intensity of the diffracted wave to the intensity of the undisturbed wave I/I_0. From Eq. (5), d/λ the diameter expressed in wave-lengths was computed for values of β from 0.0 to 9.0π. Figures 10a′, b′, c′, and d′ are plots of I/I_0 against diameter of aperture for four distances f along the axis from the center of the aperture of 0.5, 1.0, 2.0, and 5.0 wave-lengths. The envelope of the curve approaches asymptotes indicated by broken lines at I/I_0 equal to 0.25 and 2.25.

The points indicated by circles are of experimental data. As a theoretical development, Kirchhoff's theory does not take into account currents over the surface surrounding the aperture. It assumes constant intensity, constant phase, and constant direction of polarization over the aperture, none of which is experimentally true. Since Kirchhoff's theory contains so many false assumptions, the deviations in Fig. 10 of experimental data from the results of Kirchhoff's theory are to be expected. These results of Kirchhoff's simple theory are still sufficiently precise to be useful.

Any correct theoretical prediction of the diffraction pattern of the aperture would be made on the basis of the known distribution of fields in the plane of the aperture and currents over the surface surrounding the aperture. The distributions along the line of intersection of the H plane and the plane of the aperture shown in Figs. 3a, b, c, d, e appeared simple to analyze. However, because the resistance between the leaves of the iris was variable, the distribution in the E plane was not symmetrical and, therefore, was difficult to analyze. Before the distribution in the E plane can be analyzed, data will have to be taken for a set of apertures in solid metal sheets.

It is a pleasure to acknowledge the support throughout this study of W. C. White and E. D. McArthur of the General Electric Research Laboratory, to thank Professor J. R. Collins of Cornell University for reading the paper and Dr. Emory Cook of Johns Hopkins University for a written status report on the theory of diffraction.

PHYSICAL REVIEW VOLUME 71, NUMBER 11 JUNE 1, 1947

Equivalence of the Riesz Method and the λ-Limiting Process for the Classical Electromagnetic Field of a Point Source

S. T. MA
The Institute for Advanced Study, Princeton, New Jersey
(Received February 10, 1947)

It is shown generally that the Riesz method of analytic continuation and the λ-limiting process give, in general, the same results for both the classical electromagnetic potential of a point source and all its derivatives with respect to the coordinates of the field point.

I. INTRODUCTION

IT is well-known that the λ-limiting process developed by Wentzel, Dirac, and Pauli[1] leads to divergence-free results for classical wave fields of a point source. In the case of the electromagnetic field, the λ-limiting process gives, for a field point not on the world line of the particle, the Lienard-Wiechert retarded field just as in the ordinary theory. On the other hand, for a point on the world line, where the ordinary mathematical treatment gives divergent results, the λ-limiting process gives one-half of the radiation field, i.e., half the difference of the retarded and advanced fields, which is finite on the world line. Dirac[2] studied in detail the field strengths of the radiation field of a point charge. Generalized investigations for the fields of point sources possessing higher multipole moments were later made by Bhabha and Harish-Chandra for both the electromagnetic and meson fields.[3]

An alternative mathematical treatment of the problem was introduced by M. Riesz.[4] The application of Riesz' method has recently been developed by Gustafson[5] for the quantum theory and by Fremberg[6] for the classical theory. Fremberg has shown that, for the wave fields of a point charge, the Riesz method gives the same results as the λ-limiting process for the following field quantities: (i) the retarded potentials and field strengths for a point not on the world line; (ii) half the radiation field strengths for a point on the world line.

Unlike the retarded field quantities given by the formula of Lienard and Wiechert, the values on the world line of the derivatives of the radiation field potentials, with respect to the coordinates of the field point, cannot be derived from the corresponding values of the potentials by simple differentiation. The agreement of the two methods found by Fremberg therefore raises the question of the equivalence of the two methods in general. It is the main purpose of the present investigation to give a general proof of the equivalence of the two methods for the electromagnetic field generated by a point source. The case of the meson field can be studied in a similar manner.

It follows from the general equivalence of the two methods that the Riesz method provides us with an additional method of calculating the radiation fields. This is of practical importance for the sake of computation, as the Riesz method is usually simpler and more straightforward for evaluating the higher derivatives of the radiation fields, which appear in the equation of motion of a particle having a multipole moment.

Before giving the proof, we shall first derive in Section II a new expression for the Riesz field, which will help bring out the connection between the two methods. Explicit results for the potential and its first two derivatives on the world line will be given in Section III, which will be seen to agree with those of the λ-process. A general proof of the equivalence of the two methods will be given in Section IV.

II. THE RIESZ FIELD

We begin by considering the electromagnetic field generated by a source distribution **J** which

[1] G. Wentzel, Zeits. f. Physik **86**, 479 and 635 (1933); **87**, 726 (1934); P. A. M. Dirac, Ann. de l'Inst. Poincaré **9**, 13 (1939); W. Pauli, Phys. Rev. **64**, 332 (1943).
[2] P. A. M. Dirac, Proc. Roy. Soc. **167**, 148 (1938).
[3] H. J. Bhabha and Harish-Chandra, Proc. Roy. Soc. **A185**, 250 (1946); Harish-Chandra, Proc. Roy. Soc. **A185**, 269 (1946).
[4] M. Riesz, Conference de la Réunion internat. des math. tenue à Paris en Juillet 1937 (Paris, 1939).
[5] T. Gustafson, Kgl. Fys. Sallsk. i Lund Forhandl. **15**, No. 28 (1945); **16**, No. 2 (1946).
[6] N. E. Fremberg, Meddelanden fran Lunds Univ. Mat. Seminarium **7** (1946); Proc. Roy. Soc. **188A**, 18 (1946).

may be a scalar, vector, or tensor of higher rank, and the field potential $\mathbf{A}$ determined by the wave equation

$$\Box\mathbf{A}=4\pi\mathbf{J}. \tag{1}$$

The Riesz potential is defined as

$$\mathbf{A}^{(\alpha)}(P)=\frac{1}{H_4(\alpha)}\int_{D_S{}^P}\mathbf{A}(Q)R^{\alpha-4}dQ, \tag{2}$$

where $H_4(\alpha)$ denotes the factor

$$H_4(\alpha)=\pi 2^{\alpha-1}\Gamma\left(\frac{\alpha}{2}\right)\Gamma\left(\frac{\alpha}{2}-1\right), \tag{3}$$

$D_S{}^P$ is the domain of integration bounded by the retrograde cone with its vertex at the field point P and a space-like surface S, and R is the hyperbolic distance between the points P and Q. In the case of a point source moving along a world line $\mathbf{Z}(\tau)$, the source density is of the form

$$\mathbf{J}(\mathbf{X})=\int\mathbf{S}(\tau)\delta(x_0-z_0)\delta(x_1-z_1)\times\delta(x_2-z_2)\delta(x_3-z_3)d\tau, \tag{4}$$

where τ is the proper time of the particle. In order to simplify our considerations we assume that there is a single source which begins to radiate at an instant τ_A and we take $\mathbf{S}$ to be a surface which cuts the world line at the point $\mathbf{Z}(\tau_A)$. It will also be assumed that there is no incoming field present. Under such conditions, the Riesz potential becomes

$$\mathbf{A}^{(\alpha)}(\mathbf{X})=\frac{4\pi}{H_4(\alpha+2)}\int_{\tau_A}^{\tau_r}\mathbf{S}(\tau)R^{\alpha-2}d\tau, \tag{5}$$

where τ_r is the retarded proper time and R is the length of the vector $\mathbf{X}-\mathbf{Z}$. We denote the time and space components of $\mathbf{R}$ by r_0 and $\mathbf{r}$ and denote the length of $\mathbf{r}$ by r, so that

$$R=(r_0{}^2-r^2)^{\frac{1}{2}}. \tag{6}$$

Equation (5) holds for the region $x_0-z_0(\tau_A)>0$, $(\mathbf{X}-\mathbf{Z}(\tau_A))^2>0$, i.e., the region where the Lienard-Wiechert potential does not vanish identically. The derivatives of $\mathbf{A}^{(\alpha)}(\mathbf{X})$ with respect to the coordinates of the field point $\mathbf{X}$ are of the form

$$\mathbf{F}^{(\alpha)\mu\nu\cdots}(\mathbf{X})=\frac{\partial}{\partial x_\mu}\frac{\partial}{\partial x_\nu}\cdots\mathbf{A}^{(\alpha)}(\mathbf{X}). \tag{7}$$

The field quantities are to be calculated first for a value of α large enough for the integrals to be convergent, and the final results are obtained by analytic continuation to $\alpha=0$.

It will be convenient to base our later investigation on a somewhat different expression for the Riesz potential, namely,

$$\mathbf{A}^{(\alpha)}(\mathbf{X})=\alpha\int_0^{R_A}\mathbf{A}^{\mathrm{ret}}(\mathbf{X},R)R^{\alpha-1}dR. \tag{8}$$

Here R plays the role of a variable of integration, R_A is the length of the vector $\mathbf{X}-\mathbf{Z}(\tau_A)$, and $\mathbf{A}^{\mathrm{ret}}(\mathbf{X},\mathbf{R})$ denotes the value of the potential

$$\mathbf{A}^{\mathrm{ret}}(\mathbf{X},\mathbf{R})=\mathbf{S}/(\mathbf{V},\mathbf{R}), \tag{9}$$

at the retarded time when the vector $\mathbf{X}-\mathbf{Z}(\tau)$ has the magnitude $\mathbf{R}$, and $\mathbf{V}=(v_0,\mathbf{v})$ denotes $d\mathbf{Z}/d\tau$. The retarded potential given by Eq. (9) differs from the ordinary Lienard-Wiechert potential in that the variable R is in general not zero.

To derive Eq. (8) from Eq. (6), we note that (6) may be written in the form

$$\mathbf{A}^{(\alpha)}(\mathbf{X})=\frac{4\pi}{H_4(\alpha+2)}\int_{-\infty}^{\infty}\mathbf{S}(\tau)d\tau\times\int_0^{\rho_A}\frac{\delta[r_0-(r^2+\rho^2)^{\frac{1}{2}}]}{(r^2+\rho^2)^{\frac{1}{2}}}\rho^{\alpha-1}d\rho, \tag{10}$$

where ρ_A is the length of $\mathbf{X}-\mathbf{Z}(\tau_A)$. This may be verified with the help of the general formula which states that

$$\int_0^{\rho_A}f(\rho)\delta[g(\rho)]d\rho=\int_0^{\rho_A}\frac{f(\rho)}{(dg(\rho)/d\rho)}\delta[g(\rho)]dg(\rho)=\frac{f(\rho_1)}{(dg/d\rho)_{\rho=\rho_1}}\text{ or }0 \tag{11}$$

according as $g(\rho)$ has a zero ρ_1 between 0 and ρ_A or not, f and g being two arbitrary functions with g subject to the condition $dg/d\rho>0$. We carry out the integration with respect to τ in (10) by applying (11) with ρ replaced by τ and

using the relation

$$\frac{d}{d\tau}[(r^2+\rho^2)^{\frac{1}{2}}-r_0]=\frac{v_0(r^2+\rho^2)^{\frac{1}{2}}-(\mathbf{v},\mathbf{r})}{(r^2+\rho^2)^{\frac{1}{2}}}$$

$$=\frac{(\mathbf{V},\mathbf{R})_{R=\rho}}{(r^2+\rho^2)^{\frac{1}{2}}}. \tag{12}$$

The result is

$$\mathbf{A}^{(\alpha)}(\mathbf{X})=\alpha\int_0^{\rho_A}\left[\frac{\mathbf{S}}{(\mathbf{V},\mathbf{R})}\right]_{R=\rho}\rho^{\alpha-1}d\rho,$$

which is just Eq. (8) with $\mathbf{A}^{\text{ret}}(\mathbf{X}, R)$ given by Eq. (9). The factor

$$\frac{4\pi}{H_4(\alpha+2)}=\frac{4\pi\alpha}{\pi 2^{\alpha+2}\left[\Gamma\left(\frac{\alpha}{2}+1\right)\right]^2} \tag{13}$$

has been replaced for brevity by α, as the ratio of these two factors becomes unity when $\alpha=0$ and so its omission does not make any difference in the final result.

It follows from Eq. (8) that the derivatives of $\mathbf{A}^{(\alpha)}(\mathbf{X})$ in Eq. (7) are given by

$$\mathbf{F}^{(\alpha)}(\mathbf{X})=\alpha\int_0^{R_A}\mathbf{F}^{\text{ret}}(\mathbf{X}, R)R^{\alpha-1}dR, \tag{14}$$

where $\mathbf{F}^{\text{ret}}(\mathbf{X}, R)$ denotes the field quantity that can be derived from the formula of Lienard and Wiechert by differentiation with respect to the x_μ with R kept fixed. We have neglected in Eq. (15) terms arising from the variation of R_A with the x_μ. These terms are independent of the variable R and therefore vanish when α is put equal to zero.

The analytic continuation to $\alpha=0$ is governed by the following general theorem: For any function $f(x)$ which can be expanded into a Laurent series of the form

$$f(x)=\sum_{-m}^{\infty}a_n x^n \quad (m=0, 1, 2, \cdots), \tag{15}$$

we have

$$\alpha\int_0^X f(x)x^{\alpha-1}dx\to a_0 \tag{16}$$

when analytic continuation is performed to $\alpha=0$, irrespective of the magnitude of the upper limit X. The coefficient a_0 may be regarded as the finite part ("partie finie") of the function $f(x)$. It follows from this general theorem, and Eqs. (8) and (14), that *the Riesz method consists in replacing the Lienard-Wiechert potential and its derivatives by their finite parts when R is taken as the independent variable.*

It was pointed out by M. Riesz* that the use of the square of R as the independent variable brings the retarded potential to a very simple form. Writing

$$R^2=\mathfrak{R} \tag{17}$$

and

$$\mathbf{S}(\tau)=-\tfrac{1}{2}d\mathbf{T}/d\tau, \tag{18}$$

we have from Eq. (9)

$$\mathbf{A}^{\text{ret}}=d\mathbf{T}/d\mathfrak{R}. \tag{19}$$

III. EXPLICIT EVALUATION OF THE FIELD QUANTITIES ON THE WORLD LINE

Equation (9) may be written for brevity.

$$\mathbf{A}^{\text{ret}}=\mathbf{S}/\kappa, \tag{20}$$

where

$$\kappa=(\mathbf{V},\mathbf{R}). \tag{21}$$

The derivatives of $\mathbf{A}^{\text{ret}}$ can best be calculated by a method used by Dirac in his classical theory of radiating electrons. The first two derivatives of $\mathbf{A}^{\text{ret}}$ are

$$\frac{\partial}{\partial x_\mu}\mathbf{A}^{\text{ret}}=-\frac{1}{\kappa}\frac{d}{d\tau}\left(\frac{\mathbf{S}r^\mu}{\kappa}\right), \tag{22}$$

$$\frac{\partial^2}{\partial x_\mu\partial x_\nu}\mathbf{A}^{\text{ret}}=-\frac{1}{\kappa}\left\{g^{\mu\nu}\frac{d}{d\tau}\left(\frac{\mathbf{S}}{\kappa}\right)+\frac{d}{d\tau}\left[\frac{1}{\kappa}\frac{d}{d\tau}\frac{\mathbf{S}r^\mu r^\nu}{\kappa}\right]\right\}. \tag{23}$$

* I am indebted to Professor Riesz for this remark.

For the explicit evaluation of the radiation field quantities at a point $\mathbf{X}$ on the world line, it is convenient to take as the independent variable $\sigma=\tau_0-\tau$, τ_0 being the time when $\mathbf{Z}(\tau)=\mathbf{X}$. Since

$$RdR=\kappa d\sigma, \tag{24}$$

we have

$$\mathbf{F}^{(\alpha)}(\mathbf{X})=\alpha\int_0^{\sigma_A}\kappa\mathbf{F}R^{\alpha-2}d\sigma, \tag{25}$$

with $\mathbf{F}$ given by Eqs. (20), (22), and (23) for the potential and its first two derivatives, σ_A being the value of σ corresponding to τ_A. Using the expansions

$$\mathbf{S}=\mathbf{S}_0-\left(\frac{d\mathbf{S}}{d\tau}\right)_0\sigma+\frac{1}{2}\left(\frac{d^2\mathbf{S}}{d\tau^2}\right)_0\sigma^2-\frac{1}{6}\left(\frac{d^3\mathbf{S}}{d\tau^3}\right)_0\sigma^3+\cdots, \tag{26}$$

$$\mathbf{R}=\mathbf{X}-\mathbf{Z}=\mathbf{V}_0\sigma-\frac{1}{2}\left(\frac{d\mathbf{V}}{d\tau}\right)_0\sigma^2+\frac{1}{6}\left(\frac{d^2\mathbf{V}}{d\tau^2}\right)_0\sigma^3-\frac{1}{24}\left(\frac{d^3\mathbf{V}}{d\tau^3}\right)_0\sigma^4+\cdots, \tag{27}$$

$$R=\sigma\left\{1-\frac{1}{24}\left(\frac{d\mathbf{V}}{d\tau}\right)_0^2\sigma^2+\frac{1}{24}\left(\frac{d\mathbf{V}}{d\tau},\frac{d^2\mathbf{V}}{d\tau^2}\right)_0\sigma^3+\cdots\right\}, \tag{28}$$

$$R^{\alpha-2}=\sigma^{\alpha-2}\left\{1-\frac{\alpha-2}{24}\left(\frac{d\mathbf{V}}{d\tau}\right)_0^2\sigma^2+\frac{\alpha-2}{24}\left(\frac{d\mathbf{V}}{d\tau},\frac{d^2\mathbf{V}}{d\tau^2}\right)_0\sigma^3+\cdots\right\}, \tag{29}$$

where the suffix 0 denotes the value at time τ_0, we obtain from Eq. (25) and the general relation of Eq. (16)

$$\mathbf{A}(\mathbf{X})=-(d\mathbf{S}/d\tau)_0, \tag{30}$$

$$\frac{\partial\mathbf{A}(\mathbf{X})}{\partial x^\mu}=-\left\{\tfrac{1}{3}\mathbf{S}v_\mu\left(\frac{d\mathbf{V}}{d\tau}\right)^2+\tfrac{1}{3}\mathbf{S}\left(\frac{d^2v_\mu}{d\tau^2}\right)+\frac{dv_\mu}{d\tau}\frac{d\mathbf{S}}{d\tau}+v_\mu\frac{d^2\mathbf{S}}{d\tau^2}\right\}_0; \tag{31}$$

and a rather lengthy expression for $\partial^2\mathbf{A}/\partial x_\mu\partial x_\nu$, which will not be written down here. These results are just half the corresponding quantities of the radiation field given by the λ-limiting process, namely,

$$\mathbf{A}(\mathbf{X})=\tfrac{1}{2}\{(\mathbf{S}/\kappa)_{\text{ret}}+(\mathbf{S}/\kappa)_{\text{adv}}\}, \tag{32}$$

$$\mathbf{F}^{\mu\nu\cdots}(\mathbf{X})=\frac{1}{2}\frac{\partial}{\partial x_\mu}\frac{\partial}{\partial x_\nu}\cdots\left\{\left(\frac{\mathbf{S}}{\kappa}\right)_{\text{ret}}+\left(\frac{\mathbf{S}}{\kappa}\right)_{\text{adv}}\right\}. \tag{33}$$

The calculation here is simpler than the previous calculation of the radiation field because the Riesz field has finite values on the world line from the beginning, so that we do not have to consider its values in the vicinity of the world line.

IV. GENERAL PROOF OF THE EQUIVALENCE OF THE TWO METHODS

We give now a general proof that the two methods give the same results for the classical electromagnetic field. It is obvious that the two methods are equivalent for a point not on the world line, since at such a point the retarded field quantities given by the formula of Lienard and Wiechert are finite, and therefore the finite parts given by the Riesz method are just the retarded field quantities, in agreement with the λ-limiting process.

This is no longer the case for a point on the world line where the Lienard-Wiechert potential becomes infinite. To show the equivalence of the two methods in such a case we use the expansion method introduced by Dirac and developed in detail by Bhabha and Harish-Chandra.

Let us consider a field point **X** near the world line at a distance ϵ from its "contemporary point" Z_c, i.e., the point at which $\kappa=0$. Using the suffix c to denote the value of a quantity at the contemporary point and writing $\tau-\tau_c=\Delta\tau$, we have, as shown by the above authors,

$$\mathbf{S}=\mathbf{S}_c+\left(\frac{d\mathbf{S}}{d\tau}\right)_c\Delta\tau+\frac{1}{2}\left(\frac{d^2\mathbf{S}}{d\tau^2}\right)_c(\Delta\tau)^2+\frac{1}{6}\left(\frac{d^3\mathbf{S}}{d\tau^3}\right)_c(\Delta\tau)^3+\cdots,$$

$$\kappa=-(1-\kappa_c')\Delta\tau+\tfrac{1}{2}\kappa_c''(\Delta\tau)^2+\frac{1}{6}\left(\left(\frac{d\mathbf{V}}{d\tau}\right)_c^2+\kappa_c'''\right)(\Delta\tau)^3+\cdots, \tag{34}$$

$$R^2=-\epsilon^2+(1-\kappa_c')(\Delta\tau)^2-\tfrac{1}{3}\kappa_c''(\Delta\tau)^3-\frac{1}{12}\left(\left(\frac{d\mathbf{V}}{d\tau}\right)_c^2+\kappa_c'''\right)(\Delta\tau)^4+\cdots \tag{35}$$

where κ_c', κ_c'', etc. denote $(\mathbf{R}, d\mathbf{V}/d\tau)_c$, $(\mathbf{R}, d^2\mathbf{V}/d\tau^2)_c$, etc. From Eq. (35) with R set equal to zero,

$$\Delta\tau=\pm\epsilon(1+\tfrac{1}{2}\kappa_c'+\tfrac{3}{8}\kappa_c'^2)+\tfrac{1}{6}\kappa_c''\epsilon^2\pm(1/24)(d\mathbf{V}/d\tau)_c^2\epsilon^3+\cdots, \tag{36}$$

where the upper and lower signs are to be taken for the advanced and retarded times, respectively. From Eqs. (34) and (36),

$$\left(\frac{\mathbf{S}}{\kappa}\right)_{\text{ret}}=\frac{\mathbf{S}_c}{\epsilon}+\left(-\frac{d\mathbf{S}}{d\tau}+\frac{\mathbf{S}\kappa'}{2\epsilon}\right)_c+\left[\mathbf{S}\left(\frac{3\kappa'^2}{8\epsilon}-\frac{\kappa''}{3}-\left(\frac{d\mathbf{V}}{d\tau}\right)^2\frac{\epsilon}{24}\right)-\kappa'\frac{d\mathbf{S}}{d\tau}+\frac{\epsilon}{2}\frac{d^2\mathbf{S}}{d\tau^2}\right]_c+\cdots. \tag{37}$$

The value of the same quantity at the advanced time is obtained by writing $-\epsilon$ for ϵ in the right-hand side. It follows therefore,

$$\frac{1}{2}\left[\left(\frac{\mathbf{S}}{\kappa}\right)_{\text{ret}}+\left(\frac{\mathbf{S}}{\kappa}\right)_{\text{adv}}\right]=-\left(\frac{d\mathbf{S}}{d\tau}\right)_c-\left(\frac{1}{3}\mathbf{S}\kappa''+\frac{d\mathbf{S}}{d\tau}\kappa'\right)_c+\cdots. \tag{38}$$

With the help of the formulas

$$\frac{\partial\tau_c}{\partial x_\mu}=\left(\frac{v^\mu}{1-\kappa'}\right)_c, \tag{39}$$

$$\frac{\partial r_c^\mu}{\partial x_\nu}=g^{\mu\nu}-\left(\frac{v^\mu v^\nu}{1-\kappa'}\right)_c, \tag{40}$$

$$\frac{\partial\epsilon^2}{\partial x_\mu}=-2r_c^\mu, \tag{41}$$

Bhabha and Harish-Chandra reached the conclusion that the expression in Eq. (38) and all its derivatives are of the form

$$\sum_0^\infty \mathbf{a}_n\epsilon^{2n},$$

where the $\mathbf{a}_n$ are functions of τ_c and $\mathbf{R}_c$ which are finite on the world line. It follows therefore that the radiation potential and all its derivatives are finite when $\epsilon=0$, i.e., when the point **X** lies on the world line.

For the Riesz field R is not necessarily zero. For the purpose of evaluating the finite parts, however, it is sufficient to consider values of R in the neighborhood of zero. We can then take R to be a small number and solve again Eq. (35) for $\Delta\tau$, the result being

$$\Delta\tau=\pm(1+\tfrac{1}{2}\kappa'+\tfrac{3}{8}\kappa'^2)_c(\epsilon^2+R^2)^{\frac{1}{2}}+\tfrac{1}{6}\kappa_c''(\epsilon^2+R^2)\pm(1/24)(d\mathbf{V}/d\tau)_c^2(\epsilon^2+R^2)^{\frac{1}{2}}+\cdots \tag{42}$$

for the advanced and retarded times respectively. Equation (42) differs from Eq. (36) only in having $(\epsilon^2+R^2)^{\frac{1}{2}}$ instead of ϵ. Similarly,

$$\left(\frac{\mathbf{S}}{\kappa}\right)_{\text{ret}}=\frac{\mathbf{S}_c}{(\epsilon^2+R^2)^{\frac{1}{2}}}+\left[-\frac{d\mathbf{S}}{d\tau}+\frac{\mathbf{S}\kappa'}{2(\epsilon^2+R^2)^{\frac{1}{2}}}\right]_c$$

$$+\left[\mathbf{S}\left(\frac{3\kappa'^2}{8(\epsilon^2+R^2)^{\frac{1}{2}}}-\frac{\kappa''}{3}-\frac{(\epsilon^2+R^2)^{\frac{1}{2}}}{24}\left(\frac{d\mathbf{V}}{d\tau}\right)^2\right)-\kappa'\frac{d\mathbf{S}}{d\tau}+\frac{(\epsilon^2+R^2)^{\frac{1}{2}}}{2}\frac{d^2\mathbf{S}}{d\tau^2}\right]_c+\sum_0^\infty \mathbf{a}_n(\epsilon^2+R^2)^n+\sum_0^\infty \mathbf{b}_n(\epsilon^2+R^2)^{n+\frac{1}{2}}, \tag{43}$$

where the $\mathbf{b}_n$ denote functions similar to the $\mathbf{a}_n$. Using the formulas (39), (40), (41) and

$$\frac{\partial(\epsilon^2+R^2)}{\partial x_\mu}=\frac{\partial\epsilon^2}{\partial x_\mu}=-2r_c^\mu, \tag{44}$$

we see that both the expression in Eq. (43) and all its derivatives are of the form

$$\sum_0^\infty \mathbf{a}_n(\epsilon^2+R^2)^n+\sum_{-m}^\infty \mathbf{b}_n(\epsilon^2+R^2)^{n+\frac{1}{2}}, \tag{45}$$

when m is either zero or a positive integer.

The expansion in Eq. (45) contains the results of both methods for the field quantities on the world line. The λ-limiting process consists in putting $R=0$, taking the mean value

$$\frac{1}{2}\left\{\left(\sum_0^\infty \mathbf{a}_n\epsilon^{2n}+\sum_{-m}^\infty \mathbf{b}_n\epsilon^{2n+1}\right)+\left(\sum_0^\infty \mathbf{a}_n\epsilon^{2n}-\sum_{-m}^\infty b_n\epsilon^{2n+1}\right)\right\}=\sum_0^\infty \mathbf{a}_n\epsilon^{2n} \tag{46}$$

and finally putting $\epsilon=0$. On the other hand, the Riesz method consists in putting $\epsilon=0$ and replacing the expansion

$$\sum_0^\infty \mathbf{a}_nR^{2n}+\sum_{-m}^\infty \mathbf{b}_nR^{2n+1} \tag{47}$$

by its finite part. We see therefore quite generally that the two methods are equivalent.

I am indebted to Professor W. Pauli for a discussion which suggested the present investigation, and for his advice.

On Relativistic Wave Equations

HARISH-CHANDRA
Gonville and Caius College, Cambridge, England

(Received May 14, 1946)

The problem of the relativistic invariance of a first-order wave equation with matrix coefficients β_k is examined. It is found that it is intimately connected with the structure of the enveloping algebra of the β-matrices. In particular the center of this algebra can contain only elements of a very restricted type. This fact provides a powerful means for the investigation of the abstract β-algebra, as is illustrated in the general s-dimensional case of the Dirac and the Duffin-Kemmer matrices. Relativistic invariance imposes severe restrictions on the spurs of the β-matrices and their multiple products. Conversely, these restrictions insure relativistic invariance. The theory is applied to the case of particles of higher spin.

1. INTRODUCTION

THE wave equation for a particle of arbitrary spin can be written in the form

$$i\beta^k\partial_k\psi+\chi\psi=0, \quad (\partial_k=\partial/\partial x^k) \tag{1}$$

where χ is a constant determining the mass of the particle, and $\beta^k(k=0, 1, 2, 3)$ are square matrices operating on ψ which itself is a one-column matrix. The object of the present paper is to investigate the conditions which the β's must satisfy in order that Eq. (1) may be relativistically invariant. The conditions so obtained are also found to be largely sufficient. They insure the invariance of Eq. (1) under *proper* Lorentz transformations.

The method of this paper seems to provide a powerful means for the investigation of the algebra generated by the β's, and therefore for the determination of their irreducible representations. In order to find all the irreducible representations of a semi-simple algebra one has to obtain a linearly independent basis for its center.[1] It will be shown, however, that only quantities of a very restricted type can belong to the center, and therefore the task of obtaining a basis becomes much easier. Moreover, once such a basis has been obtained, one can immediately decide whether or not a particular representation is equivalent to its complex conjugate, transposed or Hermitian conjugate. The question of the invariance of the representation under reflection can also be answered at once. It will be shown also that considerable information concerning the spurs of the β's and their multiple products can be deduced from the relativistic invariance of Eq. (1). Conversely, if the spurs of the β's and their multiple products satisfy certain conditions, the invariance of Eq. (1) for the full Lorentz group is ensured.

As an illustration of these general results, the algebras of the Dirac and the Duffin-Kemmer matrices in the general case of s dimensions are discussed briefly. Although most of our results have already been obtained by Schrödinger[2] and Kemmer,[3] they serve to illustrate the power of the new method.

In the scheme of equations proposed by Dirac[4] one must impose certain other subsidiary conditions on ψ in addition to Eq. (1). However, as is well known, these subsidiary conditions in general become inconsistent with Eq. (1) when the electromagnetic interaction is introduced in the usual manner. A way out of this difficulty has been indicated by Fierz and Pauli,[5] but their method, though logically consistent, is rather cumbersome and consequently lacking in elegance. It therefore seems worth while to investigate alternative methods of approach to the problem. Bhabha[6] has recently proposed a formalism in which the subsidiary conditions are completely eliminated, so that the interaction can be introduced in the usual manner without difficulty. But the particle in general no longer

[1] The center of an algebra consists of the set of elements which commute with all elements of the algebra.

[2] E. Schrödinger, Proc. Roy. Irish Acad. [A] **48**, 135 (1943).
[3] N. Kemmer, Proc. Camb. Phil. Soc. **39**, 189 (1943).
[4] P. A. M. Dirac, Proc. Roy. Soc. [A] **155**, 447 (1936).
[5] M. Fierz and W. Pauli, Proc. Roy. Soc. [A] **173**, 211 (1939).
[6] H. J. Bhabha, Rev. Mod. Phys. **17**, 200 (1945).

obeys the second-order wave equation

$$\partial_k \partial^k \psi + \chi^2 \psi = 0 \tag{2}$$

in the force-free case. The physical result of this circumstance is that the particle described by Bhabha's equation would possess several different mass values. However, on grounds of simplicity, it seems desirable to try to discover a scheme in which the difficulty concerning the subsidiary conditions may be avoided without abandoning the second-order equation. Such an attempt is made in this paper.

As shown by Pauli,[7] the connection between spin and statistics is really based on the relativistic invariance of the wave Eq. (1). It therefore remains valid in the present case, as indeed in every other where the wave equation is relativistically invariant (e.g., for the equations proposed by Bhabha).[6,8]

2. ALGEBRAIC THEORY

For the relativistic invariance of Eq. (1) it is necessary that for every Lorentz transformation (t_k^l) there should exist a non-singular matrix T satisfying the condition

$$\beta_k' = t_k^l \beta^l = T \beta_k T^{-1}.$$

However, the problem considered in this paper may be stated somewhat more generally. *If β_k $(k=1, 2, \cdots, s)$ be an irreducible[9] set of s matrices, what are the conditions which the β's must satisfy in order that, for every transformation of the real orthogonal[10] group, there should exist a non-singular matrix T such that*

$$\beta_k' = t_k^l \beta_l = T \beta_k T^{-1}, \tag{3a}$$

$$t_k^m t_l^n g_{mn} = g_{kl}, \tag{3b}$$

$$g_{kl} = \begin{cases} 0 & k \neq l, \\ 1 & k = l; \end{cases} \tag{4}$$

and are these conditions sufficient to insure the invariance[11] of the β-representation under the orthogonal group?

Let $\mathfrak{A}(\beta)$ denote the enveloping algebra of the β-matrices,[12] i.e., the algebra consisting of all quantities of the type

$$c = c^k \beta_k + c^{kl} \beta_k \beta_l + c^{klm} \beta_k \beta_l \beta_m + \cdots, \tag{5}$$

where $c^{k\cdots}$ are numerical coefficients belonging to the field $\mathfrak{F}$ of complex numbers.[13] Since the β_k are irreducible, $\mathfrak{A}(\beta)$ is simple. Let u_p $(p=1, \cdots, h)$ be a linearly independent basis for $\mathfrak{A}$. As elements of $\mathfrak{A}(\beta)$, u_p, must be expressible in the form (5) and therefore one may write $u_p = u_p(\beta)$. On replacing each β_k by β_k' in $u_p(\beta)$ one obtains $u_p(\beta') = u_p(t\beta)$. Now $u_p(t\beta)$ is also an element of $\mathfrak{A}$ and therefore is expressible linearly in terms of the basis $u_p(\beta)$; that is,

$$u_p(t\beta) = \sum_q T_p^q u_q(\beta), \tag{6}$$

where[14] $T_p^q \varepsilon \mathfrak{F}$, and may be regarded as coefficients of a transformation T in the u-space. Thus every transformation t in the β-space induces a transformation T in the u-space. It is easy to verify that the correspondence $t \to T$ is a homomorphism with respect to addition and multiplication and therefore the set of transformations T is a representation of the orthogonal group $O(s)$. Now, it is well known that every representation of $O(s)$ is fully reducible and therefore the u-space can be decomposed into a direct sum of irreducible invariant sub-spaces. Let U denote the entire u-space and let the irreducible invariant sub-spaces be denoted by $V(1)$, $V(2)$, $\cdots$, $V(n)$ such that[15] $(V(m):\mathfrak{F}) = h_m$. Now all irreducible representations of $O(s)$ are known.[16] Any such *single valued* representation of the

[7] W. Pauli, Phys. Rev. **58**, 716 (1940).

[8] H. J. Bhabha, Proc. Ind. Acad. Sci. **21**, 291 (1945).

[9] In order to insure that Eq. (1) describes an "elementary" particle, which should be an entity of the simplest possible kind, we assume that the set of matrices β_k is irreducible.

[10] For the moment only the real orthogonal group is considered, but it will be shown in section 3 that the corresponding problem concerning other real groups (for example, the Lorentz group) associated with indefinite ground forms, is intimately connected with the present one, and has an almost identical solution.

[11] The property of the existence of a non-singular matrix satisfying Eq. (3) corresponding to every transformation t_k^l of a particular group G, can be briefly denoted as the property of the "invariance of the β-representation under G." The full (real) orthogonal group in s dimensions will be denoted by $O(s)$ while $O^+(s)$ will denote the corresponding *proper* orthogonal group.

[12] The whole set of matrices $\beta_k (k=1, 2, \cdots, s)$ is conveniently denoted by β. In the same way it is also convenient to abbreviate Eq. (3) to $\beta' = t\beta$, where t is now to be looked upon as a transformation operator acting on the set β and transforming it to β'.

[13] The summation convention for contracted indices is used throughout in this paper.

[14] This symbolism indicates that the coefficients T_p^q belong to the field $\mathfrak{F}$.

[15] If V is a vector space over $\mathfrak{F}$, then $(V:\mathfrak{F})$ denotes the dimension of V over $\mathfrak{F}$.

[16] H. Weyl, *The Classical Groups* (Princeton University Press, Princeton, New Jersey, 1939).

entire group $O(s)$ is equivalent to the set of transformations of a tensor of suitable rank and symmetry properties. It is therefore possible to find a linearly independent basis ${}^{(m)}v_p$ ($p=1, \cdots, h_m$) for $V(m)$ such that T transforms ${}^{(m)}v_p$ as components of a tensor of rank f_m with suitable symmetry properties. Thus, one can define a tensor ${}^{(m)}v_{k_1\cdots k_{f_m}}$ (of suitable symmetry) such that its h_m independent components are equal to the ${}^{(m)}v_p$'s and

$$v_{[k]}(t\beta)=t_{[k]}{}^{[l]}\cdot v_{[l]}(\beta). \tag{7}$$

Here the superscript (m) has been omitted for simplicity, and the symbol $[k]$ is used to denote the entire set of tensor indices $k_1, \cdots, k_f$. $t_{[k]}{}^{[l]}$ is merely a convenient abbreviation for $t_{k_1}{}^{l_1}t_{k_2}{}^{l_2}\cdots t_{k_f}{}^{l_f}$. At this point we need the following lemma.

Lemma 1. If $D_{[k]}(\beta)$ is a set of quantities belonging to $\mathfrak{A}(\beta)$ which transform as a tensor of rank f for all orthogonal transformations of the β-space so that

$$D_{[k]}(t\beta)=t_{[k]}{}^{[l]}\cdot D_{[l]}(\beta), \tag{8a}$$

then

$$D_{[k]}(\beta)=d_{[k]}(g)+d_{[k]l_1}(g)\cdot\beta^{l_1}+d_{[k]l_1l_2}(g)\cdot\beta^{l_1}\beta^{l_2}+\cdots, \tag{8b}$$

where $d_{[k]}\ldots(g)$ are tensors constructed out of g_{kl} alone i.e.

$$d_{[k]}\ldots(g)=\sum a(\alpha,\beta,\gamma,\delta,\cdots)g_{\alpha\beta}g_{\gamma\delta}\cdots \tag{9}$$

where $a(\alpha,\beta,\gamma,\delta\cdots)\epsilon\mathfrak{F}$ and the sum is to be taken over all permutations $\alpha,\beta,\gamma,\delta\cdots$ of the indices $k_1\cdots k_f, \cdots$ occurring on the left hand side of Eq. (9). The sum in Eq. (8b) is, of course, finite. When the total number of indices $k_1, \cdots k_f, \cdots$ is odd, a relation such as Eq. (9) is impossible and so in this case $d_{[k]}\ldots(g)=0$.

Proof: Put

$$D=\xi^{[k]}\cdot D_{[k]}(\beta),$$

where

$$\xi^{[k]}=\xi^{(1)k_1}\ldots\xi^{(f)k_f},$$

and $\xi^{(r)k}$ are indeterminates transforming contravariantly[17] to β_k. Clearly D is invariant under the transformations of $O(s)$. Since $O(s)$ is a topologically compact group, it is possible to perform the process of averaging over the entire group manifold.[16] Let $\langle D\rangle$ be the average of D over $O(s)$.

From Eq. (5), D must be of the form

$$D=\xi^{[k]}\cdot\{d_{[k]l_1}\beta^{l_1}+d_{[k]l_1l_2}\beta^{l_1}\beta^{l_2}+\cdots\}, \tag{10a}$$

where $d_{[k]}\ldots$ are suitable numerical coefficients. Therefore

$$\langle D\rangle=\xi^{[k]}\cdot\{\langle d\rangle_{[k]l_1}\beta^{l_1}+\langle d\rangle_{[k]l_1l_2}\beta^{l_1}\beta^{l_2}+\cdots\}, \tag{10b}$$

where $\langle d\rangle_{[k]}\ldots$ are the averaged coefficients. Consider the forms

$$D(\eta)=\xi^{[k]}\cdot\{d_{[k]l_1}\eta^{(1)l_1}+d_{[k]l_1l_2}\eta^{(1)l_1}\eta^{(2)l_2}+\cdots\}, \tag{11a}$$

and

$$\langle D\rangle(\eta)=\xi^{[k]}\cdot\{\langle d\rangle_{[k]l_1}\eta^{(1)l_1}+\langle d\rangle_{[k]l_1l_2}\eta^{(1)l_1}\eta^{(2)l_2}+\cdots\}, \tag{11b}$$

where $\eta^{(r)k}$ are also indeterminates transforming contravariantly to β_k. Notice that Eqs. (11a) and (11b) are derived from Eqs. (10a) and (10b) by replacing the first β in each multiple product of the β's by $\eta^{(1)k}$, the second β by $\eta^{(2)k}$, and so on. Also $\langle D\rangle(\eta)$ is the average of $D(\eta)$, and, therefore, clearly $\langle D\rangle(\eta)$ is an absolute invariant of the orthogonal group $O(s)$. Since $x^ky_k=x^ky^lg_{kl}$ is the only typical basic invariant of $O(s)$,[16] $\langle D\rangle(\eta)$ must be expressible as a rational integral function of the scalar products of the ξ's and η's. This, in turn, means that the coefficients $\langle d\rangle_{[k]}\ldots$ are of the form of Eq. (9). Now, because of the invariance of D, $D=\langle D\rangle$ and therefore Eq. (8b) holds.

Lemma 2. If Eq. (8a) is true at least for all transformations $t\epsilon O^+(s)$, then

$$D_{[k]}(\beta)=d_{[k]}(g,\epsilon)+d_{[k]l_1}(g,\epsilon)\cdot\beta^{l_1}+\cdots, \tag{12}$$

where $d_{[k]}\ldots(g,\epsilon)$ are tensors constructed out of g_{kl} and $\epsilon_{k_1\cdots k_s}$[18] only.

The proof is similar to that of Lemma 1 with the difference that $O^+(s)$ now has two typical basic invariants x^ky_k and $\epsilon_{k_1\cdots k_s}x^{(1)k_1}x^{(2)k_2}\cdots x^{(s)k_s}$. Since the product of two ϵ's can be expressed in terms of the g's, we need consider only terms linear in ϵ.

From Eq. (7) and Lemma 1 it follows directly that

$$v_{[k]}(\beta)=v_{[k]}(\beta,g) \tag{13}$$

i.e., as in Eq. (8b) $v_{[k]}(\beta,g)$ is a tensor composed of the β's and g's only. Now ${}^{(m)}v_{[k]}(\beta,g)$ taken to-

[17] Although the difference between co-variant and contra-variant vectors disappears for orthogonal transformations, it is convenient to recognize it formally.

[18] $\epsilon_{k_1\ldots k_s}$ is anti-symmetrical in every pair of indices, and $\epsilon_{12\ldots s}=1$.

gether for all values of m form a complete basis for $\mathfrak{A}(\beta)$. Hence the product of any two v's is again expressible as a linear sum of the v's so that

$$^{(m)}v_{[k]}(\beta)\cdot{}^{(m')}v_{[l]}(\beta) + \sum_{m''} {}^{(m,m')}_{\quad(m'')}\Gamma_{[k][l]}{}^{[j]}\cdot{}^{(m'')}v_{[j]}(\beta) \quad (14)$$

where ${}^{(m,m')}_{\quad(m'')}\Gamma_{[k][l]}{}^{[j]}$ are certain numerical coefficients. (Here the summation convention is used for the j's.) On imposing suitable symmetry properties on the Γ's corresponding to those of the v's in respect to permutations of the j's, they are uniquely determined by Eq. (14). Now from the similarity of the matrices β and $t\beta$ it follows that the correspondence $\beta\leftrightarrow t\beta$ is an automorphism of $\mathfrak{A}(\beta)$. Therefore

$$^{(m)}v_{[k]}(t\beta)\cdot{}^{(m')}v_{[l]}(t\beta) = \sum_{m''} {}^{(m,m')}_{\quad(m'')}\Gamma_{[k][l]}{}^{[j]}\cdot{}^{(m'')}v_{[j]}(t\beta). \quad (15)$$

So that from Eqs. (7), (14), and (15) one finds on omitting the m's that

$$t_{[k]}{}^{[i]}\cdot t_{[l]}{}^{[j]}\cdot\Gamma_{[i][j]}{}^{[a]} = t_{[b]}{}^{[a]}\cdot\Gamma_{[k][l]}{}^{[b]}.$$

Put

$$\Gamma_{[k][l][a]} = g_{[a][b]}\cdot\Gamma_{[k][l]}{}^{[b]}, \quad (16)$$

where

$$g_{[a][b]} = g_{a_1b_1}g_{a_2b_2}\cdots g_{a_fb_f}.$$

Now put

$$\Gamma = \xi^{[k]}\eta^{[l]}\zeta^{[a]}\cdot\Gamma_{[k][l][a]},$$

where $\zeta^{(r)k}$ is a third set of indeterminates transforming contravariantly to β_k. Then Γ is an absolute invariant of $O(s)$ and, therefore,

$$\Gamma_{[k][l][a]} = \Gamma_{[k][l][a]}(g) \quad (17)$$

where the right side denotes a tensor constructed out of the g's only. Equation (14) can therefore be written as

$$^{(m)}v_{[k]}(\beta,g)\cdot{}^{(m')}v_{[l]}(\beta,g) = \sum_{m''} {}^{(m,m')}_{\quad(m'')}\Gamma_{[k][l][j]}(g)\cdot{}^{(m'')}v^{[j]}(\beta,g). \quad (18)$$

Equation (18) has the form

$$c_{k_1k_2\cdots}(\beta,g) = 0. \quad (19)$$

Since $^{(m)}v_{[k]}(\beta,g)$ form a complete basis for $\mathfrak{A}(\beta)$, Eq. (18) describes the structure of $\mathfrak{A}(\beta)$ completely. Therefore *the relations determining completely the structure of an algebra can always be put in the tensor form of Eq. (19), provided the correspondence $\beta\to t\beta$ is an automorphism of $\mathfrak{A}(\beta)$ for every orthogonal transformation t.*

Conversely, let one or more equations of the type (19) be given to *define* β_k. From Eqs. (19) and (3b) it is clear that

$$c_{k_1k_2\cdots}(t\beta,g) = t_{k_1}{}^{l_1}t_{k_2}{}^{l_2}\cdots c_{l_1l_2\cdots}(\beta,g) = 0, \quad (20)$$

so that $t\beta$ satisfy the same relations as Eq. (19). Hence $\beta\to t\beta$ is an endomorphism of $\mathfrak{A}(\beta)$. Similarly, $\beta\to t^{-1}\beta$ is also an endomorphism. The product of these two endomorphisms is the identical automorphism $\beta\to\beta$. Hence each of the two endomorphisms must be an automorphism. Next, assume that the defining relations of Eq. (19) are such that the abstract algebra $\mathfrak{A}(\beta)$ is finite and simple. Now every automorphism of a simple algebra is an inner automorphism. Hence there exists a unit (i.e., a regular element) $T(\beta)\epsilon\mathfrak{A}(\beta)$ such that

$$t\beta = T(\beta)\cdot\beta\cdot T^{-1}(\beta). \quad (21)$$

This shows that in any representation of $\mathfrak{A}(\beta)$ the matrices β and $t\beta$ are similar. *Thus in order that an irreducible β-representation be invariant under the orthogonal group O, it is necessary and sufficient that the algebra $\mathfrak{A}(\beta)$ be finite and simple and its structure be completely described by relations of the type (19).*

Notice that if $e(\beta)$ is an element belonging to the center of $\mathfrak{A}(\beta)$, then from Eq. (21)

$$e(t\beta) = T(\beta)\cdot e(\beta)\cdot T^{-1}(\beta) = e(\beta).$$

Hence, $e(\beta)$ is invariant under transformations of the orthogonal group, i.e., it transforms as a scalar. Hence, from Lemma 1,

$$e(\beta) = e(g,\beta),$$

that is, $e(\beta)$ is a scalar constructed by contracting all the indices of β^k in the multiple products among themselves. As is well known, the center of a simple algebra over the field $\mathfrak{F}$ of complex numbers consists of $\mathfrak{F}$. 1 where 1 is the unity quantity of $\mathfrak{A}(\beta)$. Hence $1 = e(\beta)$ where $e(\beta)$ is a 'scalar.' One can therefore allow a multiple of 1 to appear in Eq. (19) without spoiling the tensor character of the equations.

Since it is not usually easy to see from a set of equations such as (19) whether the algebra $\mathfrak{A}(\beta)$ is simple or not, we drop the restriction about the simplicity of $\mathfrak{A}$. Assume, therefore, that a set of equations such as (19) is given, defining an algebra $\mathfrak{A}(\beta)$ of a finite order. We wish to investigate the invariance of an irreducible representation of $\mathfrak{A}(\beta)$ under $O(s)$. Let $\beta_k\to{}'\beta_k$ be an

irreducible representation of $\mathfrak{A}(\beta)$ by the matrices $'\beta_k$. Since $\beta\to t^{-1}\beta$ is an automorphism of $\mathfrak{A}$, $t^{-1}\beta\to{}'\beta$ is also an irreducible representation of $\mathfrak{A}$. Hence $\beta\to{}'\beta$ and $\beta\to t'\beta$ are both irreducible representations of $\mathfrak{A}$. Choose

$$t_k{}^l=\delta_k{}^l+\epsilon_k{}^l, \quad (\epsilon_{kl}=-\epsilon_{lk}), \tag{22a}$$

where ϵ_{kl} is an infinitesimal quantity ($t_k{}^l$ corresponds to an infinitesimal rotation). Then

$$\beta_k\to{}'\beta_k, \tag{22b}$$

$$\beta_k\to{}'\beta_k+\epsilon_k{}^l\,{}'\beta_l, \tag{22c}$$

are both irreducible representations of $\mathfrak{A}$. Now every finite algebra has only a finite number of irreducible representations apart from equivalence. Therefore from continuity, Eqs. (22b) and (22c) must be equivalent representations. Since all *proper* orthogonal transformations can be generated from the infinitesimal transformations, the representations $\beta\to{}'\beta$ and $\beta\to t^+{}'\beta$ where $t^+\epsilon O^+(s)$ are equivalent. *Hence every irreducible representation of $\mathfrak{A}(\beta)$ is invariant under the proper orthogonal group O^+.*

Let $\mathfrak{N}(\beta)$ be the radical of $\mathfrak{A}$. Clearly the radical is invariant under any automorphism of $\mathfrak{A}$. Hence exactly as before, one can find a tensor basis ${}^{(m)}\eta_{[k]}(\beta, g)$ for $\mathfrak{N}$. In any irreducible representation of $\mathfrak{A}$ all elements of $\mathfrak{N}$ are represented by zero. Hence all the irreducible representations of $\mathfrak{A}$ are the same as those of $\mathfrak{S}(\beta)$, where $\mathfrak{S}(\beta)$ is defined by Eq. (19) and the further equations ${}^{(m)}\eta_{[k]}(\beta, g)=0$. Clearly the radical of $\mathfrak{S}(\beta)$ is zero and therefore $\mathfrak{S}$ is semi-simple. Also $\mathfrak{S}(\beta)$ is defined by proper tensor equations, so that $\beta\to t\beta$ is an automorphism of $\mathfrak{S}$. Now every semi-simple algebra is expressible as a direct sum of simple algebras.[19] Therefore,

$$\mathfrak{S}(\beta)=\mathfrak{A}_1(\beta)\oplus\mathfrak{A}_2(\beta)\oplus\cdots\oplus\mathfrak{A}_r(\beta) \tag{23}$$

where $\mathfrak{A}_u(\beta)$ $(u=1, \cdots, r)$ are all simple. This decomposition of $\mathfrak{S}$ is unique apart from the order of $\mathfrak{A}_u$ in the decomposition. Hence under any automorphism θ of $\mathfrak{S}$, the simple algebra goes over into some $\mathfrak{A}_u'$ or in symbols

$$\mathfrak{A}_u\theta=\mathfrak{A}_u'. \tag{24}$$

In particular let θ be the automorphism $\beta\to t\beta$, where t is given by Eq. (21a). Then as before it follows from continuity considerations that $u'=u$ in Eq. (24), and so the transformation $\beta\to t^+\beta$ for $t^+\epsilon O^+(s)$ is an automorphism of $\mathfrak{A}_u$. Corresponding to Eq. (23) one has

$$\beta=\beta^{(1)}+\beta^{(2)}+\cdots+\beta^{(r)}, \quad \beta^{(u)}\epsilon\mathfrak{A}_u. \tag{25}$$

Hence $\mathfrak{A}_u$ is the algebra generated by $\beta^{(u)}$. The automorphism $\beta\to t^+\beta$ of $\mathfrak{S}$ corresponds to the automorphism $\beta^{(u)}\to t^+\beta^{(u)}$ of $\mathfrak{A}_u$. Since the latter must be an inner automorphism of $\mathfrak{A}_u$ there exists a unit $T^{+(u)}\epsilon\mathfrak{A}_u$ such that

$$t^+\beta^{(u)}=T^{+(u)}\beta^{(u)}(T^{+(u)})^{-1}. \tag{26}$$

Put

$$T^+=T^{+(1)}+T^{+(2)}+\cdots+T^{+(r)},$$

then

$$(T^+)^{-1}=(T^{+(1)})^{-1}+(T^{+(2)})^{-1}+\cdots+(T^{+(r)})^{-1},$$

since if $a_u\epsilon\mathfrak{A}_u$ and $b_v\epsilon\mathfrak{A}_v$, then $a_ub_v=0$ if $u\neq v$, and

$$1=e_1+\cdots+e_r, \tag{27}$$

where 1 is the unity quantity of $\mathfrak{S}$ and $e_u\epsilon\mathfrak{A}_u$ is the unity quantity of $\mathfrak{A}_u$. Thus

$$t^+\beta=T^+\beta(T^+)^{-1}. \tag{28}$$

Now if $c(\beta)$ is an element belonging to the center of $\mathfrak{S}$, then $c(t^+\beta)=T^+c(\beta)(T^+)^{-1}=c(\beta)$. Hence $c(\beta)$ is invariant under proper orthogonal transformations. Therefore, from Lemma 2,

$$c(\beta)=c(\beta, g, \epsilon). \tag{29a}$$

By the improper orthogonal transformation J, which reverses the direction of the x_1-axis, $c(\beta)$ goes over into

$$c(J\beta)=c(\beta, g, -\epsilon). \tag{29b}$$

The center of $\mathfrak{S}$ is obviously invariant under all automorphisms of $\mathfrak{S}$. Hence $c(J\beta)$ also belongs to the center of $\mathfrak{S}$. Therefore both

$$c_{sc}(\beta)=\tfrac{1}{2}c(\beta, g, \epsilon)+\tfrac{1}{2}c(\beta, g, -\epsilon),$$

and

$$c_{ps}(\beta)=\tfrac{1}{2}c(\beta, g, \epsilon)-\tfrac{1}{2}c(\beta, g, -\epsilon),$$

belong to the center of $\mathfrak{S}$. c_{sc} is the "scalar" part of c, while c_{ps} is the "pseudo-scalar" part. It is therefore sufficient to consider only those quantities of the center which are either pure scalars or pure pseudo-scalars.

The number of inequivalent irreducible representations of $\mathfrak{S}$ is r, which is the number of simple sub-algebras in the decomposition Eq. (23). Also,

[19] A. A. Albert, *Structure of Algebras* (Am. Math. Soc. Coll. Pub., New York, 1939).

$(e_1, \cdots, e_r)$ form a linearly independent basis for the center of $\mathfrak{S}$. Hence the number of irreducible representations is the same as the dimension of the center over $\mathfrak{F}$. One has, therefore, merely to obtain all scalar or pseudo-scalar quantities in $\mathfrak{S}$ which commute with β_k and choose from them a linearly independent set. Let $(c_1(\beta), \cdots, c_r(\beta))$ be such a set. In an irreducible representation of $\mathfrak{S}$ these quantities are represented by multiples of the unit matrix, i.e., by numbers in $\mathfrak{F}$. In general, two irreducible representations of $\mathfrak{S}$ are equivalent only if $c_u(\beta)(u=1, \cdots, r)$ are represented by the same numbers in the two representations. In particular, suppose the c's are so numbered that $c_1(\beta)$, $c_2(\beta)$, $\cdots$, $c_\mu(\beta)$ are scalars, while $c_{\mu+1}(\beta)$, $\cdots$, $c_r(\beta)$ are pseudo-scalars. Then an irreducible β-representation is reflection-invariant only if $c_{\mu+1}=\cdots=c_r=0$ for it.

From the point of view of the physical application it is desirable that the matrices β_k should be equivalent to their transposed $\beta_k^{\ddagger}$ and Hermitian conjugate $\beta_k^{\dagger}$. Hence $\beta_k^{\ddagger}$ also satisfy Eq. (19) i.e.,

$$c_{kl\ldots}(\beta^{\ddagger})=0. \tag{30a}$$

Taking the transposed of (30a) one obtains

$$c_{kl\ldots}{}^{T}(\beta)=0, \tag{30b}$$

where $c_{kl\ldots}{}^{T}(\beta)$ is derived from $c_{kl\ldots}(\beta)$ by reversing the order of the factors in the multiple products. Hence from Eqs. (19) and (30b),

$$c_{kl\ldots}(\beta)+c_{kl\ldots}{}^{T}(\beta)=0, \tag{31a}$$

$$c_{kl\ldots}(\beta)-c_{kl\ldots}{}^{T}(\beta)=0. \tag{31b}$$

Since Eq. (19) follows from Eqs. (31a and b), the latter define $\mathfrak{S}(\beta)$ completely. Hence the defining equations of $\mathfrak{S}$ can always be put in the form

$$c_{kl\ldots}(\beta, g)=0 \tag{32}$$

where $c_{kl\ldots}{}^{T}=\pm c_{kl\ldots}$. From the equivalence of β_k, $\beta_k^{\ddagger}$ and $\beta_k^{\dagger}$ it follows that β_k is equivalent to its complex conjugate β_k^{*}. Hence from Eq. (32) $c_{kl\ldots}(\beta^{*}, g)=0$. Taking the complex conjugate one finds

$$c_{kl\ldots}{}^{*}(\beta, g)=0 \tag{33}$$

where $c_{kl\ldots}{}^{*}$ is derived from $c_{kl\ldots}$ by applying the automorphism $i\rightarrow -i$ of $\mathfrak{F}$ to the numerical coefficients in $c_{kl\ldots}$. Hence from Eqs. (32) and (33)

$$c_{kl\ldots}(\beta, g)+c_{kl\ldots}{}^{*}(\beta, g)=0, \tag{34a}$$

$$ic_{kl\ldots}(\beta, g)-ic_{kl\ldots}{}^{*}(\beta, g)=0. \tag{34b}$$

Equation (32) follows from Eq. (34), and so (34) defines $\mathfrak{S}(\beta)$ completely. Therefore the defining equations of $\mathfrak{S}$ can be written in the form

$$c_{kl\ldots}(\beta, g)=0 \tag{35}$$

where $c_{kl\ldots}{}^{T}=\pm c_{kl\ldots}$ and $c_{kl\ldots}{}^{*}=c_{kl\ldots}$. Thus (35) is an equation with real coefficients. If the algebra $\mathfrak{S}(\beta)$ so defined by Eq. (35) be simple, then apart from equivalence it is capable of only one irreducible representation, say $\beta_k\rightarrow\mathfrak{B}_k$ where $\mathfrak{B}_k$ are irreducible matrices. Clearly $\mathfrak{B}_k{}^{\dagger}$ and $\mathfrak{B}_k{}^{\ddagger}$ are also irreducible and satisfy Eq. (35), so that they also constitute a representation of $\mathfrak{S}$. All these representations must therefore be equivalent. *Hence if (35) defines a finite simple algebra and β_k be an irreducible set of matrices satisfying (35), then β, $\beta^{\ddagger}$, β^{*}, $\beta^{\dagger}$, and $t\beta$ (for any $t\epsilon O(s)$) are all equivalent.*

In the general case when $\mathfrak{S}(\beta)$ is semi-simple, Eq. (35) is not sufficient to ensure the equivalence of β, $\beta^{\dagger}$, and $\beta^{\dagger}$. Of course, as shown above, it is still necessary; i.e., if for every irreducible representation of $\mathfrak{S}$, β, $\beta^{\dagger}$ and $\beta^{\dagger}$ are equivalent, then the defining equation's of $\mathfrak{S}$ can always be put in the form Eq. (35). To find under what conditions the irreducible sets β, $\beta^{\dagger}$, and $\beta^{\dagger}$ are equivalent we go back to the general criterion for deciding the equivalence of two representations. Take $(c_1(\beta), \cdots, c_r(\beta))$ to be a linearly independent basis for the center of $\mathfrak{S}$. Clearly $c_u{}^{T}(\beta)$ and $c_u{}^{*}(\beta)$ also belong to the center. Therefore, for a particular irreducible representation, β and $\beta^{\dagger}$ are equivalent only if $c_u(\beta)=c_u{}^{T}(\beta)$ for this representation. Similarly, the equivalence of β and $\beta^{\dagger}$ requires that $c_u(\beta)=c_u{}^{T*}(\beta)$.

From Eq. (26) it follows in the usual way that there exist elements $I_{kl}{}^{(u)}$ in $\mathfrak{A}_u$ such that

$$I_{kl}{}^{(u)}=-I_{lk}{}^{(u)} \text{ and}$$
$$[\beta_k{}^{(u)}, I_{lm}{}^{(u)}]=g_{kl}\beta_m{}^{(u)}-g_{km}\beta_l{}^{(u)}, \tag{36a}$$

$$[I_{kl}{}^{(u)}, I_{mn}{}^{(u)}]=-g_{km}I_{ln}{}^{(u)}+g_{lm}I_{kn}{}^{(u)}$$
$$+g_{kn}I_{lm}{}^{(u)}-g_{ln}I_{km}{}^{(u)}, \tag{36b}$$

where $[A, B]=AB-BA$. It is easy to prove that the choice of $I_{kl}{}^{(u)}$ is unique since if $J_{kl}{}^{(u)}$ were another set satisfying the same equations then

$$C_{kl}{}^{(u)}=J_{kl}{}^{(u)}-I_{kl}{}^{(u)}$$

would commute with $\beta_k{}^{(u)}$ and would therefore

belong to the center of $\mathfrak{A}_u$. Hence

$$0=[I_{kl}^{(u)}, I_{mn}^{(u)}]-[J_{kl}^{(u)}, J_{mn}^{(u)}]$$
$$=g_{km}C_{ln}^{(u)}-g_{lm}C_{kn}^{(u)}-g_{kn}C_{lm}^{(u)}+g_{ln}C_{km}^{(u)}$$

from which it follows that $C_{kl}^{(u)}=0$ unless $s=2$. So assuming that $s\neq 2$, $I_{kl}^{(u)}$ is uniquely determined. Put

$$I_{kl}=I_{kl}^{(1)}+\cdots+I_{kl}^{(r)}. \tag{37}$$

Then $I_{kl}=-I_{lk}$ and

$$[\beta_k, I_{lm}]=g_{kl}\beta_m-g_{km}\beta_l, \tag{38a}$$

$$[I_{kl}, I_{mn}]=-g_{km}I_{ln}+g_{lm}I_{kn}$$
$$+g_{kn}I_{lm}-g_{ln}I_{km}. \tag{38b}$$

I_{kl} is also uniquely defined by Eq. (37), since from Eq. (23) every I_{kl} is decomposable uniquely in the form (37), and $I_{kl}^{(u)}$, in consequence of Eqs. (37) and (38), must satisfy Eq. (36) and therefore are uniquely determined. I_{kl} is an element of $\mathfrak{S}(\beta)$ and hence is expressible in the form of Eq. (5). Write it as $I_{kl}(\beta)$. Consider the automorphism $\beta\rightarrow t^{-1}\beta$ of $\mathfrak{S}$. It is then easy to see from Eqs. (38) that

$$I'_{kl}=t_k{}^m t_l{}^n I_{mn}(t^{-1}\beta)$$

satisfy the same equations as (38). Hence

$$I_{kl}(t\beta)=t_k{}^m t_l{}^n I_{mn}(\beta)$$

so that $I_{kl}(\beta)$ transforms as a tensor. Applying Lemma 1, we immediately get

$$I_{kl}(\beta)=I(\beta_k\beta_l-\beta_l\beta_k)$$
$$+[\sum P^{\cdots}(\beta)\beta_k Q^{\cdots}_{\cdots}(\beta)\beta_l R\ldots(\beta)]_-, \tag{39}$$

where I is a numerical constant, $P^{\cdots}$, $Q^{\cdots}_{\cdots}$, $R\ldots$ are tensors constructed from β and g only, and the dots denote contracted indices. $\sum$ denotes a sum over similar terms and the minus sign at the end means that terms with l and k interchanged are to be subtracted. The first term $I(\beta_k\beta_l-\beta_l\beta_k)$ is of the simplest possible kind and has been purposely separated out. Bhabha's theory[6,8] is based on this simplest substitution

$$I_{kl}=I(\beta_k\beta_l-\beta_l\beta_k).$$

By an entirely similar consideration of the other two automorphisms of $\mathfrak{S}$ one concludes that $I_{kl}(\beta)=-I_{kl}{}^T(\beta)$ and $I_{kl}{}^*(\beta)=I_{kl}(\beta)$. Hence

$$I_{kl}(\beta)=I(\beta_k\beta_l-\beta_l\beta_k)$$
$$+\tfrac{1}{2}[\sum P^{\cdots}(\beta)\beta_k Q^{\cdots}_{\cdots}(\beta)\beta_l R\ldots(\beta)$$
$$-P^{T\cdots}(\beta)\beta_k Q^{T\cdots}_{\cdots}(\beta)\beta_l R^T\ldots(\beta)]_- \tag{40}$$

where the numerical coefficients in Eq. (40) are all real.

3. EXTENSION TO INDEFINITE GROUND FORMS

Let us now consider instead of O, other groups G of linear transformations with real coefficients which leave the indefinite ground form

$$g_{kl}x^k x^l=0, \tag{41a}$$

$$g_{kl}=0, \quad k\neq l, \quad g_{kk}=+1 \text{ or } -1 \tag{41b}$$

unchanged. As usual, we use g_{kl} to raise or lower the tensor indices. For every co-variant tensor $A_{k_1\cdots k_n}$ define

$$\mathbf{A}_{k_1\cdots k_n}=(i)^r A_{k_1\cdots k_n}$$

where r is the number of indices k_m among $(k_1\cdots, k_n)$ such that $g_{k_m k_m}=-1$. In this way for every co-variant tensor in the x-space one constructs a co-variant tensor in the $\mathbf{x}$-space. In particular, $\mathbf{g}_{kl}$ is now the same as defined by Eq. (4). We regard $\mathbf{g}_{kl}$ as the metric tensor of the $\mathbf{x}$-space and use it (instead of g_{kl}) to raise tensor indices in the $\mathbf{x}$-space. It is then easy to see that the tensor corresponding to $A_{k_1k_2}\cdots B^{\cdots l_1 l_2}$ is $\mathbf{A}_{k_1k_2}\cdots\mathbf{B}^{\cdots l_1 l_2}$ where the dots denote contracted indices. Thus every tensor equation can be taken over from the x-space to the $\mathbf{x}$-space by just using boldface type. However, a real transformation t of the x-space corresponds in general to a complex transformation of the $\mathbf{x}$-space. But it is well known that the necessary and sufficient condition for the invariance of a set of matrices β_k under G is that there should exist matrices $I_{kl}=-I_{lk}$ satisfying Eqs. (38) (now with the altered meaning of g_{kl}), and further that there be a non-singular matrix R such that

$$R\beta R^{-1}=J\beta, \tag{42}$$

where J is the transformation in G corresponding to the reversal of the direction of the x_1-axis. But these conditions are equivalent to

$$[\boldsymbol{\beta}_k, \mathbf{I}_{lm}]=\mathbf{g}_{kl}\boldsymbol{\beta}_m-\mathbf{g}_{km}\boldsymbol{\beta}_l, \tag{43a}$$

$$[\mathbf{I}_{kl}, \mathbf{I}_{mn}]=-\mathbf{g}_{km}\mathbf{I}_{ln}+\mathbf{g}_{lm}\mathbf{I}_{kn}$$
$$+\mathbf{g}_{kn}\mathbf{I}_{lm}-\mathbf{g}_{ln}\mathbf{I}_{km} \tag{43b}$$

and

$$R\boldsymbol{\beta}R^{-1}=J\boldsymbol{\beta}, \tag{43c}$$

since $\mathbf{J}=J$. Equations (43), however, are just the conditions that the $\boldsymbol{\beta}$-matrices be invariant under

O. Thus it is sufficient to examine the invariance of $\mathfrak{G}$ under O. This we have already done. Hence all our results in section 2 are still valid, provided that each tensor $A_{k_1\cdots}$ is replaced by $\mathbf{A}_{k_1\cdots}$. On going back from the $\mathbf{x}$-space to the x-space we have to revert to the normal type for the symbols. Therefore, all our conclusions which are expressed as tensor equations remain unaltered in form also when the new meaning is attributed to g_{kl}.

4. THE SPURS

The invariance of the β-representation under G leads to important restrictions on the spurs of the β-matrices and their products. Put

$$Sp(\beta_{k_1}\cdots\beta_{k_n}) = s_{k_1\cdots k_n}, \tag{44}$$

where clearly $s_{k_1\cdots k_n}$ are numerical quantities. Under the transformation $\beta\to\beta'=t\beta$, Eq. (44) goes over to

$$Sp(\beta_{k_1}'\cdots\beta_{k_n}') = t_{k_1}^{l_1}\cdots t_{k_n}^{l_n} s_{l_1\cdots l_n}.$$

But from Eq. (3a)

$$Sp(\beta_{k_1}'\cdots\beta_{k_n}') = Sp(T\beta_{k_1}\cdots\beta_{k_n}T^{-1}) = Sp(\beta_{k_1}\cdots\beta_{k_n}),$$

so that

$$t_{k_1}^{l_1}\cdots t_{k_n}^{l_n} s_{l_1\cdots l_n} = s_{k_1\cdots k_n}.$$

From this we deduce as before that

$$s_{k_1\cdots k_n} = s(g)_{k_1\cdots k_n}. \tag{45}$$

Since $s_{k_1\cdots k_n}$ cannot be constructed from g_{kl} when n is odd, it follows that

$$Sp(\beta_{k_1}\cdots\beta_{k_{2n+1}}) = 0, \tag{46}$$

and in particular

$$Sp(\beta_k) = 0.$$

Now if β_k and $\beta_k^{\ddagger}$ are equivalent,

$$Sp(\beta_{k_1}\cdots\beta_{k_n}) = Sp(\beta_{k_n}^{\ddagger}\cdots\beta_{k_1}^{\ddagger}) = Sp(\beta_{k_n}\cdots\beta_{k_1})$$

i.e.,

$$s(g)_{k_1\cdots k_n} = s(g)_{k_n\cdots k_1}. \tag{47}$$

Also further, if β_k and $\beta_k^{\dagger}$ and, therefore, β_k^{*} are equivalent, the numerical coefficients in Eq. (45) are all real. Conversely if β_k are an irreducible set of matrices satisfying Eqs. (45) and (47) with $s(g)_{k_1\cdots k_n} = s^{*}(g)_{k_1\cdots k_n}$, then the β-representation is invariant under G and β_k, $\beta_k^{\ddagger}$, $\beta_k^{\dagger}$, and β_k^{*} are all equivalent. To prove this it is sufficient to show that if there exists a correspondence $\beta_k\to\beta_k'$ between two sets of *irreducible* matrices such that

$$Sp(\beta_{k_1}\cdots\beta_{k_n}) = Sp(\beta_{k_1}'\cdots\beta_{k_n}'),$$

then β_k and β_k' are equivalent. Consider the algebra $\mathfrak{A}(B)$ generated by the matrices B_k which are the direct sum of β_k and β_k' i.e.,

$$B_k = \begin{array}{|c|c|}\hline \beta_k & 0 \\ \hline 0 & \beta_k' \\ \hline \end{array}. \tag{48}$$

Clearly $\mathfrak{A}(B)$ is semi-simple, and therefore either it is simple or a direct sum of two or more simple algebras. In the first case it is capable of only one irreducible representation apart from equivalence. Since $B_k\to\beta_k$, and $B_k\to\beta_k'$ are both representations of $\mathfrak{A}(B)$ they must be equivalent. On the other hand, in the second case

$$\mathfrak{A}(B) = \mathfrak{A}_1(B)\oplus\mathfrak{A}_2(B)\oplus\cdots,$$

where $\mathfrak{A}_1, \mathfrak{A}_2, \cdots$ are all simple. In case β_k and β_k' are not equivalent, they are equivalent to the regular representations of two different simple sub-algebras, say $\mathfrak{A}_1$ and $\mathfrak{A}_2$, respectively. Consider the unity quantities $e_1(B)$ and $e_2(B)$ of $\mathfrak{A}_1$ and $\mathfrak{A}_2$, respectively. We have, $e_1e_2=0$. In the β-representation e_1 is represented by the unit matrix and e_2 by the zero matrix, while in the β'-representation $e_1=0$ and $e_2=1$. Hence

$$Sp(e_1(\beta)) \neq Sp(e_1(\beta')), \tag{49}$$

where $e_1(\beta)$ and $e_1(\beta')$ are both obtained from $e_1(B)$ by replacing B_k by β_k and β_k', respectively. Equation (49) therefore contradicts the hypothesis. Hence β_k and β_k' are equivalent.

5. THE DIRAC AND THE DUFFIN-KEMMER ALGEBRAS

As an illustration of the above general theory, let us consider the algebra generated by the Dirac and the Duffin-Kemmer matrices in the general case of s-dimensions. It is well known that in both of these cases

$$I_{kl} = I(\beta_k\beta_l - \beta_l\beta_k)$$

where I is a constant. Therefore, as pointed out by Bhabha,[6] any representation of these algebras is a representation of the orthogonal group $O(s+1)$. Since every representation of the orthogonal group is fully reducible, it follows that every representation of the Dirac (or the Duffin-

Kemmer) algebra is also fully reducible. In particular, the regular representations of these algebras are fully reducible, and so the two algebras are semi-simple.

The Dirac matrices α_k are defined by the commutation rules[20]

$$\alpha_k\alpha_l+\alpha_l\alpha_k=2g_{kl} \tag{50}$$

so that

$$\alpha_k\alpha^k=s. \tag{51}$$

In any scalar quantity all the indices are contracted, and on using Eq. (50) the contracted indices can always be brought adjacent to each other. Therefore, from Eq. (51) every scalar quantity is a multiple of 1. In the same way it is easy to see that every pseudo-scalar quantity must be a multiple of

$$\omega=\frac{1}{s!}\epsilon^{k_1\cdots k_s}\alpha_{k_1}\cdots\alpha_{k_s}. \tag{52}$$

Now, ω commutes or anti-commutes with α_k according as s is odd or even. Clearly 1 and ω are linearly independent, since a pseudo-scalar cannot be linearly dependent on a scalar. Thus a basis for the center of the algebra consists of $(1, \omega)$ or 1 according as s is odd or even. Thus the algebra has one or two inequivalent irreducible representations according as s is even or odd. Hence, for s even, α, $\alpha^\ddagger$, $\alpha^\dagger$, α^* are all equivalent. For s odd, α and $J\alpha$ are inequivalent since $\omega^2=(-1)^{\frac{1}{2}s(s-1)}\neq 0$. Also $\omega^T=(-1)^{\frac{1}{2}s(s-1)}\omega$. Hence α and $\alpha^\ddagger$ are equivalent only if $\frac{1}{2}s(s-1)$ is even, i.e., if s is of the form $4n+1$. In a particular representation ω is represented by $\pm\omega_0$ where $\omega_0=i^{\frac{1}{2}s(s-1)}$. Therefore, α and α^* are equivalent only if $\omega_0=\omega_0^*$, i.e., if $s=4n+1$. α and $\alpha^\dagger$ are always equivalent.

The Duffin-Kemmer matrices are defined by

$$\beta_k\beta_l\beta_m+\beta_m\beta_l\beta_k=g_{kl}\beta_m+g_{ml}\beta_k. \tag{53}$$

Put $\beta_k\beta^k=B$, so that

$$\beta_kB+B\beta_k=(s+1)\beta_k, \tag{54a}$$

that is,

$$\beta_kB=(s+1-B)\beta_k, \tag{54b}$$

$$\beta^k\beta_l\beta_k=\beta_l. \tag{55}$$

Two contracted indices in a scalar expression can, from Eq. (53), be brought either adjacent to each other, or immediately to the left and right of a β_k, so that from Eqs. (54) and (55) every scalar is expressible as a polynomial $f(B)$ in B. Further, if $f(B)$ belongs to the center,

$$f(B)\beta_k=\beta_kf(s+1-B)=\beta_kf(B). \tag{56}$$

Since the algebra, being semi-simple, has a 1 which must be expressible as a scalar $e(\beta)$, it follows from Eq. (56) on multiplying on the left by $e^k(\beta)$, where $e^k(\beta)\beta_k\equiv e(\beta)$, that

$$f(s+1-B)=f(B)=\tfrac{1}{2}\{f(s+1-B)+f(B)\}.$$

Put

$$\tfrac{1}{2}(s+1)-B=\Delta \quad\text{and}\quad f\left(\frac{s+1}{2}-\Delta\right)\equiv\varphi(\Delta).$$

Then every scalar quantity of the center is of the form $\frac{1}{2}\varphi(\Delta)+\frac{1}{2}\varphi(-\Delta)\equiv\psi(\Delta^2)$ where $\psi(\Delta^2)$ is a polynomial in Δ^2. Now $\Delta^2=\frac{1}{4}(s+1)^2-B(s+1-B)$. Put

$$\theta=B(s+1-B). \tag{57}$$

Then every scalar quantity in the center is expressible as a polynomial in θ.

In a similar way, it follows that every pseudo-scalar quantity is of the form $\omega f(B)$, where f is a polynomial in B and

$$\omega=\epsilon^{k_1\cdots k_s}\beta_{k_1}\cdots\beta_{k_s}. \tag{58}$$

Now

$$\begin{aligned}\beta_{k_1}\omega=\epsilon^{k_1k_2\cdots k_s}\{&\beta_{k_1}{}^2\beta_{k_2}\cdots\beta_{k_s}-\beta_{k_1}\beta_{k_2}\beta_{k_1}\beta_{k_3}\cdots\beta_{k_s}\\&+\beta_{k_1}\beta_{k_2}\beta_{k_3}\beta_{k_1}\beta_{k_4}\cdots\beta_{k_s}\\&+\cdots+(-1)^s\beta_{k_1}\beta_{k_2}\cdots\beta_{k_s}\beta_{k_1}\}\end{aligned}$$

where there is no summation over the index k_1. Using Eq. (53) and remembering that $k_1, k_2, \cdots, k_s$ are all different, we get

$$\beta_{k_1}\omega=\left[\frac{s+1}{2}\right]\epsilon^{k_1k_2\cdots k_s}\beta_{k_1}{}^2\beta_{k_2}\cdots\beta_{k_s}, \tag{59a}$$

where $[n]$ denotes the integral part of n. Similarly,

$$\omega\beta_{k_1}=\left[\frac{s+1}{2}\right]\epsilon^{k_2\cdots k_sk_1}\beta_{k_2}\cdots\beta_{k_s}\beta_{k_1}{}^2. \tag{59b}$$

Remembering that $\beta_k{}^2\beta_l=\beta_l(1-\beta_k{}^2)$ for $k\neq l$, one finds from Eq. (59) that

$$\beta_k\omega-\omega\beta_k$$

$$=\begin{cases}0 \text{ if } s \text{ is odd}, & \text{(60a)}\\ \left[\dfrac{s+1}{2}\right]\epsilon_k{}^{k_2\cdots k_s}\beta_{k_2}\cdots\beta_{k_s} \text{ if } s \text{ is even}. & \text{(60b)}\end{cases}$$

[20] For convenience we take g_{kl} as defined in Eq. (4).

Also, from Eq. (59b),

$$\omega\beta_{k_1}^2=\left[\frac{s+1}{2}\right]\epsilon^{k_2\cdots k_s\hat{k}_1}\beta_{k_2}\cdots\beta_{k_s}\beta_{\hat{k}_1}.$$

Hence

$$\omega B=\sum_{k_1}\omega\beta_{k_1}^2=\left[\frac{s+1}{2}\right]\omega. \tag{61}$$

Therefore any pseudo-scalar quantity $\omega f(B)$ is really a numerical multiple of ω. Now it is clear from Eqs. (60) that ω belongs to the center only if s is odd. Hence the center contains pseudo-scalar elements only if s is odd and then they are numerical multiples of ω.

Consider the expression

$$B_r=\sum_{(k_1\cdots k_r)}\beta_{k_1}^2\cdots\beta_{k_r}^2 \tag{62}$$

where the summation is to be taken over all possible values of $k_1, \cdots, k_r$ such that no two of the k's are the same. Notice that

$$B_rB=\sum_{(k_1\cdots k_r)}\beta_{k_1}^2\cdots\beta_{k_r}^2\sum_{k_{r+1}}\beta_{k_{r+1}}^2.$$

Now β_k^2 and β_l^2 always commute, and $\beta_k^4=\beta_k^2$. Hence the right side is

$$\sum_{(k_1\cdots k_{r+1})}\beta_{k_1}^2\cdots\beta_{k_r}^2\beta_{k_{r+1}}^2+r\sum_{(k_1\cdots k_r)}\beta_{k_1}^2\cdots\beta_{k_r}^2,$$

so that

$$B_{r+1}=B_r(B-r).$$

But $B_1=B$ and, therefore,

$$B_r=B(B-1)\cdots(B-r+1). \tag{63}$$

Clearly, $B_{s+1}=0$ since $k_1, \cdots, k_{s+1}$ cannot all be different. Hence

$$B(B-1)\cdots(B-s)=0. \tag{64a}$$

Notice that $B=B_1, B_2, \cdots, B_s$ are all linearly independent and so $B, B^2, \cdots, B^s$ are also linearly independent over $\mathfrak{F}$. Put $f(B)=B(B-1)\cdots(B-s)$. Then $f(B)=0$ and so belongs to the center. Therefore, $f(B)=f(s+1-B)=0$; i.e.,

$$(s+1-B)(s-B)\cdots(1-B)=(-1)^{s+1}(B-1)\cdots(B-s)\times(B-(s+1))=0. \tag{64b}$$

Hence from Eqs. (64a) and (64b),

$$(B-1)(B-2)\cdots(B-s)=0. \tag{65}$$

Equation (65) is the minimum equation for B, since otherwise $B, B^2, \cdots, B^s$ would not be linearly independent. From Eqs. (65) and (57) it follows that the minimum equation for θ is

$$(\theta-1\cdot s)(\theta-2(s-1))\cdots\times(\theta-[\tfrac{1}{2}(s+1)][\tfrac{1}{2}(s+2)])=0. \tag{66}$$

Hence $1, \theta, \theta^2, \cdots, \theta[\frac{1}{2}(s+1)]-1$ form a linearly independent complete scalar set in the center. When s is even, this set is a basis for the center. On the other hand, when s is odd, ω must be added to it to obtain a complete basis. Therefore the dimension of the center over $\mathfrak{F}$ is $[\frac{1}{2}(s+1)]$ or $[\frac{1}{2}(s+1)]+1$, according as s is even or odd. Hence the algebra has $\frac{1}{2}s$ or $\frac{1}{2}(s+3)$ irreducible inequivalent representation, according as s is even or odd.

From Eq. (61) it follows that ω is zero in all representations except those in which B can have the eigenvalue $[\frac{1}{2}(s+1)]$, i.e., in which θ has the eigenvalue $[\frac{1}{2}(s+1)][\frac{1}{2}(s+2)]$. But θ is in the center and so

$$\theta=\left[\frac{s+1}{2}\right]\left[\frac{s+2}{2}\right]\equiv\theta_0$$

for this representation.

Proceeding as in Eq. (59a), one easily finds that

$$\beta_{k_2}\beta_{k_1}\omega=\left[\frac{s+1}{2}\right]\left[\frac{s}{2}\right]\epsilon^{k_1k_2k_3\cdots k_s}\times(1-\beta_{k_1}^2)\beta_{k_2}^2\beta_{k_3}\cdots\beta_{k_s},\quad(k_1\neq k_2),$$

and, similarly,

$$\beta_{k_s}\beta_{k_{s-1}}\cdots\beta_{k_1}\omega=\left[\frac{s+1}{2}\right]\left[\frac{s}{2}\right]\cdots\times\left[\frac{2}{2}\right]\epsilon^{k_1\cdots k_s}\beta_{k_s}^2(1-\beta_{k_{s-1}}^2)\beta_{k_{s-2}}^2(1-\beta_{k_{s-3}}^2)\cdots,$$

where $k_1, \cdots, k_s$ are all different. Therefore

$$\omega^2=(-1)^{[\frac{1}{2}s(s-1)]}\left[\frac{s+1}{2}\right]\cdots\left[\frac{2}{2}\right]\times P_{(k_1\ldots k_s)}\beta_{k_s}^2\beta_{k_{s-2}}^2\cdots(1-\beta_{k_{s-1}}^2)(1-\beta_{k_{s-3}}^2)\cdots, \tag{67}$$

where $P_{(k_1\cdots k_s)}$ denotes a sum over all permu-

tations of $(1, 2, \cdots s)$. It is easy to see from Eqs. (67) and (63) that

$$\omega^2=(-1)^{[\frac{1}{2}s(s-1)]}\left[\frac{s+1}{2}\right]\left[\frac{s}{2}\right]\cdots\left[\frac{2}{2}\right]$$
$$\times\left\{B_{[\frac{1}{2}(s+1)]}-\left[\frac{s}{2}\right]B_{[\frac{1}{2}(s+3)]}+\frac{\left[\frac{s}{2}\right]\left[\frac{s-2}{2}\right]}{2!}B_{[\frac{1}{2}(s+5)]}\right.$$
$$\left.-\frac{\left[\frac{s}{2}\right]\left[\frac{s-2}{2}\right]\left[\frac{s-4}{2}\right]}{3!}B_{[\frac{1}{2}(s+7)]}+\cdots+(-1)^{[\frac{1}{2}s]}B_s\right\}. \quad (68)$$

Using Eqs. (63) and (61), it follows that

$$\omega^3=(-1)^{[\frac{1}{2}s(s-1)]}\left\{\left[\frac{s+1}{2}\right]\left[\frac{s}{2}\right]\cdots\left[\frac{2}{2}\right]\right\}^2\omega. \quad (69)$$

Now ω^2 is a scalar and hence a polynomial in B, as is also clear from Eq. (68). Hence ω^2 can be written in the form

$$\omega^2=P(\theta)+Q(\theta)\cdot B$$

where P and Q are polynomials in θ. Since ω^2 vanishes for all representations except those for which $\theta=\theta_0$, it follows that

$$\omega^2=\phi(\theta)\{p+qB\}, \quad (70)$$

where

$$\phi(x)\equiv(x-1\cdot s)\cdots\left(x-\left[\frac{s-1}{2}\right]\left[\frac{s+4}{2}\right]\right).$$

In view of Eq. (66), p and q can be taken to be constants. From Eqs. (61), (70), and (66) one finds that

$$\omega^4=\phi(\theta_0)\left(p+q\left[\frac{s+1}{2}\right]\right)\omega^2, \quad (71)$$

while on multiplying Eq. (70) by $(s+1-B)$ one gets

$$\omega^2\left[\frac{s+2}{2}\right]=\phi(\theta)\{p(s+1)+q\theta_0-pB\}. \quad (72)$$

From Eqs. (69), (70), (71), and (72) it is easy to deduce that

$$\omega^2=\begin{cases}(-1)^{[\frac{1}{2}s(s-1)]}(\frac{1}{2}s!)^4\dfrac{\phi(\theta)}{\phi(\theta_0)}\\ \qquad\times\left\{\dfrac{s}{2}+1-B\right\}, & (s \text{ even}), \quad (73a)\\ (-1)^{[\frac{1}{2}s(s-1)]}\left(\dfrac{s+1}{2}\right)^2\\ \qquad\times(\tfrac{1}{2}(s-1)!)^4\dfrac{\phi(\theta)}{\phi(\theta_0)}, & (s \text{ odd}). \quad (73b)\end{cases}$$

Now notice that it follows from Eq. (59a) that

$$\beta_{k_1}\omega\beta_{k_1}=\left[\frac{s+1}{2}\right]\epsilon^{k_1k_2\cdots k_s}\beta_{k_1}^2\beta_{k_2}\cdots\beta_{k_s}\beta_{k_1}$$
$$=\left[\frac{s+1}{2}\right]\epsilon^{k_1k_2\cdots k_s}\beta_{k_2}\cdots\beta_{k_s}(1-\beta_{k_1}^2)\beta_{k_1}$$
$$=0, \quad (s \text{ even}). \quad (74)$$

It will presently be shown in Section 6 that Eq. (74) necessarily implies

$$\beta_k\omega\beta_l+\beta_l\omega\beta_k=0, \quad (s \text{ even}). \quad (75)$$

Now consider $\omega\beta_k\omega$. It is a vector and hence must be expressible in the form $\beta_k f(B)$ where $f(B)$ is a polynomial in B. Then

$$\beta_k^2\omega\beta_k\omega=\beta_k^3 f(B)=\beta_k f(B)=\omega\beta_k\omega.$$

But the left side is zero from Eq. (74), when s is even. Hence

$$\omega\beta_k\omega=0, \quad (s \text{ even}). \quad (76)$$

Further it is easy to see from Eq. (61) that

$$\beta_{k_1}^2\omega+\omega\beta_{k_1}^2=\omega, \quad (s \text{ even}).$$

As shown in Section 6, this implies that

$$(\beta_k\beta_l+\beta_l\beta_k)\omega+\omega(\beta_k\beta_l+\beta_l\beta_k)=2\omega g_{kl}, \quad (s \text{ even}).$$

But ω is a pseudo-scalar and therefore commutes with I_{kl} i.e.,

$$(\beta_k\beta_l-\beta_l\beta_k)\omega-\omega(\beta_k\beta_l-\beta_l\beta_k)=0.$$

Adding the two equations, one gets

$$\beta_k\beta_l\omega+\omega\beta_l\beta_k=\omega g_{kl}, \quad (s \text{ even}). \quad (77)$$

Moreover, Eq. (73a) gives

$$\beta_k\omega^2+\omega^2\beta_k=(-1)^{[\frac{1}{2}s(s-1)]}(\tfrac{1}{2}s!)^4\frac{\phi(\theta)}{\phi(\theta_0)}\beta_k. \quad (78)$$

Put

$$\omega_0=\frac{i^{[\frac{1}{2}s(s-1)]}}{\left[\frac{s+1}{2}\right]\cdots\left[\frac{2}{2}\right]}\cdot\omega.$$

Then $\omega_0^3=\omega_0$. The only irreducible representations in which $\omega_0\neq 0$ are those in which $\theta=\theta_0$. In these representations

$$\omega_0^2=\begin{cases}\frac{1}{2}s+1-B & (s \text{ even}), \quad (79a)\\ 1 & (s \text{ odd}). \quad (79b)\end{cases}$$

In view of Eqs. (75), (76), (77), and (78), one can put $\beta_{s+1}=\omega_0$, (s even) for the representation $\theta=\theta_0$, and allow the indices to run from *1* to $s+1$ in Eq. (53). Also notice that for this representation the matrices γ_k defined by

$$\gamma_k=\beta_k\omega_0+\omega_0\beta_k \quad (80)$$

satisfy the same commutation rules as Eq. (53). In fact

$$\gamma_k=(1+\omega_0-\omega_0^2)\beta_k(1+\omega_0-\omega_0^2); \quad (81)$$

and since $(1+\omega_0-\omega_0^2)^2=1$, γ and β are equivalent. Since $1+\omega_0-\omega_0^2$ is a pseudo-scalar quantity it commutes with I_{kl}. Also clearly it commutes with B and ω_0; therefore

$$\gamma_k\gamma_l-\gamma_l\gamma_k=\beta_k\beta_l-\beta_l\beta_k, \quad \gamma^k\gamma_k=\beta^k\beta_k,$$
$$\epsilon^{k_1\cdots k_s}\gamma_{k_1}\cdots\gamma_{k_s}=\epsilon^{k_1\cdots k_s}\beta_{k_1}\cdots\beta_{k_s}.$$

Since $\theta=\theta^*=\theta^T$ it follows that for even s, any irreducible β-representation is equivalent to $J\beta$, β^*, $\beta^\ddagger$, $\beta^\dagger$. For s odd, β, $J\beta$, β^*, $\beta^\ddagger$, $\beta^\dagger$ are equivalent for the representations for which $\theta\neq\theta_0$, $\omega=0$. In the other two $\theta=\theta_0$,

$$\omega=\pm i^{[\frac{1}{2}s(s-1)]}\tfrac{1}{2}(s+1)(\tfrac{1}{2}(s-1)!)^2.$$

Clearly here β and $J\beta$ are inequivalent. β and β^* are equivalent only when s is of the form $4n+1$. The same holds for β and $\beta^\ddagger$, while β and $\beta^\dagger$ are always equivalent.

6. PHYSICAL APPLICATION

We now come to the physical application of the above abstract theory. The tensor indices now run from 0 to 3 only and $g_{00}=-g_{11}=-g_{22}=-g_{33}=1$. Consider the wave equation (1). Let the minimum equation for β_0 be

$$(\beta_0)^n+a_1(\beta_0)^{n-1}+a_2(\beta_0)^{n-2}+\cdots+a_n=0, \quad (82)$$

with a's in $\mathfrak{F}$. Write it in the form

$$(\beta_0)^n+g_{00}a_2(\beta_0)^{n-2}+(g_{00})^2a_4(\beta_0)^{n-4}+\cdots$$
$$+\{a_1(\beta_0)^{n-1}+g_{00}a_3(\beta_0)^{n-3}+\cdots\}=0.$$

Since β and $t\beta$ are equivalent, t now being a Lorentz transformation, it follows that $\beta_0'=t_0^k\beta_k$ has the same minimum equation. Put $t_0^k=y^k$. Then

$$y^ky_k=t_0^kt_0^lg_{kl}=g_{00}=1 \quad (83)$$

and $\beta_0'=y^k\beta_k$. Therefore

$$\{(y^l\beta_l)^n+a_2y^{k_1}y^{k_2}g_{k_1k_2}(y^l\beta_l)^{n-2}$$
$$+a_4(y^{k_1}y^{k_2}g_{k_1k_2})^2(y^l\beta_l)^{n-4}+\cdots\}$$
$$+\{a_1(y^l\beta_l)^{n-1}+a_3y^{k_1}y^{k_2}g_{k_1k_2}(y^l\beta_l)^{n-3}+\cdots\}=0.$$

Now the y's are arbitrary except for Eq. (83). Hence put

$$y^l=\frac{z^l}{(g_{mn}z^mz^n)^{\frac{1}{2}}}\equiv\frac{z^l}{Z},$$

where the z's are independent indeterminates. Then on multiplying by Z^n one finds

$$\{(z^l\beta_l)^n+a_2z^{k_1}z^{k_2}g_{k_1k_2}(z^l\beta_l)^{n-2}+\cdots\}$$
$$+Z\{a_1(z^l\beta_l)^{n-1}+\cdots\}=0. \quad (84)$$

This must be an identity in z. Therefore from the irrationality of Z in z it follows that

$$a_1(z^l\beta_l)^{n-1}+\cdots=0.$$

Put $z^0=1$, $z^l=0$, $l\neq 0$. Then

$$a_1(\beta_0)^{n-1}+\cdots=0.$$

If a_1, a_3, $\cdots$ are not all zero, this is an equation, of a degree lower than the minimum equation. Since this contradicts the definition of the minimum equation, it follows that $a_1=a_3=a_5=\cdots=0$. Hence only the terms in the first bracket in Eq. (84) remain. Equating coefficients one gets

$$P_{(k_1\cdots k_n)}(\beta_{k_1}\cdots\beta_{k_n}+a_2g_{k_1k_2}\beta_{k_3}\cdots\beta_{k_n}$$
$$+a_4g_{k_1k_2}g_{k_3k_4}\beta_{k_5}\cdots\beta_{k_n}+\cdots)=0, \quad (85)$$

where $P_{(k_1\cdots k_n)}$ denotes a sum over all permutations of $k_1\cdots k_n$. From Eq. (85) it follows that

$$\{(\partial^l\beta_l)^n+a_2\partial^k\partial_k(\partial^l\beta_l)^{n-2}$$
$$+a_4(\partial^k\partial_k)^2(\partial^l\beta_l)^{n-4}+\cdots\}\psi=0.$$

On making use of Eq. (1), this can be written as

$$\{(i\chi)^n+a_2(i\chi)^{n-2}\partial^k\partial_k$$
$$+a_4(i\chi)^{n-4}(\partial^k\partial_k)^2+\cdots\}\psi=0. \quad (86)$$

Equation (86) is the differential equation (with numerical coefficients) of the lowest order which the most general solution ψ of Eq. (1) would satisfy if no subsidiary conditions were imposed. Now, if we demand that (86) be the usual second-order equation, we must have[21] $a_4=a_6=\cdots=0$ and $a_2=-1$. Equation (85) then becomes

$$P_{(k_1\cdots k_n)}(\beta_{k_1}\cdots\beta_{k_n}-g_{k_1k_2}\beta_{k_3}\cdots\beta_{k_n})=0. \quad (87)$$

Equation (87) is completely equivalent to

$$(z^l\beta_l)^n=z^kz_k(z^l\beta_l)^{n-2}, \quad (88)$$

where z's are indeterminates. Equation (88) is the natural generalization of the well-known cases of the Dirac and the Duffin-Kemmer matrices, for which

$$(z^l\beta_l)^2=z^kz_k$$

and

$$(z^l\beta_l)^3=z^kz_k(z^l\beta_l),$$

respectively.

Since Eq. (87) is already in a proper tensor form, one might at first sight think that the invariance of an irreducible representation under the proper Lorentz group is insured. This, however, is in general not the case, since for $n\geqslant 3$ Eq. (87) does *not* generate a *finite* algebra. Some other stronger tensor condition compatible with Eq. (87) is needed to make the algebra finite. An example of such a condition for $n=3$ is provided by the Duffin commutation rules

$$\beta_k\beta_l\beta_m+\beta_m\beta_l\beta_k-g_{kl}\beta_m-g_{ml}\beta_k=0.$$

In the Dirac and the Duffin-Kemmer case it is possible to choose a representation in which β's are Hermitian (i.e., $\beta_0=\beta_0^\dagger$ and $\beta_k=-\beta_k^\dagger$, $k=1, 2, 3$). But this is clearly impossible when $n>3$, since if β_0 is Hermitian it can be brought to the diagonal from. Now, its minimum equation is

$$\beta_0{}^{n-2}(\beta_0{}^2-1)=0, \quad (89)$$

and hence its eigenvalues are ±1, 0. But then, since β_0 is diagonal, it clearly satisfies the equation

$$\beta_0(\beta_0{}^2-1)=0.$$

Hence $n\leqslant 3$.

I have not been able to establish the existence of an irreducible relativistically invariant set β_k satisfying Eq. (87) for $n>3$, but not for $n\leqslant 3$.[22] All the obvious commutation rules which are compatible with Eq. (87) and with the general restrictions laid down in Section 3, and which make the resulting algebra finite, either turn out to be inconsistent or are found, on closer investigation, to degenerate into the already known cases of the Dirac or the Duffin-Kemmer rules. On the other hand, there seems to be no obvious way of proving that such a representation is impossible for $n>3$. If it be true that no such β-representation could exist for $n>3$, our results should be interpreted to mean that no higher spins are possible.

It is comparatively easy to find an explicit expression for β_k with $n=4$; e.g.,

$$\beta_k=\frac{1}{\sqrt{2}}\{\alpha_k(\tfrac{3}{2})X\omega+i\cdot 1X\alpha_k(\tfrac{1}{2})\}$$

where $\alpha_k(\frac{3}{2})$ and $\alpha_k(\frac{1}{2})$ are matrices constructed in the way proposed by Bhabha,[8] which satisfy the minimum equations

$$(\alpha_0{}^2-\tfrac{1}{4})(\alpha_0{}^2-9/4)=0, \quad \text{and} \quad (\alpha_0{}^2-\tfrac{1}{4})=0,$$

respectively. ω is uniquely[23] defined by $\omega^2=1$ and

$$\alpha_k(\tfrac{1}{2})\omega+\omega\alpha_k(\tfrac{1}{2})=0.$$

$\alpha_k(\frac{1}{2})$ are really $\frac{1}{2}$ times the usual Dirac matrices. X denotes Kronecker product. It is easy to see that this representation is relativistically invariant (including reflection) and is equivalent to its Hermitian conjugate. But since it is not certain that it is irreducible, one cannot rule out the possibility that the irreducible part may satisfy an equation such as (89) with $n\leqslant 3$.

[21] It is assumed here that $\chi\neq 0$, so that one can divide out $(i\chi)^{n-2}$.

[22] Since the manuscript was sent to the press, one such representation has been found corresponding to $n=4$.

[23] Apart from ambiguity in sign, which is immaterial.

Absorption Line Width in the Rotation Spectrum of Atmospheric Water Vapor*

ARTHUR ADEL
McMath-Hulbert Observatory of the University of Michigan Ann Arbor, Michigan

(Received February 28, 1947)

Grating measurements at oblique incidence are employed as a means of obtaining the narrow slits essential to the direct observation of line width. Correction for the finite width of slit is small. It is accomplished by empirical extrapolation to zero slit in one instance, and by numerical estimation of slit influence in another. The absorption coefficient half-width at half-height for the atmospheric water vapor lines at 18.64 mu and 15.99 mu is found to be 0.12 cm^{-1} and 0.11 cm^{-1}, respectively.

FOR a spectrometer of unlimited resolving power the fractional transmission of radiation through an absorption line is given by the expression,

$$T=\epsilon^{-k(\nu)\cdot t},$$

and the fractional absorption by $A=1-T$. By the width of the line is meant the width of the absorption coefficient $k(\nu)$. In the infra-red, broadening by thermal collisions is the principal agent in shaping an absorption line, and the absorption coefficient has the Lorentz dispersion form

$$k(\nu)=\frac{J}{\pi}\frac{D_0}{(\nu-\nu_0)^2+D_0^2},$$

where ν_0 marks the center of the line, and

$$J=\int_{-\infty}^{+\infty}k(\nu)d\nu$$

is the total intensity of the line. The distance from ν_0 to the point at which $k(\nu)$ falls to half its maximum value is D_0, the half-width of the line, that is, half the width at half the height of the curve of absorption coefficient. J and D_0 are important in the problem of radiative transfer. In an absorption line of moderate depth the rate at which energy is absorbed is proportional to

$$(JD_0t)^{\frac{1}{2}},$$

where t is the length of path.[1]

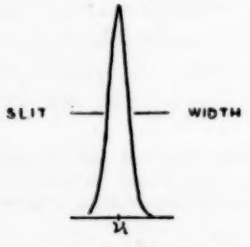

FIG. 1. The intensity distribution within the spectral interval transmitted by the exit slit of a spectrometer with equal entrance and exit slits.

For the purpose of measuring widths, the curve of absorption coefficient can always be obtained from the absorption line following correction of the latter for the finite slits of the spectrometer. This correction can be made directly for a line of any strength by using a graduated series of slits and extrapolating the curve of apparent line width *versus* slit width to zero slit width. The correction can also be made indirectly by application of the simple theory of slit influence to a line of moderate depth.[2] Both methods will be applied to atmospheric water vapor—the empirical to the line at 18.64 mu, the numerical to the line at 15.99 mu.

Infra-red lines are generally exceedingly narrow. It has been shown, for example, that the directly observed absorption line half-width in N_2O, at a pressure of 30 cm Hg, even prior to correction for slit width is but 0.09 cm^{-1}.[2] The need for narrow slits is evident, since one may hope to explore a line significantly only if the slit is narrower than the line.

The spectral width of a slit depends more importantly upon the available dispersion than upon actual slit opening. The intensity distribution within the spectral interval transmitted by

* This paper is based on work done for the Office of Scientific Research and Development under Contract OEMsr-1361 with the University of Michigan.

[1] D. M. Dennison, Phys. Rev. **31**, 503 (1928).
[2] Arthur Adel and E. F. Barker, Rev. Mod. Phys. **16**, 236 (1944).

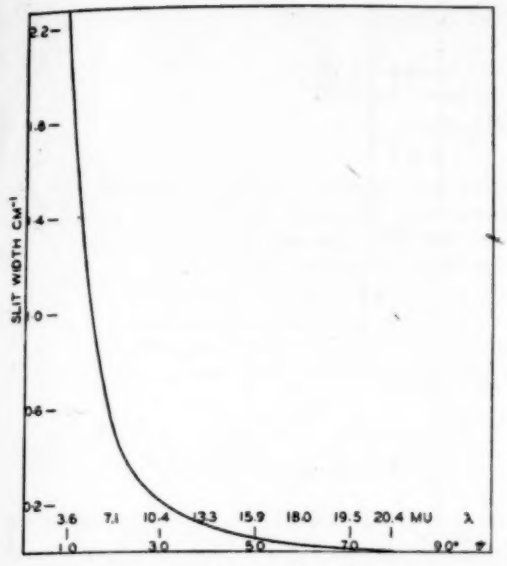

FIG. 2. Effective slit width as a function of wave-length or grating angle for the spectrometer $\lambda_\mu = 20.764 \sin\vartheta$, with 2400 line grating and slits of angular width one minute of arc.

the exit slit of a spectrometer with equal entrance and exit slits is shown in Fig. 1. This is the frequency pattern received by the thermopile at the frequency setting ν_i. The width of the slit is the width of the slit distribution function at half-height. The functional dependence of spectral slit width on slit opening and dispersion can be obtained from the spectrometer equation

$$\lambda = 2a \cos\tfrac{1}{2}\varphi \sin\vartheta,$$

where a is the grating constant, φ is the angle between the incident and diffracted beams, and ϑ is the angle between the grating normal and the bisector of φ.

For entrance and exit slits of equal angular width $d\varphi$ the spectral slit width is given by

$$d\tilde{\nu}_L = \frac{10^4 \cdot d\varphi}{2K_\mu \sin\vartheta}(\cot\vartheta - \tan\tfrac{1}{2}\varphi) \text{ cm}^{-1},$$

where

$$K_\mu = 2a \cos\tfrac{1}{2}\varphi\mu.$$

$d\tilde{\nu}_L$ must not be confused with $d\tilde{\nu}_C$, the spectral interval which sweeps past a point in the exit slit when the grating turns through a small angle $d\vartheta = d\varphi$; for the grating sweeps the spectrum across the exit slit faster than would a mirror a ray of light, that is,

$$d\tilde{\nu}_C = \frac{10^4 d\vartheta}{K_\mu \sin\vartheta}\cot\vartheta > 2d\tilde{\nu}_L,$$

when $d\vartheta = d\varphi$, the slit width. $d\tilde{\nu}_L$ may also be written

$$d\tilde{\nu}_L = \frac{10^4 \cdot d\varphi}{2K_\mu \sin\vartheta}\frac{\cos(\vartheta + \tfrac{1}{2}\varphi)}{\sin\vartheta \cdot \cos\tfrac{1}{2}\varphi},$$

from which it is clear that $d\tilde{\nu}_L = 0$ at grazing incidence, that is, when $\vartheta + \tfrac{1}{2}\varphi = \tfrac{1}{2}\pi^{(r)}$, and remains very small at oblique incidence.

In the experiment described in this paper a grating with 2400 lines per inch was used, thus making $2a = 127/6$ mu. From the spectrometer constant, $K_\mu = 20.764$ mu, it is found that $\tfrac{1}{2}\varphi = 11° 20'$. Figure 2 is a plot of $d\tilde{\nu}_L$ *versus* ϑ (or λ) for a grating with 2400 lines per inch and an angular slit width of one minute of arc, according to the equation

$$d\tilde{\nu}_L = 0.07\frac{\cot\vartheta - 0.2004}{\sin\vartheta}\text{cm}^{-1}.$$

The technique of oblique incidence has been applied to the atmospheric water vapor lines at 15.991 mu, 16.667 mu, 18.018 mu ($7_4 - 6_0$), and 18.64 mu ($6_5 - 5_1$). All are extremely narrow and essentially of the same width. Only the two at 15.991 mu and 18.64 mu will be treated in detail. The line at 18.64 mu was examined with a variety of slit widths ranging from 0.62 cm^{-1} to 0.061 cm^{-1}. The reduction appears in Fig. 3,[3]

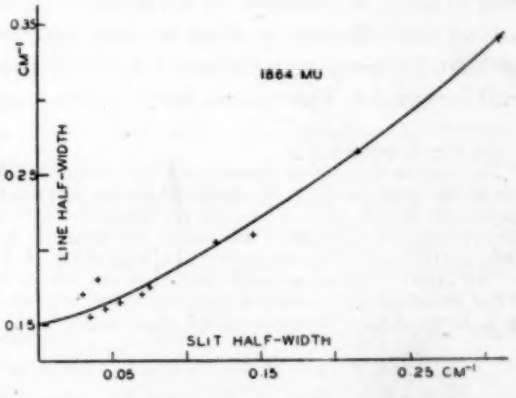

FIG. 3. Observed dependence of absorption line width on spectrometer slit width.

[3] Line half-width is here plotted against slit half-width.

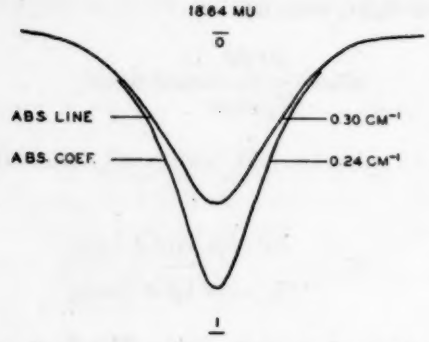

FIG. 4. The atmospheric absorption line at 18.64μ and its absorption coefficient.

which has the form indicated by theoretical considerations.[4] The extrapolation to zero slit is short and can certainly lead to a value no greater than 0.15 cm^{-1} for the half-width at half-height, at the observed fractional absorption of 56 percent. The line, and the curve of $k(\nu)\cdot t$ deduced from it, appear in Fig. 4. $k(\nu)\cdot t$ and $k(\nu)$ possess the same half-width, since t is a constant factor. The half-width at half-height of $k(\nu)$ is 0.12 cm^{-1}.

It also seems worth while to correct for finite slits by computing the effect of slit-width on apparent line width, in contrast to the empirical extrapolation just concluded. The elementary theory of slit influence has been applied to the problem of line width[2,5] in N_2O. Figure 5 is taken from this work. Here the apparent half-width of the line, in units of true half-width, is plotted against the apparent half-width, in units of slit half-width. The abscissa is an observable. Thus D/D_0 may be read from the curve, D being known, D_0 follows. It is assumed in this analysis that the line is weak so that line half-width and absorption coefficient half-width are sensibly equal.[6] The atmospheric water vapor

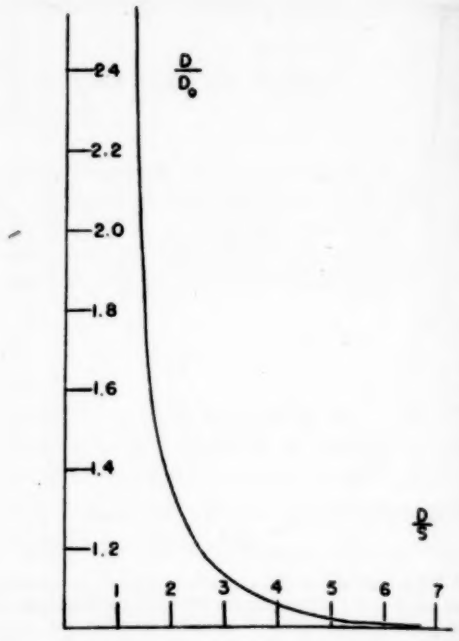

FIG. 5. Infra-red absorption line width in units of absorption coefficient width as a function of absorption line width in units of slit width.

line at 15.991 mu was observed to have a half-width at half-height of 0.145 cm^{-1}, at a time when the maximum absorption was 39 percent, and the slit half-width was 0.075 cm^{-1}. Since $D/S=2$, $D/D_0=1.35$, and $D_0=0.11$ cm^{-1}, in substantial agreement with the value obtained for the line at 18.64 mu.

Since this work was done, in the summer of 1944,[7] several investigators have determined the half-width of the water vapor line $(6_{-5}-5_{-1})$ at $\lambda 1.35$ cm in the microwave region. See, for example, G. E. Becker and S. H. Autler,[8] who found values of 0.087 cm^{-1} and 0.107 cm^{-1} for low and high density of water vapor, respectively, in good agreement with the results given in this paper.

[4] See Fig. 6, reference 2.

[5] The author takes this opportunity to correct a small error in the work on N_2O. $d\bar{\nu}_C$ rather than $d\bar{\nu}_L$ was used to compute slit width, and, as a result, the line half-width was overcorrected to 0.07 cm^{-1}. By using the true slit half-width of 0.02 cm^{-1}, the apparent line half-width of 0.09 cm^{-1} for N_2O is reduced to 0.08 cm^{-1}, true line half-width.

[6] For an observed central absorption of 39 percent the line is of moderate strength rather than weak, and the computed half-width will be conservative, that is, slightly too large.

[7] Div. 14, NDRC. Report No. 320, October 10, 1944; and an unpublished letter to Professor G. E. Uhlenbeck, dated February 1, 1945.

[8] G. E. Becker and S. H. Autler, Phys. Rev. 70, 300 (1946).

Finite Elastic Strain of Cubic Crystals*

FRANCIS BIRCH
Harvard University, Cambridge, Massachusetts

(Received February 24, 1947)

Murnaghan's theory of finite strain is developed for a medium of cubic symmetry subjected to finite hydrostatic compression, plus an arbitrary homogeneous infinitesimal strain. The free energy is developed for cubic symmetry to include terms of the third order in the strain components. The effect of pressure upon the second-order elastic constants is found and compared with experiment, with particular reference to the compressibility; the pressure-volume relation in several approximations is compared with the measurements to 100,000 kg/cm². The simplest approximation is shown to give a satisfactory account of most of the experimental data. The results are also compared with some of the calculations based on Born's lattice theory.

1. INTRODUCTION

MURNAGHAN[1] has published an exact treatment of finite deformation of elastic solids, with application to several questions involving isotropic media. The theory is not restricted to the case of isotropy, and it will be developed below for the case of cubic symmetry.

Finite *elastic* strain is in practice limited to finite hydrostatic strain plus superimposed infinitesimal strain of an arbitrary type. Excluding such special materials as rubber, non-hydrostatic strains large enough to require treatment as "finite" are generally beyond the elastic limit. On the other hand, hydrostatic strain of whatever magnitude is "elastic" and may be accompanied by elastic infinitesimal strain of any kind. The hydrostatic strain affects the response of the medium to the infinitesimal additional strain, giving rise to an effect of pressure upon the elastic constants. Such a strain is of fundamental interest in many problems concerning the interior of the earth, to a few of which the theory has been applied.[2] A large body of experimental data, almost entirely the work of Bridgman, may be used to find the change of compressibility with pressure; there are also a few determinations of the effect of pressure upon the rigidity of quasi-isotropic materials.

Born[3] has treated this kind of deformation from the point of view of lattice theory, and has carried out with several collaborators detailed computations for various monatomic cubic lattices. The results are of great interest, showing plausible pressure and temperature coefficients for the elastic constants. Born appears to have accepted as general the theorem of the classical theory of elasticity, which holds that the stress components are the partial derivatives of the free energy density with respect to the corresponding strain components. Murnaghan has shown that this is valid only for infinitesimal strain, and in consequence, some of the calculations according to Born's method are subject to a correction which increases with the amount of compression.

Another paper on this general topic has been published by Fürth,[4] who combines certain results of Born and Misra[5] concerning the third-order terms of the elastic potential with an incorrect application of Murnaghan's stress-strain relation. Except in the special case of hydrostatic pressure, Fürth's calculations are consequently wrong, and with the same exception, they deal with unrealizable examples of finite elastic strain.

In the following sections, the theory is developed for a medium of cubic symmetry subjected to a strain consisting of (1) a hydrostatic compression of any amount, plus (2) a homogeneous infinitesimal strain of general type. The exact stress-strain relations for this case are found and

* Paper No. 100 published under the auspices of the Committee on Experimental Geology and Geophysics, and the Division of Geological Sciences at Harvard University.

[1] F. D. Murnaghan, Am. J. Math. **49**, 235 (1937).

[2] F. Birch, Bull. Seis. Soc. Am. **29**, 463 (1939); K. E. Bullen, *ibid.* **30**, 235 (1940).

[3] Max Born, J. Chem. Phys. **7**, 591 (1939); also a series of papers in Proc. Camb. Phil. Soc.

[4] R. Fürth, Proc. Roy. Soc. **A180**, 285 (1942).

[5] Max Born and R. D. Misra, Proc. Camb. Phil. Soc. **36**, 466 (1940).

decomposed into a hydrostatic pressure plus a general stress related to the infinitesimal strain. A general form for the free energy is given, to the third order in the strain components, and used to find the variation of the elastic constants with pressure. Particular attention is given to the effect of pressure on compressibility and on volume, and to the relevant experimental data. Since there apparently exists some misunderstanding concerning the application of Murnaghan's theory, most of the developments are carried along according to both of the alternative methods which Murnaghan has formulated; this naturally lengthens the treatment, but it is perhaps worth while to show clearly that no ambiguity arises. The particular case of hydrostatic pressure could have been dealt with more directly, and indeed, since cubic crystals are isotropic with respect to such a stress, this case has already been covered in the studies of isotropic media.[1,6] The general theory is given for the sake of comparison with Born's lattice theory, and with experimental data which should be obtainable.

2. THE STRAIN

Throughout the following, rectangular Cartesian coordinates are employed, the axes taken to coincide with the axes of fourfold symmetry; the same coordinate system is used for the description of the initial and final configurations. The usual notation of Cartesian tensors is used, repetition of an index signifying summation over the values 1, 2, 3 for this index. The coordinates of a point before strain are denoted by (a_1, a_2, a_3), after strain by (x_1, x_2, x_3). These points determine a displacement vector with components (x_1-a_1), (x_2-a_2), (x_3-a_3).

We now consider a special strain composed of two parts: (1) a hydrostatic compression by which every line in the crystal is shortened by the factor $(1-\alpha)$, where α, intrinsically positive, may have any value from 0 to 1; (2) a subsequent homogeneous strain expressed in terms of six coefficients β_{rs}, which will be treated as infinitesimals, whereas all powers of α are retained. By the hydrostatic strain, a point initially at (a_1, a_2, a_3) is brought to the point (x_1^0, x_2^0, x_3^0), given by $x_p^0=(1-\alpha)a_p$, with $p=1, 2, 3$. The additional displacements resulting from the strain β_{rs} will be

$$\begin{aligned} u_1' &= \beta_{11}x_1^0+\beta_{12}x_2^0+\beta_{13}x_3^0, \\ u_2' &= \beta_{21}x_1^0+\beta_{22}x_2^0+\beta_{23}x_3^0, \\ u_3' &= \beta_{31}x_1^0+\beta_{32}x_2^0+\beta_{33}x_3^0, \end{aligned} \tag{1}$$

with $\beta_{rs}=\beta_{sr}$. The final coordinates are $x_r=x_r^0+u_r'$, or

$$\begin{aligned} x_1 &= (1-\alpha)[(1+\beta_{11})a_1+\beta_{12}a_2+\beta_{13}a_3], \\ x_2 &= (1-\alpha)[\beta_{21}a_1+(1+\beta_{22})a_2+\beta_{23}a_3], \\ x_3 &= (1-\alpha)[\beta_{31}a_1+\beta_{32}a_2+(1+\beta_{33})a_3]. \end{aligned} \tag{2}$$

From these we find the partial derivatives:

$$\begin{aligned} \partial x_r/\partial a_s &= (1-\alpha)(\delta_{rs}+\beta_{rs}); \\ \partial a_r/\partial x_s &= (\delta_{rs}-\beta_{rs})/(1-\alpha); \\ r, s &= 1, 2, 3. \end{aligned} \tag{3}$$

Here δ_{rs} is equal to 1 for $r=s$, to 0 for $r\neq s$; squares of β_{rs} have been neglected.

Putting ρ_0 for the initial unstrained density, ρ for the density in the strained state, with V_0 and V for the corresponding specific volumes, we have the mathematical identities,

$$\rho/\rho_0 = V_0/V = \begin{vmatrix} \frac{\partial a_1}{\partial x_1} & \frac{\partial a_1}{\partial x_2} & \frac{\partial a_1}{\partial x_3} \\ \frac{\partial a_2}{\partial x_1} & \frac{\partial a_2}{\partial x_2} & \frac{\partial a_2}{\partial x_3} \\ \frac{\partial a_3}{\partial x_1} & \frac{\partial a_3}{\partial x_2} & \frac{\partial a_3}{\partial x_3} \end{vmatrix}$$

$$= 1 \div \begin{vmatrix} \frac{\partial x_1}{\partial a_1} & \frac{\partial x_1}{\partial a_2} & \frac{\partial x_1}{\partial a_3} \\ \frac{\partial x_2}{\partial a_1} & \frac{\partial x_2}{\partial a_2} & \frac{\partial x_2}{\partial a_3} \\ \frac{\partial x_3}{\partial a_1} & \frac{\partial x_3}{\partial a_2} & \frac{\partial x_3}{\partial a_3} \end{vmatrix}. \tag{4}$$

Using the relations (3) and neglecting squares and higher powers of the β_{rs}, we obtain

$$V_0/V = (1-\beta_{11}-\beta_{22}-\beta_{33})/(1-\alpha)^3. \tag{5}$$

[6] F. Birch, J. App. Phys. 9, 279 (1938).

For all β's equal to zero, we have the exact formula, $V=V_0(1-\alpha)^3$.

Murnaghan has shown how finite strain may be treated rigorously from either of two viewpoints; by analogy with the similar situation in hydrodynamics these are termed the "Lagrangian" and the "Eulerian." In the "Lagrangian" scheme, the strain is described with the initial or unstrained coordinates (a_p) as the independent variables; in the "Eulerian" scheme, the coordinates (x_p) of the strained state are taken as independent. The two alternative sets of strain components are then, using Murnaghan's notation,

the Lagrangian strain components,

$$\eta_{rs}=\tfrac{1}{2}\left(\frac{\partial x_p}{\partial a_r}\frac{\partial x_p}{\partial a_s}-\delta_{rs}\right), \tag{6}$$

or the Eulerian strain components,

$$\epsilon_{rs}=\tfrac{1}{2}\left(\delta_{rs}-\frac{\partial a_p}{\partial x_r}\frac{\partial a_p}{\partial x_s}\right). \tag{7}$$

Except for a factor of $\frac{1}{2}$ for $r\neq s$, the η_{rs} are identical with the strain components given by Love for finite strain. They are also equal to $\frac{1}{2}\xi_{rs}$, where ξ_{rs} are the strain components used by Born and Misra and by Fürth. For infinitesimal strains, the η_{rs} and ϵ_{rs} become identical and (except for the factor $\frac{1}{2}$ for $r\neq s$) equal to the strain components of the classical theory.

For the particular strain defined by (2), these become

$$\begin{aligned}\eta_{rs}&=\delta_{rs}\eta+\beta_{rs}(1+2\eta),\\ \text{and}\qquad \epsilon_{rs}&=\delta_{rs}\epsilon+\beta_{rs}(1-2\epsilon),\end{aligned} \tag{8}$$

where η and ϵ are defined by

$$(1-\alpha)^3=(1+2\eta)^{\frac{1}{2}}=(1-2\epsilon)^{-\frac{1}{2}}. \tag{9}$$

The relations between the quantities α, η and ϵ and the density for hydrostatic compression, are tabulated for convenience in Table 1.

TABLE I. Comparative values of ϵ, α, and η for hydrostatic compression.

ρ/ρ_0	V/V_0	$-\epsilon$	α	$-\eta$
1.0	1.0	0	0	0
1.1	.909	0.0328	0.0313	0.0308
1.2	.833	.0646	.0590	.0572
1.3	.769	.0955	.0837	.0802
1.4	.714	.1257	.1061	.1005
1.5	.667	.1551	.1264	.1185
2.0	.500	.2937	.2063	.1850
3.0	.333	.5400	.3067	.2596
4.0	.250	.7599	.3700	.3016
5.0	.200	.9620	.4152	.3290
∞	0	∞	1.0000	.5000

3. STRESS-STRAIN RELATIONS

Murnaghan's fundamental contribution is the discovery that for finite, elastic, isothermal strain, the exact relation between the stress components T_{rs} and the strain is of the form

$$T_{rs}=\rho\frac{\partial\phi}{\partial\eta_{pq}}\frac{\partial x_r}{\partial a_p}\frac{\partial x_s}{\partial a_q}\equiv-2\rho\frac{\partial\phi}{\partial j_{pq}}\frac{\partial a_p}{\partial x_r}\frac{\partial a_q}{\partial x_s}; \tag{10}$$

$$r, s, p, q=1, 2, 3.$$

Here $j_{rs}=(\partial a_r/\partial x_p)(\partial a_s/\partial x_p)$, and tension is taken positive. In developing these expressions, all nine partial derivatives are to be formed; in this procedure we ignore the symmetry relations, $\eta_{pq}=\eta_{qp}$. Furthermore, it is supposed that the rotation has been removed from the strain, so that the matrix $\partial(x)/\partial(a)$ is symmetric.

The function ϕ is the Helmholtz free energy ($=E-TS$) per unit mass; for a given material, it is assumed to depend only on the strain components η_{rs} and the temperature. The second equality in (10) is the Eulerian form of the first; the two are identically equal. ϕ is equivalent to the function A of Born, who, while using finite strain components equivalent to η_{rs}, has used the "infinitesimal" form of (10) for finding the stress.

In an isotropic medium, ϕ depends upon the strain components by way of the strain invariants (for arbitrary rotation of coordinate axes) of the first, second and third orders and their various products. In this simplest case, the Eulerian form becomes

$$T_{rs}=\rho\left(\frac{\partial\phi}{\partial\epsilon_{rs}}-2\epsilon_{rp}\frac{\partial\phi}{\partial\epsilon_{ps}}\right). \tag{11}$$

Even in this case the stress matrix does not in general possess the same principal axes as the strain matrix η_{rs}, whereas the principal axes of the matrices T_{rs} and ϵ_{rs} coincide. Fürth's pro-

cedure amounts to taking the expression (11) for the isotropic medium, substituting η_{rs} for ϵ_{rs}, and finally applying this result, incorrect even for the isotropic case, to the problem of cubic symmetry. Only for the degenerate case of hydrostatic compression does this give a correct result.

4. THE FREE ENERGY FOR CUBIC SYMMETRY

In a crystalline medium, the form of the free energy ϕ must conform with the symmetry of the crystal; in other words, ϕ must be invariant for rotations of the coordinate axes corresponding to the covering operations. The forms of ϕ appropriate for the various classes of crystals have been developed for terms of the second order in the strain components, and constitute the basis of the classical theory of crystal elasticity. For the present work, it is desirable to extend the development to include terms of the third order in the strain components. The details of this process are given in the Appendix, where it is found that the third-order terms involve 6 new elastic constants for the most symmetrical classes of cubic crystals, 8 for the cubic classes of lower symmetry, and 56 for triclinic symmetry. Most actual cubic crystals belong to the class of highest symmetry and the further developments pertain to this case; the required modification for the other case is slight and easily made.

The free energy, including third-order terms but omitting terms independent of strain, is thus:

$$\begin{aligned}\rho_0\phi=&(c_{11}/2)(\eta_{11}^2+\eta_{22}^2+\eta_{33}^2)+c_{12}(\eta_{11}\eta_{22}+\eta_{22}\eta_{33}+\eta_{33}\eta_{11})+c_{44}(\eta_{12}^2+\eta_{21}^2+\eta_{23}^2+\eta_{32}^2+\eta_{13}^2+\eta_{31}^2)\\&+C_{111}(\eta_{11}^3+\eta_{22}^3+\eta_{33}^3)+C_{112}\{\eta_{11}^2(\eta_{22}+\eta_{33})+\eta_{22}^2(\eta_{11}+\eta_{33})+\eta_{33}^2(\eta_{11}+\eta_{22})\}\\&+C_{123}\eta_{11}\eta_{22}\eta_{33}+C_{456}(\eta_{12}\eta_{23}\eta_{31}+\eta_{21}\eta_{13}\eta_{32})+(C_{144}/2)\{\eta_{11}(\eta_{23}^2+\eta_{32}^2)+\eta_{22}(\eta_{13}^2+\eta_{31}^2)\\&+\eta_{33}(\eta_{12}^2+\eta_{21}^2)\}+(C_{166}/2)\{(\eta_{11}+\eta_{22})(\eta_{12}^2+\eta_{21}^2)+(\eta_{22}+\eta_{33})(\eta_{23}^2+\eta_{32}^2)\\&+(\eta_{33}+\eta_{11})(\eta_{13}^2+\eta_{31}^2)\}. \qquad (12)\end{aligned}$$

For ease in forming the relations (11) the equalities $\eta_{rs}=\eta_{sr}$ have been ignored in (12). Rather than ϕ, the product $\rho_0\phi$ has been expanded so that the second-order coefficients will equal those of Voigt, which are derived from the energy per unit volume. The C's with triple indices are the new "third-order" coefficients. For a given material, the c's and C's are functions only of the temperature. This differs from Born's development of the free energy in which the c's are functions of both pressure and temperature.

This expansion is based on the assumption that there is always a state of zero strain under no external forces for any temperature at which the crystal can exist. Energy dependent upon the temperature alone may be included in an additive term which, being independent of the strain, plays no part in the following treatment of isothermal processes. Thermal expansion does not constitute a strain in the sense of the present theory, and no special significance is attached to absolute zero.

The third-order terms of the free energy have been given by Born and Misra[5] for a cubic Bravais lattice with central forces between particles at absolute zero. In this special case, Cauchy's relation holds: $c_{12}=c_{44}$, and by comparison with (12) the following relations among third-order coefficients are found:

$$C_{456}=8C_{123};\quad C_{144}=2C_{123};\quad C_{166}=4C_{112}. \qquad (13)$$

Cauchy's relation is rarely satisfied by real crystals, and it seems probable that the relations (13) are also rarely valid.

When, however, (13) is assumed to hold, the third-order coefficients may be expressed in terms of the 5 lattice sums computed by Born and Misra, as follows:

$$\begin{aligned}&c_{11}=8\mathfrak{C}(2), && C_{111}=8\mathfrak{C}(3),\\&c_{12}=8\mathfrak{C}(1,1), && C_{123}=48\mathfrak{C}(1,1,1), \qquad (14)\\& && C_{112}=24\mathfrak{C}(2,1).\end{aligned}$$

The expansion of ϕ in terms of the matrix j_{rs} might prove awkward in the general case, but for the particular strain (2) it is possible to express the j_{rs} in terms of the Eulerian strains,

ϵ_{rs}. Since

$$j_{pq}=\frac{\partial a_p}{\partial x_r}\frac{\partial a_q}{\partial x_r}, \quad \text{and} \quad \frac{\partial a_p}{\partial x_r}=(1-\alpha)^{-1}(\delta_{pr}-\beta_{pr}),$$

we find

$$j_{pq}=(1-\alpha)^{-2}(\delta_{pq}-2\beta_{pq})=\delta_{pq}-2\epsilon_{pq}. \quad (15)$$

Assuming that in this case, ϕ is expressible in terms of ϵ_{pq}, we may replace $\partial\phi/\partial j_{pq}$ by $-\frac{1}{2}(\partial\phi/\partial\epsilon_{pq})$. Also ϕ must have the same symmetry in terms of the ϵ_{rs} as in terms of the η_{rs}, and the second-order coefficients must be the same, since the expressions must coincide for infinitesimal strain, where ϵ_{rs} and η_{rs} become indistinguishable. Thus we obtain an expansion for $\rho_0\phi$ in terms for ϵ_{rs} exactly like (12), except that we write ϵ_{rs} instead of η_{rs}, and introduce new third-order coefficients, D_{111} and so on in place of the corresponding C's.

These expressions for ϕ must be identical, and hence there must be relations between the C's and the D's. One such relation is readily found by considering a hydrostatic strain, letting $\beta_{rs}=0$, and putting both expressions in terms of α. We have first, in terms of η,

$$\rho_0\phi=\tfrac{3}{2}\eta^2C_2+\eta^3C_3+\eta^4C_4+\cdots;$$

in terms of ϵ, (16)

$$\rho_0\phi=\tfrac{3}{2}\epsilon^2C_2+\epsilon^3D_3+\epsilon^4D_4+\cdots;$$

where

$$C_2=c_{11}+2c_{12}; \quad C_3=3C_{111}+C_{123}+6C_{112};$$
$$D_3=3D_{111}+D_{122}+6D_{112};$$

and C_4, $D_4\cdots$ are possible coefficients of higher order terms. On substituting α for ϵ and η according to (9), and identifying the coefficients of like powers of α in the two expressions, we obtain:

$$D_3=C_3+6C_2; \quad D_4=C_4+6C_3+18C_2, \text{ etc.} \quad (17)$$

Evidently the identity of the two formulations can be assured to any power of α by the addition of terms of higher order. Where C_3 has been calculated from lattice theory or otherwise, D_3 may be found by (17). Other relations may be found by taking other types of strain. Thus if we take $\beta_{12}\neq 0$, we find

$$D_{144}+2D_{166}=C_{144}+2C_{166}+16c_{44}+4c_{11}+8c_{12}. \quad (18)$$

In deriving this identity, care must be taken to include second-power terms of β_{12}; the approximations (8) should not be used.

These formulations of the free energy are not dependent upon the form of the potential between particles, except insofar as the numerical values of the coefficients, c's, C's, and D's, are concerned.

5. EFFECT OF PRESSURE ON ELASTIC CONSTANTS

The symmetry of a cubic crystal is preserved under hydrostatic compression, so that the relations between the additional stresses and the infinitesimal additional strains must have the same form as for a cubic crystal under infinitesimal strain at zero pressure, but the effective elastic "constants" will depend upon the pressure. These relations now follow; the algebra, which is tedious, is omitted. By substituting in (10) and noting that the density is given by (5) and (9), we find, for example,

$$T_{11}=(1+2\eta)^{-\frac{1}{2}}(1+\beta_{11}-\beta_{22}-\beta_{33})(\partial\phi/\partial\eta_{11}), \quad (19)$$

neglecting higher powers of the β's.

We now set $T_{11}=-P+T_{11}'$ and write T_{11}' in terms of the β's and a new set of elastic constants, c_{11}', c_{12}', and c_{44}', which depend upon P. Expanding (19) and identifying the coefficients, we find

$$T_{11}'=c_{11}'\beta_{11}+c_{12}'(\beta_{22}+\beta_{33}); \quad (20)$$

$$-P=\eta(1+2\eta)^{-\frac{1}{2}}(c_{11}+2c_{12}+\eta C_3+\cdots); \quad (21)$$

$$c_{11}'=(1+2\eta)^{-\frac{1}{2}}\{c_{11}+\eta(3c_{11}+2c_{12}+6C_{111}+4C_{112})+\eta^2(15C_{111}+C_{123}+14C_{112})+\cdots\};$$
$$c_{12}'=(1+2\eta)^{-\frac{1}{2}}\{c_{12}+\eta(C_{123}+4C_{112}-c_{11})+\eta^2(C_{123}+2C_{112}-3C_{111})+\cdots\}. \quad (22)$$

Similarly, expanding $T_{12}=T_{12}'=2c_{44}'\beta_{12}$,

$$2c_{44}'=(1+2\eta)^{-\frac{1}{3}}\{2c_{44}+\eta(4c_{44}+2c_{11}+4c_{12}+C_{144}+2C_{166})$$
$$+\eta^2(6C_{111}+2C_{123}+12C_{112}+2C_{144}+4C_{166})+\cdots\}. \quad (23)$$

To the first power in η these become

$$c_{11}'=c_{11}+\eta(2c_{11}+2c_{12}+6C_{111}+4C_{112});$$
$$c_{12}'=c_{12}+\eta(C_{123}+4C_{112}-c_{11}-c_{12}); \quad (24)$$
$$c_{44}'=c_{44}+\eta(c_{44}+c_{11}+2c_{12}+C_{144}/2+C_{166});$$

also

$$c_{11}'+2c_{12}'=c_{11}+2c_{12}+2\eta C_3=C_2+2\eta C_3. \quad (25)$$

The three parameters c_{11}', c_{12}', and c_{44}' determine completely the response of the compressed crystal to the additional small strains. The constants for the bending, extension, or twisting of variously oriented bars or plates under pressure are found by substituting these parameters in Voigt's formulas in place of the c_{11}, c_{12}, and c_{44}. The equations of small motion in the compressed medium are found from T_{rs} in the usual way, the displacements being the u_p' defined in (1). For uniform pressure, the stress equations of equilibrium involve only the derivatives of T_{rs}'.

Parallel development in the Eulerian form leads to:

$$T_{11}=-P+T_{11}'=(1-2\epsilon)^{5/2}(1-3\beta_{11}-\beta_{22}-\beta_{33})(\partial\phi/\partial\epsilon_{11}); \quad (26)$$

$$-P=\epsilon(1-2\epsilon)^{5/2}[c_{11}+2c_{12}+\epsilon D_3+\cdots]; \quad (27)$$

$$c_{11}'=(1-2\epsilon)^{5/2}\{c_{11}-\epsilon(5c_{11}+6c_{12}-6D_{111}-4D_{112})-\epsilon^2(21D_{111}+3D_{123}+26D_{112})+\cdots\};$$
$$c_{12}'=(1-2\epsilon)^{5/2}\{c_{12}-\epsilon(c_{11}+4c_{12}-D_{123}-4D_{112})-\epsilon^2(3D_{111}+3D_{123}+14D_{112})+\cdots\};$$
$$2c_{44}=(1-2\epsilon)^{5/2}\{2c_{44}-\epsilon(4c_{44}+2c_{11}+4c_{12}-D_{144}-2D_{166})$$
$$-\epsilon^2(6D_{111}+2D_{123}+12D_{112}-2D_{144}-4D_{166})+\cdots\}. \quad (28)$$

To the first power in ϵ,

$$c_{11}'=c_{11}-\epsilon(10c_{11}+6c_{12}-6D_{111}-4D_{112}),$$
$$c_{12}'=c_{12}-\epsilon(c_{11}+9c_{12}-D_{123}-4D_{112}), \quad (29)$$
$$c_{44}'=c_{44}-\epsilon(7c_{44}+c_{11}+2c_{12}-D_{144}/2-D_{166});$$

also

$$c_{11}'+2c_{12}'=c_{11}+2c_{12}-\epsilon(12C_2-2D_3)=C_2-\epsilon(12C_2-2D_3). \quad (30)$$

In this form it is clear that the c''s will all increase with the pressure if the D's are sufficiently small.

Since for small compressions, α, η and ϵ are all equal to the first order, we obtain further identified among the C's and D's:

$$D_{123}+4D_{112}\equiv C_{123}+4C_{112}+8c_{12};$$
$$3D_{111}+2D_{112}\equiv 3C_{111}+2C_{112}+6c_{11}+4c_{12}; \quad (31)$$

as well as the relations (17) and (18) already given. Since it appears that the C's are usually negative, while the second-order coefficients must be positive, the D's will be numerically smaller than the C's.

The relations between pressure and volume, and between pressure and compressibility, are of special interest as they offer the possibility of rationalizing a large mass of experimental data. For hydrostatic strain, we may set all $\beta_{rs}=0$, or we may put $\beta=\beta_{11}=\beta_{22}=\beta_{33}$, with the other β's zero. The former method is more direct; the latter may serve as a check. With the β's all zero, we have from (21), with $V_0/V=(1+2\eta)^{-\frac{1}{3}}$,

$$P=\tfrac{1}{2}[(V/V_0)^{-\frac{1}{3}}-(V/V_0)^{\frac{1}{3}}][C_2-C_3/2+(C_3/2)(V/V_0)^{\frac{1}{3}}+\cdots]. \quad (32)$$

Denoting the ordinary compressibility, $-(1/V_0)(\partial V/\partial P)_T$ by χ_0 and its reciprocal, the "bulk modulus" or "incompressibility" by K_0, we find for the limiting case of zero pressure,

$$(\partial K_0/\partial P)_{P=0}=1-(2C_3/3C_2). \tag{33}$$

In terms of ϵ, with $V_0/V=(1-2\epsilon)^{\frac{1}{2}}$,

$$P=\tfrac{1}{2}[(V_0/V)^{7/3}-(V_0/V)^{5/3}][C_2+D_3/2-(D_3/2)(V_0/V)^{2/3}+\cdots]. \tag{34}$$

$$(\partial K_0/\partial P)_{P=0}=5-(2D_3/3C_2). \tag{35}$$

But since $D_3=C_3+6C_2$, (33) and (35) are identical.

The same result is of course obtained if we put $\beta_{rs}=\beta\delta_{rs}$, where β is a small constant. In this case, we have $-\Delta P=T_{11}'=\beta(c_{11}'+2c_{12}')$, and $\Delta V/V_0=3\beta(1-\alpha)^3=3\beta(1-2\epsilon)^{-\frac{1}{2}}$; $K_0=-(V_0\Delta P)/\Delta V$, so that $K_0=\frac{1}{3}[C_2-\epsilon(15C_2-2D_3)+\cdots]=C_2/3+P(5-2D_3/3C_2)+\cdots$. Thus in the limit, for $P=0$, we have again (35). The combination $3/(c_{11}'+2c_{12}')$, gives the "instantaneous" compressibility, that is, the compressibility referred to the volume at the pressure P, rather than to the volume at zero pressure.

We may remark that all of these expressions become identical with those of the isotropic medium[6] on setting $c_{11}=\lambda+2\mu$, $c_{12}=\lambda$, and $c_{44}=\mu$.

It is also noteworthy that (33) and (35) are unchanged by the introduction of higher order terms in the free energy; terms contributed by powers of the strain higher than the third, disappear in passing to the limit of zero pressure. Equation (33) has also been found by Fürth.[4]

6. RELATIONSHIP TO OTHER THEORIES

Since ϕ is the Helmholtz free energy, it must satisfy the thermodynamic relation, $-P=(\partial\phi/\partial V)_T=-\rho^2(\partial\phi/\partial\rho)_T$, when the stress system degenerates to a hydrostatic pressure P. In this case, the stress-strain equations (10) take the form

$$-P=T_{11}=\rho\frac{\partial\phi}{\partial\eta_{11}}(1+2\eta_{11})=\rho\frac{\partial\phi}{\partial\epsilon_{11}}(1-2\epsilon_{11}). \tag{36}$$

But

$$\rho/\rho_0=[(1+2\eta_{11})(1+2\eta_{22})(1+2\eta_{33})]^{-\frac{1}{2}}$$
$$=[(1-2\epsilon_{11})(1-2\epsilon_{22})(1-2\epsilon_{33})]^{\frac{1}{2}}.$$

Hence

$$\partial\rho/\partial\eta_{11}=-\rho(1+2\eta_{11})^{-1},$$

and

$$\partial\rho/\partial\epsilon_{11}=-\rho(1-2\epsilon_{11})^{-1}.$$

Since for this case,

$$\partial\phi/\partial\eta_{11}=(\partial\phi/\partial\rho)(\partial\rho/\partial\eta)_{11}$$

and

$$\partial\phi/\partial\epsilon_{11}=(\partial\phi/\partial\rho)(\partial\rho/\partial\epsilon_{11}),$$

we verify at once that $-P=-\rho^2(\partial\phi/\partial\rho)_T$.

We might also have proceeded to find the compressibility and its change with pressure by successive differentiation of this general equation. Thus we have

$$K_0=-V_0(\partial P/\partial V)_T=V_0(\partial^2\phi/\partial V^2),$$

and

$$(\partial K_0/\partial P)_{P=0}=-V_0(\partial^3\phi/\partial V^3)_0/(\partial^2\phi/\partial V^2)_0;$$

or if we take a linear dimension such that $V=r^3$, we find

$$(\partial K_0/\partial P)_0=2-r_0(\partial^3\phi/\partial r^3)_0/3(\partial^2\phi/\partial r^2)_0. \tag{37}$$

The partial derivatives with respect to the volume may be obtained from (12) or its equivalent in terms of ϵ or η by using (5) and (9); we return to the relations already found.

If, however, the form of ϕ is known or assumed in terms of the interparticle distances and force constants, additional relations may be derived. With the power-law favored by Born, where the potential between two isolated particles is of the form $-ar^{-m}+br^{-n}$, (37) leads at once to the well-known expression $(\partial K_0/\partial P)_0=(9+m+n)/3$; this is strictly valid only for $T=0$. Thus we find that $D_3/C_2=3-(m+n)/2$ and $C_3/C_2=-3-(m+n)/2$. Conversely, if $(\partial K_0/\partial P)_0$ is known, the sum $(m+n)$ is determined. This method has been applied by Fürth[7]

[7] R. Fürth, Proc. Roy. Soc. **A183**, 87 (1944–45).

TABLE II. Relative values of third-order coefficients for power-law potential.

$(m+n)$	C_3/C_2	D_3/C_2	$(\partial K_0/\partial P)_0$
3	−4.5	+1.5	4.0
4	−5.0	+1.0	4.33
5	−5.5	+0.5	4.67
6	−6.0	0	5.00
7	−6.5	−0.5	5.33
8	−7.0	−1.0	5.67
9	−7.5	−1.5	6.00
10	−8.0	−2.0	6.33
11	−8.5	−2.5	6.67
12	−9.0	−3.0	7.00
14	−10.0	−4.0	7.67
16	−11.0	−5.0	8.33
18	−12.0	−6.0	9.00

in an effort to show that consistent values of m and n can be found from several independent experimental quantities.

As m and n are intrinsically positive, D_3 will always be smaller than C_3; values of the ratios of these coefficients to C_2 for various values of $(m+n)$ are shown in Table II. Since, as it will appear later, the most common experimental values for $(\partial K_0/\partial P)_0$ are in the neighborhood of 5, it may be justifiable for many purposes to neglect D_3/C_2 where the neglect of C_3/C_2 would introduce serious error. It is thus advantageous to treat most of the questions involving large compressions in terms of the Eulerian strain; the same results may be obtained with the Lagrangian form, but at the price of retaining terms of higher order.

Pressure-volume relations are furnished by Born and co-workers for a number of special cases, but the results are given in numerical form and comparison is not immediate, except for zero temperature. At $T=0$, however, it is readily found that the power-law potential leads to the general form,

$$P=\text{constant} \times[(V_0/V)^{(3+m)/3}-(V_0/V)^{(3+n)/3}]. \quad (38)$$

This equals (34) for $m=2$, $n=4$, in which case $D_3=0$. For other values of m and n, these expressions will be equal only with the inclusion of higher order terms in (34).

The higher order coefficients may be found for the special case of hydrostatic pressure by developing the power-law potential in terms of ϵ and of η. Putting $V_0/V=(r_0/r)^3$, we have $(r_0/r)=(1-2\epsilon)^{\frac{1}{2}}=(1+2\eta)^{-\frac{1}{2}}$. Then if

$$\rho_0\phi=A\left[\frac{1}{m}\left(\frac{r_0}{r}\right)^m-\frac{1}{n}\left(\frac{r_0}{r}\right)^n\right],$$

it follows that

$$\begin{aligned}\rho_0\phi=\text{constant}&+A\{(n-m)\epsilon^2/2!\\&-[(n-2)(n-4)-(m-2)(m-4)]\epsilon^3/3!\\&+[(n-2)(n-4)(n-6)\\&-(m-2)(m-4)(m-6)]\epsilon^4/4!-\cdots\}; \quad (39)\end{aligned}$$

and also that, alternatively,

$$\begin{aligned}\rho_0\phi=\text{constant}&+A\{(n-m)\eta^2/2!\\&-[(n+2)(n+4)-(m+2)(m+4)]\eta^3/3!\\&+[(n+2)(n+4)(n+6)\\&-(m+2)(m+4)(m+6)]\eta^4/4!-\cdots\}. \quad (39a)\end{aligned}$$

Whenever m and n are both even integers, the development in ϵ becomes simply a polynomial; if either m or n is odd, (39) gives an infinite series which ultimately diverges for very high compressions (see Table I). It is hardly to be expected that the assumed power-law potential remains valid for such compressions, regardless of its suitability for small volume changes. The expression in η is always convergent, since $|\eta|$ never exceeds $\frac{1}{2}$, for compression; but also it is never a polynomial. The terminating property of (39) possibly accounts in part for its usefulness in dealing with reasonably large compressions. Except for ionic crystals, good approximations to the potential can probably always be obtained with even values of m and n (within the scope of usefulness of the power-law form of potential) and it seems unlikely that the larger of these

TABLE III. c_{44}'/c_{44} as function of volume.

ξ	-2ϵ	V_0/V	c_{44}'/c_{44} (Birch)	c_{44}'/c_{44} (Gow)
				$m=6$, $n=12$
0	0	1.000	1.000	1.000
0.05	0.0164	1.0247	1.125	1.193
.10	.0323	1.0488	1.247	1.405
.15	.0477	1.0724	1.363	1.635
				$m=4$, $n=8$
0.05	0.0247	1.0375	1.189	1.207
.10	.0495	1.075	1.378	1.436
.15	.0818	1.125	1.625	1.711

need ever exceed 12. For $n=12$, the expansion terminates with the sixth power of ϵ. Smaller values seem more suitable for most of the metals. The expansion in ϵ is given below for several pairs of values of m and n.

For $m=2$, $n=4$; $\rho_0\phi=\text{constant}+A\epsilon^2$.
For $m=2$, $n=6$; $\rho_0\phi=\text{constant}+A'\epsilon^2(1-\frac{3}{4}\epsilon)$.
For $m=4$, $n=8$; $\rho_0\phi=\text{constant}+A''\epsilon^2(1-2\epsilon+\epsilon^2)$.
For $m=1$, $n=8$; a good approximation for most of the alkali halides,[8] $\rho_0\phi=\text{constant}+A'''\epsilon^2\times(1-\epsilon+\frac{3}{4}\epsilon^2+\frac{1}{4}\epsilon^3+\cdots)$.

These expressions are found from the power-law potential and hence possess the same restriction to zero temperature, but it appears probable that the differential effect of temperature upon the coefficients of the various powers of ϵ will not be great, at least for moderate temperatures, and hence that the values for such ratios as D_3/C_2, D_4/C_2 and so on, which are immediately obtainable from the above expansions for zero, will be approximately valid at higher temperatures. We notice that for $m=2$, $n=4$, we have D_3 and all higher order D's equal to zero, and the pressure is given by the relatively simple expression, $P=\text{constant}\times[(V_0/V)^{7/3}-(V_0/V)^{5/3}]$. D_3 depends only upon $(n+m)$ but the other terms depend upon the individual values of n and m. Thus for $m=2$, $n=6$, D_4 and higher coefficients are zero, while for $m=1$, $n=7$, $D_4/C_2=9/8$, $D_5/C_2=3/8$, and so on.

In treatments which deal only with the case of hydrostatic pressure, development of the potential in terms of strain components is of course unnecessary; any function of the volume may serve, subject to certain restrictions. Thus Slater expands the free energy in terms of $(1-r/r_0)$. This is equal to $1-(1+2\eta)^{\frac{1}{2}}$ which becomes approximately $-\eta$ for small compressions. If, however, the individual elastic constants are of interest and not merely the compression and its various derivatives, it is necessary to expand the free energy in terms of the strain components, as has been done by Born and his associates, using the equivalent of η_{rs}. It is possible that in the general case, as well as in the special case of hydrostatic compression, the use of the ϵ_{rs} instead of the η_{rs} might lead to more rapidly convergent results.

[8] J. C. Slater, *Introduction to Chemical Physics* (McGraw-Hill Book Company, Inc., New York, 1939), p. 393.

TABLE IV. Calculated effect of pressure on c_{44}' for several substances.

Substance	$7+(c_{11}+2c_{12})/c_{44}$	$\frac{1}{c_{44}}\frac{\partial c_{44}'}{\partial P}$ (P in bars)
Na	9.85	70.2×10^{-6}
Cu	12.60	2.97
Ag	13.86	4.63
Au	20.2	3.83
Al	15.28	6.59
W	13.02	1.41
Fe	11.46	2.22
MgO	10.0	2.15
NaCl	12.74	17.2
KBr	14.22	31.8
CaF_2	14.52	5.7

A paper by Miss Gow[9] gives the variation with pressure (and temperature) of all of the elastic constants for face-centered monatomic cubic lattices, using a potential of the form just considered; the lowest values of m and n for which calculations are presented are $m=4$, $n=8$. The results are given in numerical tables, in terms of a parameter ξ related to the volume by $(1+\xi)=(V_0/V)^{(n-m)/3}$. Comparison with the results of this paper can be carried out by computing the changes of the corresponding elastic constants for the same changes of volume. This has been done for c_{44} in Table III, where we have taken the approximate form of (29), neglecting the third-order coefficients D_{144} and D_{166}:

$$c_{44}'/c_{44}=1-\epsilon[7+(c_{11}+2c_{12})/c_{44}]. \quad (40)$$

As shown in Table IV, the coefficient of ϵ in (40) varies between 10 and 20 for various materials, most of the values falling near 14. In Table III, the figure 15.28, the value for aluminum, has been used.

Miss Gow gives

$$c_{44}/P_0=(V_0/V)[A_3/u+B_4T/\theta],$$

where A_3/u and B_4 are tabulated as functions of ξ; P_0, θ are constants, T the absolute temperature. This c_{44} is equivalent to our c_{44}'. For comparison with (29), we form the ratio for $T=0$, $c_{44}'(\xi)/c_{44}(0)=(V_0/V)[A_3(\xi)/A_3(0)]$; this ratio is not greatly affected by including the

[9] Margaret M. Gow, Proc. Camb. Phil. Soc. 40, 151 (1944).

TABLE V. Experimental values of change of compressibility with pressure: elements (pressure in bars).*

Element	t°C	$10^6 a$	$10^{12} b$	$2b/a^2=(\partial K_0/\partial P)_0$
W	30	0.32	0.1	2
	75	.32	.2	4
Pt	30	.363	.3	5
Rh	30	.364	1.5	23
Cr	30	.525	.9	7
Ni	30	.535	.9	6
	75	.541	.8	5
Pd	30	.534	.9	6
Co	30	.546	.8	5
B	30	.558	.8	5
Au	30	.584	2.0	12
	75	.577	.8	5
Cb	30	.577	.9	5
Fe	24	.5941	.83	4.7 (to 30,000)
(Ebert)**	20	.603	1.37	7.5 (to 5,000)
V	30	.617	1.35	7.1
Cu	30	.729	1.6	6.0
		.7182	.9	4 (to 30,000)
(Ebert)**	20	.731	2.6	9.7 (to 5,000)
Mn	30	.803	4.2	13
Ag	30	1.002	3.7	7.4
(Ebert)**	20	1.025	1.9	3.6 (to 5,000)
Al	30	1.365	4.9	5.3
		1.328	3.7	4.2 (to 30,000)
(Ebert)**	20	1.370	3.1	3.3 (to 5,000)
(Birch)	23	1.378	7.2	7.6 (to 10,000)
Ge	30	1.435	4.8	4.6
Th	30	1.850	12	7
Pb	30	2.415	19.6	6.8
		2.340	10.2	3.7 (to 30,000)
(Birch)	20	2.354	14.3	5.1 (to 10,000)
(Ebert)**	20	2.448	14.5	4.9 (to 5,000)
Pr	30	3.451	12.2	2.0
La	30	3.578	13.9	2.2
Ca	30	5.805	65	3.9 see Table VIII
Sr	30	8.278	103	3.0
Ba	30	10.39	133	2.5

* Unless otherwise noted, the measurements are by P. W. Bridgman, and the range is 12,000 kg/cm². Several corrections have been applied to the values published in the original papers and in *The Physics of High Pressure* (Bell and Sons, London, England, 1931), notably for the new value of b for iron given in Proc. Am. Acad. Arts Sci. **74**, 11–20 (1940). See also Proc. Am. Acad. Arts Sci. **70**, 285–317 (1935), and Rev. Mod. Phys. **18**, 1 (1946). Corrected values, expressed as above in bars rather than in the original kg/cm², are tabulated in *Handbook of Physical Constants*, Special Paper No. 36, published by the Geological Society of America, Section 4. Values of a and b for the new measurements on Cu, Pb and Al, still unpublished, were computed by Birch. Entries marked "Ebert" are from H. Ebert, Physik. Zeits. **36**, 388 (1935). Those marked "Birch" are from F. Birch and R. R. Law, Bull. Geol. Soc. Am. **46**, 1219 (1935).

** Single crystal.

temperature terms. Values of the ratio, as a function of volume, are given in Table III, for $m=6$, $n=12$, and for $m=4$, $n=8$. Again it is clear that better agreement would exist for smaller values of m and n.

The magnitude of the neglected terms in (29), $(D_{144}+2D_{166})/2$, relative to the quantity retained, $(7c_{44}+c_{11}+2c_{12})$, may be estimated by using Fürth's evaluation[4] of the third-order coefficients, and the identity (18). The C's and the c's are given in terms of the quantity $\mathfrak{C}(2)$ for certain combinations of m and n. In this way, it may be estimated that for the face-centered cubic lattice, with $m=4$, $n=8$, the neglected terms would increase the pressure coefficient by about 14 percent; for $m=4$, $n=6$, the neglected terms would reduce the coefficient by about 4 percent. The few experimental determinations[10] of the effect of pressure on rigidity support the calculated values of Table IV: the measured values of the relative change of rigidity with pressure are $2.7\cdot10^{-6}$ for copper, $7.6\cdot10^{-6}$ for aluminum, and $2.36\cdot10^{-6}$ for steel (P in bars). However, these are for polycrystalline materials, and are not strictly comparable with the calculated values for a particular direction in the crystal, although it seems probable that the effect will not differ greatly for different orientations.

The correction to Born's theory arising from the stress-strain relation (10) for finite strain will apply only to the expressions for the elastic constants; the pressure-volume relation escapes this correction, since it is based on the exact thermodynamic relation for the pressure as volume derivative of the free energy. The relation (10) should be regarded as the exact extension of this thermodynamic relation to the general finite strain.

7. COMPARISON WITH MEASUREMENTS OF COMPRESSION

The compression of a large number of materials crystallizing in the cubic system has been measured over pressure ranges sufficiently great to establish a definite departure from linearity. Most of the measurements have been made by Bridgman, who has extended the working range from about 12,000 kg/cm² in his early work to 100,000 kg/cm² in recent publications. The results for the lower ranges are usually given in the form, $-\Delta V/V_0=aP-bP^2$, where ΔV is the change of volume from the initial volume V_0 at zero pressure, to the pressure P; a and b depend upon the temperature. Thus, at constant temperature, $(\partial K_0/\partial P)_0=2b/a^2$. Table V includes the measurements for all of the elements of cubic symmetry except for those of high compressibility (Table VII and VIII), and several (Mo, Ta, Ce) which show anomalous

[10] P. W. Bridgman, Proc. Am. Acad. **63**, 401 (1929); F. Birch, J. App. Phys. **8**, 129 (1937).

negative values of b. Table VI includes measurements for a number of cubic compounds. Measurements made before 1940 have been corrected to the new value determined for iron at that time; this correction amounts to a reduction of the former values for b by about $1.5 \cdot 10^{-12}$ and is thus of importance for the materials of low compressibility.

Most of the values of $2b/a^2$ in both Table V and Table VI lie between 4 and 7; if the distribution is considered to represent a normal probability curve, the most probable value for the elements is about 4.5 with a half-width of about 0.5, an amount not inconsistent with the experimental uncertainty when reasonable allowance is made for such defects of material as initial strains and porosity. Occasional deviations seem to be of this character, as for gold, where an erratic value occurs for 30°C, a normal one for 75°C. The values for rhodium and for manganese are almost certainly erratic. The most probable value for the compounds is between 5 and 6. The only significant deviation is for the sulfides and perhaps certain fluorides, where $2b/a^2$ is about 12. It is noteworthy that the latest and most precise measurements, to 30,000 kg/cm², show even lower values for $2b/a^2$ than the earlier ones for such relatively reliable materials as Al, Pb, and Cu. Figures lower than 5 mean positive values of D_3, and correspond to very small exponents in the power-law potential (Table II). Low values occur both at the beginning and end of Table V, which is arranged in the order of increasing compressibility. Not too much weight should be attached to the low value for tungsten, where the experimental error must be relatively large; but the same reasoning would suggest that the values for Ca and Sr should be very reliable. Other data for Ca in Table VIII demonstrate a more "normal" variation.

Slater[11] has concluded that 5 is probably the best general value of $2b/a^2$ for the metals; this leads to a figure of 1.833 for Gruneisen's constant, as compared with about 2.4 preferred by Fürth. An outstanding feature of Tables V and VI is the evidence that $(\partial K_0/\partial P)_0$ has approximately the same value for such diverse materials as metals and various types of ionic compounds.

[11] J. C. Slater, Phys. Rev. **57**, 744 (1940).

TABLE VI. Experimental values of change of compressibility with pressure: compounds. Measurements at 30°C (P in bars).*

Compound	$10^6 a$	$10^{12} b$	$2b/a^2$	
TiN	0.334	0.87	16	
TiC	.477	.8	7	
Pyrope (garnet)	.545	.9	6	
Fe_3O_4	.547	.82	5.5	
MgO	.598	1.0	5.5	
Andradite (garnet)	.673	.86	3.8	
Fe_2S	.68	.87	3.8	
CoAsS	.767	1.88	6.4	
CdF_2	1.120	7.5	12	
ZnS	1.303	1.28	1.5	
	1.258	5.4	6.8	(to 50,000)
CaF_2	1.226	6.49	8.7	
LiF (S)	1.53	7.6	6.5	
	1.52	5.5	4.8	
SrF_2	1.607	9.4	7.3	
PbS	1.869	7.43	4.3	
Cu_2O	1.943	19.3	10.1	
BaF_2	1.964	14	7.3	
NaF	2.11	17	7.7	
CaS	2.321	39	14.5	
SrS	2.426	38.8	13.2	
CuCl	2.508	13.3	4.2	
CuI	2.802	24.8	6.3	
BaS	2.946	52.8	12.1	
Ag_2S	3.265	49.5	9.4	
KF (S)	3.30	32	5.9	
LiCl (S)	3.40	32.3	5.6	
NaCl	4.260	51	5.6	see Table IX
LiBr (S)	4.30	51	5.6	
$NaBrO_3$	4.401	76	7.8	
$NaClO_3$	5.033	95	7.5	
NaBr (S)	5.07	63	4.9	see Table IX
KCl (S)	5.62	75	4.8	
CsCl	5.94	99.5	5.7	see Table IX
LiI	6.00	110	6.1	
KBr (S)	6.70	105	4.7	
CsBr	7.05	149	6.0	see Table IX
RbBr (S)	7.93	137	4.4	
KI (S)	8.53	155	4.3	
CsI	8.565	209	5.7	see Table IX
RbI (S)	9.56	204	4.5	

* All measurements by P. W. Bridgman (see references for Table V) except those marked "S," which are by J. C. Slater, Phys. Rev. **23**, 488 (1924).

This is understandable if the ratio $(-D_3/C_2)$, which is the part of $(\partial K_0/\partial P)_0$ which depends upon the individual peculiarities of the interparticle forces, is generally no greater than unity, or in other terms, $(m+n)$ no greater than 8 or 9.

The same conclusion may be reached by examining the striking body of data for compressions up to 100,000 kg/cm² given in two papers by Bridgman, as well as some earlier results to 45,000. The data are given as $-\Delta V/V_0$ for various pressures. In a number of instances the density was more than doubled, and in many cases, raised by 25 percent or more. Taking the pressure-volume relation in the form (34), we

TABLE VII. Compression of the alkali metals to 45,000 kg/cm², and values of F/P.*

P in 10^3 kg/cm²	Li		Na		K		Rb		Cs	
	V/V_0	F/P	V/V_0	F/P	V/V_0	F/P	V/V_0	F/P	V/V_0	F/P
5	0.957	641	0.929	113	0.884	210	0.826	374	0.818	401
10	.926	599	.883	107	.817	202	.767	301	.729	397
15	.899	584	.852	98	.770	196	.721	280	.674	387
20	.875	581	.818	100	.732	194	.684	271	.628	395
25	.855	573	.791	100	.699	196	.655	264	.586	417
30	.835	577	.767	100	.671	197	.629	261	.568	392
35	.816	581	.746	100	.647	199	.607	259	.542	400
40	.798	591	.727	101	.627	199	.587	259	.519	409
45	.782	597	.710	101	.604	206	.569	260	.499	417

* P. W. Bridgman, Phys. Rev. **57**, 237 (1940); Proc. Am. Acad. Arts Sci. **72**, 207 (1938).

TABLE VIII. Compressions to 100,000 kg/cm² and values of F/P.*

P in 10^3 kg/cm²	Li		Na		K		Rb		Ca	
	V/V_0	F/P	V/V_0	F/P	V/V_0	F/P	V/V_0	F/P	V/V_0	F/P
10	0.926	598	0.883	106	0.817	202	0.767	301	0.942	449
20	.875	581	.818	100	.732	194	.684	271	.897	451
30	.835	575	.767	100	.671	197	.629	261	.861	449
40	.798	591	.727	101	.627	199	.587	259	.832	443
50	.763	621	.690	104	.581	216	.538	288	.805	447
60	.728	668	.657	108	.543	232	.499	313	.780	454
70	.695	720	.628	112	.508	252	.461	351	(Transition)	
80	.664	776	.603	116	.478	272	.425	401		
90	.634	842	.581	120	.451	293	.392	459		
100	.606	913	.560	124	.427	316	.362	527		

* P. W. Bridgman, Proc. Am. Acad. Arts Sci. **74**, 425 (1942); or Phys. Rev. **60**, 351 (1941).

see that if it is permissible to neglect D_3/C_2, we obtain the simpler form,

$$P = FC_2/2,$$

with

$$F = [(V_0/V)^{7/3} - (V_0/V)^{5/3}]. \qquad (41)$$

The ratio F/P is in this case a constant, $2/C_2 = 2\chi_0/3$. The following test has been applied to the measurements of Tables VII, VIII, and IX: F has been formed from the measured values of V_0/V and divided by the corresponding measured pressures. The test is extremely sensitive since F varies rapidly with V_0/V. All, or nearly all, of the measurements of inorganic cubic materials have been included except those which show polymorphic changes in the pressure range, a fairly large fraction of the whole.

Let us first examine the alkali metals in the 45,000 kg/cm² range, shown in Table VII. F/P is constant within the precision of the measurements for all of these metals except Rb, where there is an abnormally high initial compressibility; the first value for Li also deviates widely. For the others, the initial compressibility can be obtained with an error of less than about 10 percent from any single volume determination. There is no particular trend which would suggest that improved agreement would result from the next approximation, with a non-zero D_3.

The measurements on the alkali metals to 100,000 kg/cm² (Table VIII), do show a definite trend, with F/P increasing beyond 50,000, by roughly 50 percent for Li and K, nearly 100 percent for Rb, and about 20 percent for Na. The values above 50,000 can be fitted by including a term in D_3, as in (34), but D_3 turns out to be large and positive and far beyond any value compatible with the measurements below 50,000. It seems fairly clear that the determinations for these two ranges are not mutually consistent. Bridgman has discussed the possible sources of fairly large errors in the higher range. In view of later determinations to 100,000, we may conclude that the abnormal behavior of the alkali metals above 50,000 is somehow connected with the method of correcting the data, which was improved in the later work. For example, as shown in Table IX, if the data for indium (a tetragonal crystal) given in the two papers (1942 and 1945) are reduced in the same way, we find that F/P increases in the former, though much less than for the alkali metals, whereas it decreases in the latter.

A decrease or approximate constancy of F/P is characteristic of the 1945 determinations, shown in Table IX. The decrease is readily accounted for by restoring D_3, which may be evaluated by plotting P/F *versus* $(V_0/V)^1$; according to (34) this should be a straight line. In a fairly typical case, we find $D_3/C_2 = -0.8$ for CsI. This corresponds to a value of 5.53 for $2b/a^2$, whereas from Table VI, we find 5.7; and from Table II, $(m+n)$ between 7 and 8.

With the retention of the constant D_3, the measurements of Table IX can all be reproduced with an error not exceeding about 3 percent on the pressure. This is probably less than the experimental error of pressure determination for this range, and there is some indication from the data that the experimental pressures may be perhaps 10 percent lower than supposed. We reach this conclusion by observing that the ratio $(F/P)_{10,000}$ to $(F/P)_{100,000}$ is close to 1.1 for 9 of

the 14 materials of Table IX; it is nearly constant for AgCl and CsBr and equal to about 1.2 for CsCl and $TlNO_3$. There appears to be no correlation with the amount of compression.

The approximate form (41) thus gives the pressure corresponding to the extreme compression in terms of the measured compression at 10,000 with an error not exceeding 20 percent, and generally less than 10 percent for the entries of Table IX. This is probably not far from the limits of experimental precision for this range of pressure.

Bardeen[12] has calculated the zero-point energy as function of density for Li and Na by approximate quantum-mechanical methods, obtaining the energy in the form, $\phi = Ay^3 + By^2 - Cy$, with $y = (V_0/V)^{\frac{1}{3}}$. A, B, and C are constants which he calculates and compares with the experimental values. This leads to a formula for the pressure which is approximately,

$$P = \text{constant}[(V_0/V)^{5/3} - (V_0/V)^{4/3}], \quad (42)$$

equivalent to the form for a power-law potential with $m=1$, $n=2$. Comparison with experiment requires a somewhat uncertain reduction to absolute zero, and the numerical agreement for the constants is not very close. If, however, the constant of (42) is determined from the measured initial compressibility, the agreement with the measured compression of the alkali metals to 45,000 is very nearly as close as for (41). Fürth[7] has applied the power-law potential to some of the measurements to 100,000, with values of m and n larger than are implied by (41); the agreement with the experimental values is less good. It appears that larger values of the exponents in the force law are required to satisfy the experimental determinations of temperature effects than to fit the measurements of pressure effects. It may be questioned whether this is mainly the consequence of an inadequacy of this form of potential, of some approximation in Born's treatment of the entropy of the lattice, or of more fundamental causes, as suggested by Bridgman in a discussion of the implications of Schottky's theorem.[13]

8. CONCLUSION

Besides the application of the theory of finite strain to find the effect of pressure upon the elasticity of cubic crystals, we have attempted a clarification of certain questions regarding the

TABLE IX. Compressions of cubic compounds and values of F/P. Compression of indium.*

P in 10^3 kg/cm²	V/V_0 NaCl	F/P	V/V_0 CsCl	F/P	V/V_0 TlCl	F/P	V/V_0 AgCl	F/P	V/V_0 NaBr	F/P	V/V_0 CsBr	F/P	V/V_0 NH_4Br	F/P
10	0.962	279	0.952	362	0.962	279	0.979	145	0.957	321	0.947	405	0.951	370
20	.932	270	.914	359	.929	285	.960	149	.922	319	.905	406	.912	369
30	.907	264	.882	359	.901	285	.942	150	.893	315	.870	409	.880	367
40	.885	260	.856	353	.877	284	.926	149	.868	313	.840	411	.853	364
50	.865	258	.834	348	.856	282	.910	152	.847	309	.814	416	.830	361
60	.848	254	.816	338	.838	279	.896	152	.829	303	.792	413	.811	354
70	.832	253	.801	329	.823	274	.883	153	.814	296	.773	411	.795	346
80	.817	253	.788	319	.809	270	.871	152	.801	288	.757	405	.781	338
90	.803	252	.777	309	.798	262	.860	151	.789	282	.742	402	.768	332
100	.790	252	.767	301	.787	258			.778	277	.728	400	.756	327

	$TlNO_3$		NaI		CsI		TlI		Indium 1940		Indium 1942		Indium 1945	
10	0.963	271	0.944	429	0.935	513	0.950	379	0.978	155	0.977	166	0.9760	170
20	.932	270	.902	424	.887	508	.910	379	.958	156	.955	168	.9558	164
30	.905	271	.868	417	.849	505	.877	378	.940	155	.936	167	.9381	162
40	.882	266	.840	411	.818	501	.848	381	.925	152	.919	167	.9219	159
50	.863	264	.816	406	.792	496	.823	384	.913	146	.903	166	.9068	157
60	.848	255	.795	404	.770	490	.802	382			.888	167	.8928	157
70	.835	246	.777	398	.751	484	.784	378			.874	168	.8798	158
80	.824	238	.761	393	.734	479	.768	373			.860	170	.8676	156
90	.815	228	.747	388	.719	473	.755	366			.847	172	.8561	158
100	.806	222	.734	383	.706	467	.744	356			.835	173	.8451	157

* P. W. Bridgman, Proc. Am. Acad. Arts Sci. 76, 1 (1945), (Halogen compounds and indium); 74, 425 (1942), (Indium); 74, 21 (1940), (Indium).

[12] J. Bardeen, J. Chem. Phys. 6, 372 (1938).

[13] P. W. Bridgman, Rev. Mod. Phys. 7, 1 (1935).

scope of this theory. It is shown that there is no ambiguity: the alternative methods developed by Murnaghan lead to identical results for comparable approximations. The choice of method is a matter of convenience; for studies of large compressions, the Eulerian form furnishes simpler, more compact relations. Lattice theory does not conflict with this method; in cases where it can be sufficiently developed, it furnishes numerical values for the elastic constants in terms of atomic parameters, but many relations of a general nature are obtainable without a detailed specification of lattice structure and forces. The present method is valid for elastic strain at any constant temperature, and hence avoids the complexities which arise in lattice theory when temperatures other than zero are considered. It is shown that a relatively simple approximation accounts for practically all of the measurements at high pressure. The fact that this first approximation is also a good one, is shown to imply values for the exponents in a power-law form of potential considerably lower than have commonly been adopted.

9. ACKNOWLEDGMENTS

The kindness of Professors P. W. Bridgman and F. D. Murnaghan in reading and commenting on the manuscript is gratefully acknowledged, as is the assistance of Professor C. S. Hurlbut, Jr. with certain points of crystallographic terminology.

APPENDIX

Derivation of Third-order Terms of the Free Energy for Cubic Crystals

The general methods of taking into account the symmetry of a crystal for various properties are described in Voigt,[14] Wooster[15] and other texts on crystal physics, and the application to the second-order elastic coefficients is given in considerable detail in Love.[16] The symmetry of all classes of cubic crystals is such as to reduce the 21 possible second-order coefficients to 3. There are 56 possible distinct third-order coefficients, and this is the actual number for a triclinic crystal. Using the customary short notation, where we write 1 for the pair of indices 11, 2 for 22, 3 for 33, 4 for 23 and 32, 5 for 31 and 13, and 6 for 12 and 21, the 56 third-order terms are as follows where evidently $C_{pqr}=C_{prq}=C_{qpr}$ and so on:

$$
\begin{aligned}
&C_{111}\eta_1^3+C_{112}\eta_1^2\eta_2+C_{113}\eta_1^2\eta_3+C_{114}\eta_1^2\eta_4+C_{115}\eta_1^2\eta_5+C_{116}\eta_1^2\eta_6\\
&\quad+C_{122}\eta_1\eta_2^2+C_{123}\eta_1\eta_2\eta_3+C_{124}\eta_1\eta_2\eta_4+C_{125}\eta_1\eta_2\eta_5+C_{126}\eta_1\eta_2\eta_6\\
&\qquad+C_{133}\eta_1\eta_3^2+C_{134}\eta_1\eta_3\eta_4+C_{135}\eta_1\eta_3\eta_5+C_{136}\eta_1\eta_3\eta_6\\
&\qquad\quad+C_{144}\eta_1\eta_4^2+C_{145}\eta_1\eta_4\eta_5+C_{146}\eta_1\eta_4\eta_6\\
&\qquad\qquad+C_{155}\eta_1\eta_5^2+C_{156}\eta_1\eta_5\eta_6\\
&\qquad\qquad\quad+C_{166}\eta_1\eta_6^2\\
&+C_{222}\eta_2^3+C_{223}\eta_2^2\eta_3+C_{224}\eta_2^2\eta_4+C_{225}\eta_2^2\eta_5+C_{226}\eta_2^2\eta_6\\
&\qquad+C_{233}\eta_2\eta_3^2+C_{234}\eta_2\eta_3\eta_4+C_{235}\eta_2\eta_3\eta_5+C_{236}\eta_2\eta_3\eta_6\\
&\qquad\quad+C_{244}\eta_2\eta_4^2+C_{245}\eta_2\eta_4\eta_5+C_{246}\eta_2\eta_4\eta_6\\
&\qquad\qquad+C_{255}\eta_2\eta_5^2+C_{256}\eta_2\eta_5\eta_6\\
&\qquad\qquad\quad+C_{266}\eta_2\eta_6^2\\
&\qquad+C_{333}\eta_3^3+C_{334}\eta_3^2\eta_4+C_{335}\eta_3^2\eta_5+C_{336}\eta_3^2\eta_6\\
&\qquad\quad+C_{344}\eta_3\eta_4^2+C_{345}\eta_3\eta_4\eta_5+C_{346}\eta_3\eta_4\eta_6\\
&\qquad\qquad+C_{355}\eta_3\eta_5^2+C_{356}\eta_3\eta_5\eta_6\\
&\qquad\qquad\quad+C_{366}\eta_3\eta_6^2\\
&\qquad\quad+C_{444}\eta_4^3+C_{445}\eta_4^2\eta_5+C_{446}\eta_4^2\eta_6\\
&\qquad\qquad+C_{455}\eta_4\eta_5^2+C_{456}\eta_4\eta_5\eta_6\\
&\qquad\qquad\quad+C_{466}\eta_4\eta_6^2\\
&\qquad\qquad+C_{555}\eta_5^3+C_{556}\eta_5^2\eta_6\\
&\qquad\qquad\quad+C_{566}\eta_5\eta_6^2+C_{666}\eta_6^3.
\end{aligned}
$$

The crystallographers have amused themselves by inventing a variety of ways of designating the 32 crystal classes and of describing the elements of symmetry. Table X shows in parallel form a few of the proposals with regard to the 5 classes of cubic or isometric symmetry. Only two of these classes are characterized by the tetragonal symmetry about the three cubic axes which one might expect to be a common property; the other three classes possess digonal symmetry

[14] W. Voigt, *Lehrbuch der Kristallphysik* (B. G. Teubner, Leipzig, Germany, 1928).
[15] W. A. Wooster, *A Textbook on Crystal Physics* (The Cambridge University Press, New York, New York, 1938).
[16] A. E. H. Love, *A Treatise on the Mathematical Theory of Elasticity* (The Cambridge University Press, New York, New York, 1937).

TABLE X. Designations and elements of symmetry of the isometric classes.

Name or symbol of class					
Dana (Groth-Rogers)	Miers	Lewis	Hermann-Mauguin	Schoenflies	Elements of symmetry
Hexoctahedral (galena)	Ditesseral central	Cubic II	$\frac{4}{m}\ \bar{3}\ \frac{2}{m}$	$O^{(h)}$	C, $3A_4$, $4A_3$, $6A_2$
Gyroidal (cuprite)	Tesseral holoaxial	Cubic I	$4\ 3\ 2$	O	$3A_4$, $4A_3$, $6A_2$
Hextetrahedral	Ditesseral polar	Cubic V	$\bar{4}\ 3\ m$	$T^{(d)}$	$4A_3$, $3A_2$
Diploidal (pyrite)	Tesseral central	Cubic IV	$\frac{2}{m}\ \bar{3}$	$T^{(h)}$	C, $4A_3$, $3A_2$
Tetartoidal	Tesseral polar	Cubic III	$2\ 3$	T	$4A_3$, $3A_2$

Note: In the last column, C denotes a center of symmetry, A_4 an axis of fourfold symmetry, A_3 an axis of threefold symmetry, A_2 an axis of twofold symmetry. The numbers before the A's denote the number of such axes. This notation is used in Dana and Hurlbut's *Manual of Mineralogy* (John Wiley and Sons, Inc., New York, 1941) and is by far the most intelligible and useful to the reader unversed in crystallography. The Hermann-Mauguin symbols are to be found in the first volume of *International Tables for the Determination of Crystal Structures* (Borntraeger, Berlin, Germany, 1935). The other notation has been extracted from Love.

about these axes. All classes possess trigonal symmetry with respect to the 4 cube diagonals. This is expressed analytically as an invariance of properties under cyclic permutation of indices. Thus if the three original axes of coordinates are $X_1\,X_2\,X_3$, coinciding with a set of cubic axes, then rotation of 120° about a trigonal axis defines a new set of axes, $X_1'\,X_2'\,X_3'$, say, such that X_2' coincides with X_1, X_3' with X_2 and X_1' with X_3, for example. This corresponds to the scheme:

	X_1'	X_2'	X_3'
X_1	0	1	0
X_2	0	0	1
X_3	1	0	0.

The strain components referred to the new axes, η_{rs}', will be related to the strain components referred to the original axes by the general transformation equation for second-order tensors, $\eta_{rs}'=\alpha_{pr}\alpha_{qs}\eta_{pq}$, $p, q, r, s=1, 2, 3$, where α_{11} is the cosine of the angle between X_1 and X_1', and so on. For this transformation, this becomes simply

$$\eta_1'=\eta_3 \qquad \eta_4'=\eta_6$$
$$\eta_2'=\eta_1 \qquad \eta_5'=\eta_4$$
$$\eta_3'=\eta_2 \qquad \eta_6'=\eta_5.$$

TABLE XI. Effect of the elements of symmetry upon the third-order elastic constants.

Trigonal symmetry 4 axes	Diagonal symmetry 3 axes	Tetragonal symmetry 3 axes
$C_{111}=C_{222}=C_{333}$	C_{111}	C_{111}
$C_{112}=C_{133}=C_{223}$	C_{112}	C_{112}
$C_{113}=C_{322}=C_{122}$	C_{113}	$=C_{112}$
$C_{114}=C_{225}=C_{336}$	$=0$	
$C_{115}=C_{226}=C_{334}$	$=0$	
$C_{116}=C_{224}=C_{335}$	$=0$	
$C_{444}=C_{555}=C_{666}$	$=0$	
$C_{445}=C_{664}=C_{556}$	$=0$	
$C_{446}=C_{665}=C_{554}$	$=0$	
$C_{124}=C_{136}=C_{235}$	$=0$	
$C_{125}=C_{134}=C_{236}$	$=0$	
$C_{126}=C_{135}=C_{234}$	$=0$	
$C_{144}=C_{366}=C_{255}$	C_{144}	C_{144}
$C_{244}=C_{166}=C_{355}$	C_{166}	C_{166}
$C_{344}=C_{266}=C_{155}$	C_{155}	$=C_{166}$
$C_{145}=C_{364}=C_{256}$	$=0$	
$C_{146}=C_{356}=C_{245}$	$=0$	
$C_{156}=C_{345}=C_{246}$	$=0$	
C_{123}	C_{123}	C_{123}
C_{456}	C_{456}	C_{456}
Non-zero distinct constants 20	8	6

Now the free energy must possess the same form with respect to the new axes as to the old; thus we must have

$$C_{111}\eta_1^3+C_{112}\eta_1^2\eta_2+\cdots=C_{111}\eta_1'^3+C_{112}\eta_1'^2\eta_2'+\cdots,$$

the C's being necessarily the same on both sides. Substitution for the η_{rs}' of their values in terms of η_{rs}, as given above, leads to equalities among the C's. By this process, the 56 constants are reduced to 20, as shown in Table XI.

In addition to the trigonal symmetry, all 5 isometric classes possess digonal symmetry about the 3 cubic axes. The corresponding transformation scheme for rotation of 180° about the X_3 axis is:

	X_1'	X_2'	X_3'
X_1	−1	0	0
X_1	0	−1	0
X_3	0	0	1,

so that

$$\eta_1'=\eta_1 \qquad \eta_4'=-\eta_4$$
$$\eta_2'=\eta_2 \qquad \eta_5'=-\eta_5$$
$$\eta_3'=\eta_3 \qquad \eta_6'=\eta_6.$$

Application of this transformation, taking into account the equalities already found, gives, for example, $C_{114}\eta_1^2\eta_4=-C_{114}\eta_1^2\eta_4$, and hence $C_{114}=0$. By this process, the 20 constants are reduced to a maximum of 8.

Finally, for two of the classes, the cubic axes are axes of tetragonal symmetry. For a rotation of 90°, we have the typical scheme

	X_1'	X_2'	X_3'
X_1	0	−1	0
X_2	1	0	0
X_3	0	0	1 ,

leading to

$$\eta_1' = \eta_2 \qquad \eta_4' = -\eta_5$$
$$\eta_2' = \eta_1 \qquad \eta_5' = \eta_4$$
$$\eta_3' = \eta_3 \qquad \eta_6' = -\eta_6.$$

We find two additional equalities, $C_{112} = C_{113}$, and $C_{155} = C_{166}$; the number of constants is thus reduced to 6. This is the minimum obtainable from considerations of symmetry alone, although further reduction may result from special assumptions about lattice structure and forces, as Born and Misra have shown.

Letters to the Editor

PUBLICATION of brief reports of important discoveries in physics may be secured by addressing them to this department. The closing date for this department is, for the issue of the 1st of the month, the 8th of the preceding month and for the issue of the 15th, the 23rd of the preceding month. No proof will be sent to the authors. The Board of Editors does not hold itself responsible for the opinions expressed by the correspondents. Communications should not exceed 600 words in length.

Radiations from As^{72}*

ALLAN C. G. MITCHELL, ED. T. JURNEY, AND MARGARET RAMSEY
Indiana University, Bloomington, Indiana
May 1, 1947

A PRELIMINARY investigation of the radiations from As^{72} has been made with the help of the coincidence counting apparatus available in this laboratory. Only meager information exists in the literature about this element. It is shown to be a positron emitter of approximately 26 hours half-life. It was of interest to this laboratory because it disintegrates to Ge^{72}. The authors have recently studied the energy levels of Ge^{72} when it is formed by beta-ray emission from Ga^{72}, and it is to be expected that a study of the radiations of As^{72} would shed further light on the levels of Ge^{72}.

As^{72} was prepared by bombarding gallium with 23 Mev alpha-particles from the cyclotron. A chemical separation was made, using arsenic carrier, and the active material showed a 26-hour period from As^{72} and a small amount (<2 percent) of an activity with a period of several days, probably from the 16-day As^{74} formed from the other isotope of gallium.

The positron end point was obtained by measuring the range of the positrons in aluminum and applying the Feather rule. The value obtained was 2.78 ± 0.10 Mev. Absorption curves were taken at various times after the end of the irradiation to make sure that this end point was that of As^{72} and not caused by the small amount of As^{74}.

The energy of the most energetic gamma-ray was obtained by placing an aluminum radiator in front of the source and measuring the range of the Compton electrons passing through two counters arranged in a coincidence circuit.[1] The range of the Compton electrons was 1.10 grams/cm² which, if one uses the curve of Curran, Dee, and Petrzilka,[2] corresponds to a gamma-ray energy of 2.4 Mev.

Positron-gamma and gamma-gamma coincidence experiments were also made. In the first instance the source was placed between two counters. With enough aluminum between source and counters to stop all positrons, the total non-particle coincidence rate was determined. This rate arises from annihilation radiation, true gamma-gamma coincidences and gamma-annihilation radiation coincidences. In the present experiments it served merely as a base for measuring particle-gamma coincidences. With the source between the two counters and enough aluminum between the source and one counter to stop all positrons, positron-gamma coincidences were measured as a function of the thickness of aluminum between the source and the other counter. The results show that positron emission probably does not lead to the ground state of Ge^{72} and that there is more than one group of positrons.

In another experiment, lead-lined counters were used to measure gamma-rays and gamma-gamma coincidences. With the counters placed in line with the source between, the number of coincidences observed from the source was the sum of annihilation-gamma, gamma-gamma, and annihilation coincidences. When the line between the source and one of the counters was perpendicular to the line between the source and the other counter, the coincidences due to annihilation radiation were greatly reduced. With the counters in line with the source, the ratio of coincidences per recorded gamma-ray was 3.89×10^{-3}; when they were out of line, the ratio was 1.06×10^{-3}.

The fact that a 2.4 Mev gamma-ray is present in the radiations from Ga^{72} as well as in those from As^{72} shows that possibly one level of Ge^{72} is excited by either disintegration.

* This research was supported by a grant from the Office of Naval Research.
[1] A. C. G. Mitchell, E. T. Jurney, and M. Ramsey, Phys. Rev. 71, 324 (1947).
[2] S. C. Curran, Dee, and Petrzilka, Proc. Roy. Soc. 169, 269 (1938).

Erratum: The Analysis of the Vibration-Rotation Band ω_3 for $C^{12}O_2^{16}$ and $C^{13}O_2^{16}$

[Phys. Rev. 68, 173 (1945)]
ALVIN H. NIELSEN* AND Y. T. YAO**
Mendenhall Laboratory of Physics, The Ohio State University, Columbus, Ohio
May 5, 1947

ON re-examination of the data from which the band analysis for ω_3 of $C^{12}O_2^{16}$ and $C^{13}O_2^{16}$ was made, it was discovered that a mistake had been made in stating that the frequencies of the rotation lines had been reduced to vacuum. Through an oversight the lines given in Tables I and II are uncorrected. The constants have been recalculated in order to determine how they would be affected by this error. The only constants given in Table III which are affected are ω_0 for both molecules. For $C^{12}O_2^{16}$ the corrected value of ω_0 is 2349.33 cm^{-1} which is now in excellent agreement with the value quoted by Herzberg[1] in his compilation of the CO_2 data. The corrected value of ω_0 for $C^{13}O_2^{16}$ is 2283.56 cm^{-1}. B_{000}, B_{001}, and α_3 are not affected because the slopes of the straight lines in Figs. 3–6 are not altered measurably.

To obtain the corrected frequencies the following table of $\Delta\nu$ may be applied:

$\nu(cm^{-1})$	$\Delta\nu(cm^{-1})$
2050	−0.532
2100	−0.545
2200	−0.571
2250	−0.584
2300	−0.597
2350	−0.610

* The University of Tennessee, Knoxville, Tennessee.
** The National University of Peking, Kunming, China.
[1] G. Herzberg, *Infrared and Raman Spectra of Polyatomic Molecules* (D. Van Nostrand Company, Inc., New York, 1945) p. 274.

Preliminary Determination of the Neutron Absorption Cross Section of Long-Lived I^{129}*

SEYMOUR KATCOFF
University of California, Los Alamos Scientific Laboratory, Santa Fe, New Mexico
April 30, 1947

THE following chain of mass number 129 is known to occur in fission:

4.2-hr. Sb→72-min. Te→long-lived I→stable Xe
↑
32-day Te.

An attempt was made by J. Seiler[1] to detect by radiochemical means the long-lived I^{129}. He isolated the iodine from a uranium slug which had undergone irradiation in the Clinton pile for 123 days. The sample decayed essentially to background, with a half-life of 8.0 days which is characteristic of I^{131}. This indicated that the half-life of I^{129} was extremely long, or that its radiations were extremely soft, or both.

In the present experiment this same iodine sample was irradiated simultaneously with two normal iodine samples for 12.8 hours in the Los Alamos homogeneous pile, just outside the BeO reflector. Normal iodine, which is known to consist only of stable I^{127}, should give on slow neutron irradiation only 25-min. I^{128}. However, the sample which also contained some I^{129} yielded several thousand counts per minute of 12.6-hr. I^{130} after irradiation. All three samples were purified radio-chemically, mounted as AgI, and counted with a mica-window Geiger counter. Absorption of the radiations of the 12.5-hr. component in aluminum indicated two beta-rays with maximum energies of 0.54 and 1.02 Mev. This compares favorably with the values for I^{130} reported in the literature of 0.61 and 1.03 Mev.

The neutron absorption cross section of I^{129} could be calculated from the data of this experiment if the number of I^{129} atoms in the samples were known. Unfortunately, this can be calculated only roughly because the isolation of the iodine from the uranium by Seiler was not done quantitatively. Two separate methods of making this estimate were used. The first is based on the fission cross section of uranium, the fission yield of the chain of mass 129 (0.7 percent), the weight of uranium, the time of irradiation, the approximate neutron flux in which the uranium slug was irradiated, and the assumptions that about 30 percent of the iodine in the slug was extracted and that the chemical yield was also about 30 percent. This leads to a value of 7.6×10^{15} for the number of I^{129} atoms and to a value of 2.5 barns (10^{-24} cm^2) for the cross section. The other method of estimation is based on an approximate measurement of the 8.0-day I^{131} activity which was present at the end of the 123-day irradiation in the iodine sample. This assumes that the bombardment of the uranium was steady, especially near the end. The fission yield of I^{131} was taken as 2.5 percent. This leads to a value of 1.9×10^{15} I^{129} atoms and to a value of 10 barns for the cross section. This is thought to be more reliable than the first value, so that a weighted average of the two gives a final value of about 8 barns, which is very probably correct to within a factor of ten.

The neutron flux passing through the iodine samples during their irradiation at the Los Alamos pile was calculated from the activity of the 25-min. I^{128} and the cross section of stable I^{127} (6.25 barns). In the calculations, corrections were made to 100 percent counter geometry, to 100 percent chemical yield, to zero absorber, and for decay.

A half-life of 10^8 years, or longer, for I^{129} is consistent with the results of Seiler's experiment. Such a long period would make it possible for I^{129} to exist in nature. In fact, the two normal iodine samples used in this experiment did show a small amount of residual activity after the decay of the 25-min. I^{128} (see Fig. 1). Some of this may be due to 13-day I^{126} formed by an $(n, 2n)$ reaction, and to impurities. However, there is some indication of a 12.9-hr. period which may be due to 12.6-hr. I^{130}. This sets an upper limit of 3 parts per million for the amount of I^{129} that might

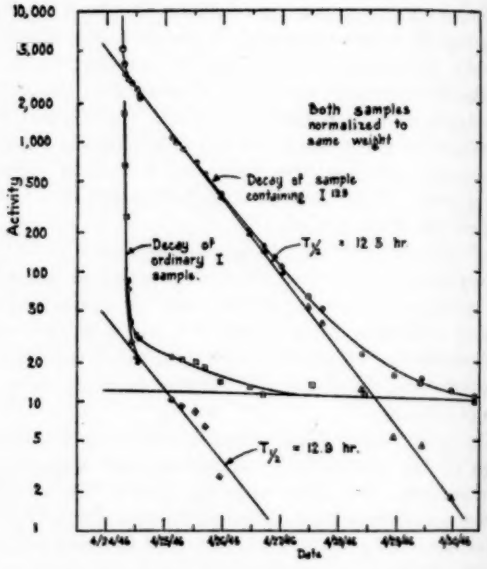

FIG. 1. Decay of 12.6-hr. I^{130} produced by neutron bombardment of long-lived I^{129}.

be present in normal iodine if a cross section of 0.8 barn is taken. The limit is only 0.3 part per million if the most probable cross section of 8 barns is used. Nier reported[2] an upper limit from mass spectrographic data of 25 parts per million. This problem can be investigated further by bombarding larger samples of normal iodine in a higher thermal neutron flux and then subjecting them to more extensive purification.

* This document is based on work performed at Los Alamos Scientific Laboratory of the University of California under Contract No. W-7405-eng-36 for the Manhattan Project, and the information contained therein originally appeared in Report LAMS-389, May 29, 1946. It will also appear in Division V of the Manhattan Project Technical Series as part of the contribution of the Los Alamos Laboratory.

[1] Manhattan Project Progress Report CN-1998, p. 2.
[2] A. O. C. Nier, Phys. Rev. 52, 937 (1937).

Solar Absorption Lines between 2950 and 2200 Angstroms

E. Durand, J. J. Oberly, and R. Tousey
Naval Research Laboratory, Washington, D. C.
April 23, 1947

SOLAR spectrograms were taken by the Naval Research Laboratory on the V-2 rocket flights of October 10, 1946[1] and March 7, 1947. The spectra obtained at 55 km and 75 km on the respective dates have been studied to identify the Fraunhofer absorption lines in the region between 3000 and 2200A. Some 300 observable absorption features were compared to a master finding list of 1100 of the principal classified lines of the arc and spark spectra of elements 1 to 30. The heavier elements will be added as time permits. The finding list was prepared in collaboration with Dr. Charlotte Moore-Sitterly, who generously made available the unpublished multiplet lists which are being compiled as an extension of the Revised Multiplet Table[2] to cover the rocket ultraviolet region. Entries included laboratory intensities, assigned multiplet numbers, and, in many cases, her solar intensity predictions.

At the available resolution of about 1A, nearly every observed line is a blend; as many as 10 possible contributors to a single line have been found. Likely contributors have been assigned to nearly every observed feature, and work is under way to estimate their relative importance.

As in the previously known region, Fe *I* and Fe *II* are dominant and clearly contribute to a majority of the lines. In Fig. 1, the matching of many of the solar lines (indicated by dots) to the Fe arc spectrum is apparent. In the regions just below 2750, 2630, 2550, and 2490A there is a piling up of intense iron lines. This causes the whole level of the solar radiation to fall off sharply as shown in Fig. 1. In addition, many strong single Fe lines are found throughout the spectrum.

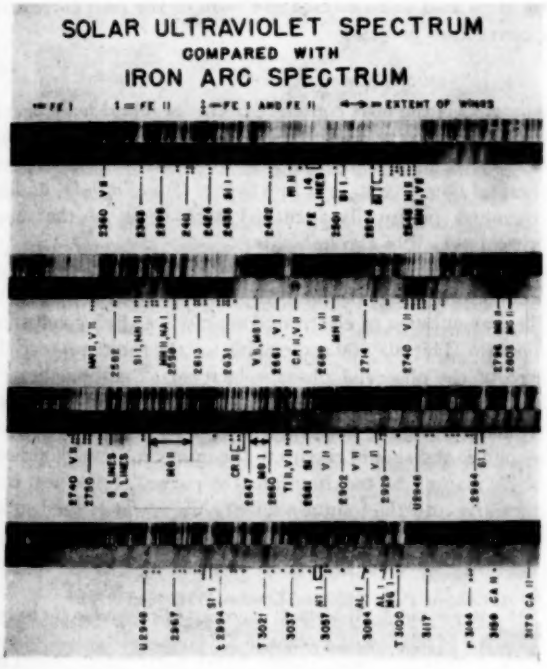

Fig. 1.

The great Mg *II* lines at 2803 and 2796A are of particular interest. They appear as two bright emission lines in the center of a great absorption band running from 2775 to 2825A.

Dr. Menzel of the Harvard Observatory offered the above explanation of the observed spectra and suggested the following explanation: A strong eruption of hydrogen occurred about 1 hour before the rocket flight, and the Mg emission may have originated in the prominence. However, similar emission lines, unresolved, may be inferred from the October 10 spectra, at which time no important prominences are known to have occurred.

Twelve lines of Si *I* of great intensity were found. The one at 2882 and the group between 2507 and 2529A showed strong wings. The existence of wings on the group between 2208 and 2219A could not be proved. A strong line of C *I* was found at 2478A.

In addition to the above elements one or more lines have been assigned as follows: definite, V *I*, V *II*, Cr *II*, Mn *II*, Co *I*, and Al *II*; probable, Na *I*, Ni *I*, Ni *II*, Cr *I*, Co *II*, Be *I*, and Al *I*; possible, P *I*, and Cu *I*. More definite assignments will be made taking into account multiplet intensity and the relative abundances of the elements.

There appear to be regions of general absorption between 2886 and 2893A and between 2442 and 2472A. The finding list contains few lines in these regions; the absorption may, therefore, be molecular.

A complete report of the analysis will be published later.

[1] W. A. Baum, F. S. Johnson, J. J. Oberly, C. C. Rockwood, C. V. Strain, and R. Tousey, Phys. Rev. **70**, 781 (1946).
[2] Charlotte E. Moore, "A revised multiplet table of astrophysical interest," Princeton Observatory.

Lower Bounds for Eigenvalues

R. J. Duffin
Department of Mathematics, Carnegie Institute of Technology, Pittsburgh, Pennsylvania
April 28, 1947

BARTA[1] has given a method for finding lower bounds for the "ground state" eigenvalue of a vibrating membrane. He does not claim that his method is as nice as the Rayleigh-Ritz method for finding upper bounds, but in a numerical example he shows that fair accuracy is obtainable.

The purpose of this note is threefold: (1) We extend Barta's method to include the Schrödinger equation, (2) the boundary conditions of Barta are relaxed, for instead of $u=0$ on the boundary we have $u\geq 0$, and this may be easier to apply in practice, (3) we give a very simple, but mathematically rigorous, proof. Barta makes use of the fact that the ground state eigenfunction is positive; the proof of this fact is very long and sophisticated.

Consider a continuous real function, ψ, which vanishes on the secondary of a region, R, and satisfies the n-dimen-

sional Schrödinger equation, $\Delta\psi+(\lambda-V)\psi=0$. For simplicity we assume that V is a finite function. Let u be any function with bounded second derivatives satisfying $u\geq\epsilon$ for a positive constant, ϵ. The continuous function $r=\psi/u$ vanishes on the boundary and may be assumed to have a positive maximum in R (otherwise take $-\psi$). At a maximum point the first derivatives of r vanish, and the second derivatives are negative or zero. Adding the second derivatives gives $\Delta r=(u\Delta\psi-\psi\Delta u)/u^2\leq 0$. Thus $\Delta u/u\geq\Delta\psi/\psi=V-\lambda$ so that $\lambda\geq V-\Delta u/u$. *A fortiori*, $\lambda\geq\min.(V-\Delta u/u)$ for all points of the region. This gives the theorem: *The eigenvalues of Schrödinger's equation satisfy the inequality* $\lambda\geq\min.(V-\Delta u/u)$ *where* u *is a positive function in the region.*

The rest of this note is mainly of mathematical interest and proves that on the boundary, S, it is only necessary to assume $u\geq 0$. In case the region is finite, we suppose that S is sufficiently regular so that there is a function, g, which satisfies $\Delta g+(h-V)g<0$ on S and $g\geq 1$ in R, where $h=\min.(V-\Delta u/u)$. If $w=u+\epsilon g$, then $\lambda\geq\min.(V-\Delta w/w)$ by what has just been shown. Clearly, $V-(\Delta u+\epsilon\Delta g)/(u+\epsilon g)\geq V+(hu-Vu-\epsilon\Delta g)/(u+\epsilon g)=h+\epsilon(Vg-hg-\Delta g)/(u+\epsilon g)$. In a neighborhood of the boundary the last term is positive, and in the remainder of the region it must vanish with ϵ, so that $\lambda\geq h$, Q. E. D.

In an infinite region we take $g=1$ in the above proof, that is, $w=u+\epsilon$. Assume, moreover, that outside a sufficiently large sphere $h-V<0$. Thus $V-\Delta w/w\geq h+\epsilon(V-h)/(u+\epsilon g)$. Outside the sphere the last term is positive, and inside the sphere it vanishes with ϵ, so that $\lambda\geq h$.

The problem discussed here could be generalized for an equation in which λ is multiplied by a positive function. On the other hand, the writer has been unable to treat by similar methods the eigenvalues of the acoustic equation, the equation of the clamped plate, or Maxwell's equations.

[1] J. Barta, Comptes rendus, **204**, 472 (1937).

On a Connection between the Fountain Effect, Second Sound, and Thermal Conductivity in Liquid Helium II

LOTHAR MEYER
Institute for the Study of Metals, University of Chicago, Chicago, Illinois
AND
WILLIAM BAND
Institute for Nuclear Studies, University of Chicago, Chicago, Illinois
April 25, 1947

WE have investigated the possible phenomenological relations between the observed properties of liquid helium II. We assume that in the absence of a constriction the internal forces responsible for the fountain effect are still present but produce an internal momentum density $\mathbf{M}$ such that

$$\mu\nabla T=\nabla p=-d\mathbf{M}/dt, \tag{1}$$

where T is the temperature and p is the fountain effect pressure difference. We then apply the first law of thermodynamics to a heat transported with the momentum

$$\nabla\cdot\mathbf{h}=\nabla\cdot(\epsilon\mathbf{M}/m)=-\rho C_v dT/dt. \tag{2}$$

We solve (1) and (2) simultaneously to give a wave equation for momentum and temperature similar to second sound. The phase velocity is

$$V_s=(\epsilon\mu/m\rho C_v)^{\frac{1}{2}}, \tag{3}$$

where μ is the fountain effect coefficient,[1,2] ρC_v is the specific heat[3] per cm^3, and ϵ is the heat associated with a mass m transported with the momentum. Empirical values of μ, V_s (second sound velocity),[4,5] and ρC_v below 1.8°K yield values of ϵ/m which fit a monotonically increasing curve from zero at 0°K to the heat content at the lambda point (T_λ).

From the equation

$$d(\epsilon\rho_s/m)/dT=\rho C_v \tag{4}$$

we calculated the concentration ρ_s/ρ of the liquid taking part in the momentum. The curve connecting these values is approximately equal to (T/T_λ),[6] going therefore through zero at 0°K and unity at T_λ, which it should do from general considerations.

The observed finite heat conductivity in liquid helium requires a wave equation having a relaxation (damping) term added to (1), namely,

$$\nabla\cdot\nabla T=\left\{\frac{d^2T}{dt^2}+\frac{1}{\tau}\frac{dT}{dt}\right\}\Big/V_s^2. \tag{5}$$

Combined with the data on thermal conductivity[3] this gives a time of relaxation τ of the order 10^{-3} to 10^{-4} sec., going to zero at T_λ. Equations (5) and (1) with the damping term lead to an alternative form of the heat current as a convection process:

$$\mathbf{h}=\rho Q\mathbf{u}_s, \tag{6}$$

where ρQ is the heat content per cm^3 of liquid helium, and $\mathbf{u}_s$ is the velocity associated with the steady momentum density as limited by the relaxation term. The data on thermal flow give $\mathbf{u}_s$ as a function of T and dT/dx, leading to values practically identical with those of the super critical velocities through slits.[2]

The relaxation causes an absorption and dispersion of second sound near the lambda point, formally analogous to the transmission of electromagnetic waves in a conducting medium. This may be responsible for the rapid approach to zero of the observed phase velocity as T approaches T_λ, and leads to the expectation that under ideal conditions (small amplitude and high frequency) the velocity of second sound should rise up to the immediate neighborhood of T_λ just as the maximum in the curves of the heat conductivity and the fountain effect shift towards the lambda point under appropriate conditions.[2]

We are studying the physical meaning of these relations.

[1] H. London, Proc. Roy. Soc. London **A171**, 484 (1939).
[2] L. Meyer and J. H. Mellink, Physica, 's-Gravenhage (to be published).
[3] W. H. Keesom, *Helium* (Amsterdam, 1942).
[4] V. P. Peshkov, Vestnik Akademii Nauk **4**, 117 (1945); Nature **157**, 200 (1946).
[5] H. Fairbank, W. Fairbank, and C. T. Lane, Phys. Rev. **71**, 477(A) (1947).

Errata: The Collision of Neutrons with Deuterons and the Reality of Exchange Forces

[Phys. Rev. 71, 558 (1947)]

H. S. W. MASSEY AND R. A. BUCKINGHAM
University College, London, England

AND

Conductivity of Sodium-Ammonia Solutions

[Phys. Rev. 71, 563 (1947)]

D. K. C. MACDONALD AND K. MENDELSSOHN
Clarendon Laboratory, Oxford, England
AND
A. J. BIRCH
Dyson Perrins Laboratory, Oxford, England

THE Editor regrets that Fig. 2 of the first of the above papers has been interchanged with Fig. 1 of the second paper. The captions, however, are right, as they stand.

Erratum: The Quadrupole Moments and Spins of Br, Cl, and N Nuclei

[Phys. Rev. 71, 644 (1947)]

C. H. TOWNES, A. N. HOLDEN, J. BARDEEN, AND F. R. MERRITT
Bell Telephone Laboratories, Murray Hill, New Jersey

THE Editor regrets that Figs. 1 and 2 of the above paper have been interchanged. The captions for the figures, however, are correct as they stand.

Isotopic Changes in Cadmium by Neutron Absorption

A. J. DEMPSTER
Argonne National Laboratory, Chicago, Illinois
May 1, 1947

IN a recent letter B. J. Moyer, B. Peters, and F. H. Schmidt[1] report that the absorption of thermal neutrons in cadmium that had been enriched in the isotope at mass 113 was six times normal, and conclude that this isotope is mainly responsible for the large absorption in this element.

The mass spectra reproduced in Fig. 1 illustrate another phenomenon that also indicates the absorbing isotope, namely, the gradual alteration of the isotopic constitution of an element by long exposure to neutrons. The upper mass spectrum shows the normal isotopes at masses 110, 111, 112, 113, and 114, with $Cd^{113}=12.3$, and $Cd^{114}=28$ percent. The faint isotopes at 106 and 108 do not show on the prints. The lower spectrum shows the changed isotopic abundance in a sample scraped from the surface of a piece of metal that had been used to absorb intense neutrons from a pile over a long period of time. These neutrons include a considerable number with energies above the thermal range.

Photometric measurements, made by using Nier's measurements of the normal cadmium abundances as standards, showed that the isotope at mass 113 was reduced

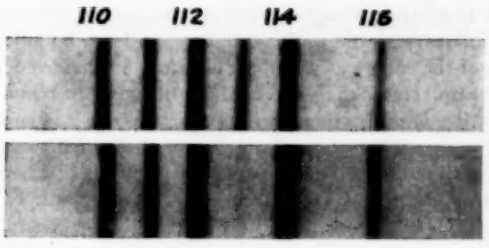

FIG. 1. Normal cadmium (above) and isotopes altered by neutron absorption (below).

to 1.6 ± 0.2 percent, about one-eighth of its normal abundance, and that the isotope at mass 114 was increased to 39.5 ± 1.5 percent. Within the limits of the accuracy attained, the increase in 114 is equal to the decrease in 113. Any changes in the abundances of the isotopes at masses 110, 111, 112, and 116 were less than five percent. It was noticed, however, that in both samples the isotopes at 110 and 111 had a greater difference in abundance than is indicated by Nier's measurements (12.8 and 13.0 percent). We may conclude that the other main isotopes have absorbing cross sections less than one-fortieth of that of Cd^{113}, and that if any $(n, 2n)$ or other reactions occur, they are comparatively rare.

[1] B. J. Moyer, B. Peters, and F. H. Schmidt, Phys. Rev. 69, 666 (1946).

Radiation from Electrons in a Synchrotron

F. R. ELDER, A. M. GUREWITSCH, R. V. LANGMUIR, AND H. C. POLLOCK
Research Laboratory, General Electric Company, Schenectady, New York
May 7, 1947

HIGH energy electrons which are subjected to large accelerations normal to their velocity should radiate electromagnetic energy.[1-4] The radiation from electrons in a betatron or synchrotron should be emitted in a narrow cone tangent to the electron orbit, and its spectrum should extend into the visible region. This radiation has now been observed visually in the General Electric 70-Mev synchrotron.[5] This machine has an electron orbit radius of 29.3 cm and a peak magnetic field of 8100 gausses. The radiation is seen as a small spot of brilliant white light by an observer looking into the vacuum tube tangent to the orbit and toward the approaching electrons. The light is quite bright when the x-ray output of the machine at 70 Mev is 50 roentgens per minute at one meter from the target and can still be observed in daylight at outputs as low as 0.1 roentgen.

The synchrotron x-ray beam is obtained by turning off the r-f accelerating resonator and permitting subsequent changes in the field of the magnet to change the electron orbit radius so as to contract or expand the beam to suitable targets. If the electrons are contracted to a target at successively higher energies, the intensity of the light radiation is observed to increase rapidly with electron energy. If, however, the electrons are kept in the beam past the

peak of the magnetic field and then expanded to a target, the intensity of the radiated light appears to be independent of the energy at which the electrons are removed from the beam. This is to be expected, for in a given machine the radiation is proportional to the fourth power of the electron energy. The light radiation is not observed if the beam is contracted before its energy is about 30 Mev. When the electron beam has been accelerated to the peak of the magnetic field and then decelerated to low energy, a rough measurement of the phase angle over which the light was visible gave a value of 90–100 degrees. The light was viewed through a slotted disk rotating at synchronous speed.

If the r-f resonator is turned off a short time before the peak of the magnetic field, the electron beam slowly contracts to a radius just larger than that of the interior target and then expands as the magnetic field decreases. In this case, the observer no longer sees a single point of light but a short line with extension in the plane of the orbit.

The light emitted from the beam is polarized with the electric vector parallel to the plane of the electron orbit. It disappears as the observer rotates a piece of Polaroid before the eye through ninety degrees. An investigation of the spectral distribution of the energy is in progress and will be reported.

This work has been supported by the Office of Naval Research under contract N5ori–178.

[1] D. Iwanenko and I. Pomeranchuk, Phys. Rev. 65, 343 (1944).
[2] J. P. Blewett, Phys. Rev. 69, 87 (1946).
[3] L. I. Schiff, Rev. Sci. Inst. 17, 6 (1946).
[4] J. S. Schwinger, Phys. Rev. 70, 798 (1946).
[5] H. C. Pollock *et al.*, Phys. Rev. 70, 798 (1946).

Proceedings of the Southeastern Section of The American Physical Society

MINUTES OF THE SALISBURY, NORTH CAROLINA, MEETING ON APRIL 4–5, 1947

THE thirteenth annual meeting of the Southeastern Section of the American Physical Society was held at Catawba College, Salisbury, North Carolina, on Friday and Saturday, April 4–5, 1947. Approximately 180 members and guests attended. Local arrangements were made by a committee headed by M. L. Braun.

The regular program consisted of thirty-nine papers, abstracts for thirty-one of which are appended hereto. Abstracts of the other papers will be found in the July–August issue of the *American Journal of Physics*. One abstract did not reach the Program Committee in time to be included in the printed program, but the paper was presented at the meeting. The title was, "On the Division of Nuclear Charge in Fission," by R. D. Present, of the University of Tennessee.

As additional features the following invited papers were presented: "Some Aspects of the Theory of Neutron Diffraction by Crystals," by Fredrick Seitz; "New Developments in Instruments for Counting and Detecting Nuclear Particles," by Walter Jordan; "Microwave Spectra," by Walter Gordy; "Report on the Oak Ridge Institute of Nuclear Studies," by W. G. Pollard; "Educational Programs in Atomic Energy for the Southeast," by Karl Morgan; and "The Training School Program at Clinton Laboratories," by Fredrick Seitz.

At the business meeting the election of the following officers for the Section was announced: Chairman, M. L. Braun; Vice-Chairman, E. H. Dixon; Secretary, Eric Rodgers; Treasurer, H. F. Henry; and Member of the Executive Committee, C. B. Crawley.

The 1948 meeting will be held at the University of Tennessee in Knoxville.

ERIC RODGERS, *Secretary*

ABSTRACTS

1. An Automatically Recording Grating Spectrograph for the Infra-Red. ALVIN H. NIELSEN, *The University of Tennessee, Knoxville.*—A recording prism-grating infra-red spectrograph with a spectral range of 1–25μ has been built in the University of Tennessee shop. Spherical mirrors are employed with the exception of the principal collimator, which is an off-axis paraboloid, and the final mirror which focusses a reduced slit image on the thermocouple. An airtight cover permits the removal of carbon dioxide and water vapor from the spectrograph. All controls emerge from the base so the instrument need be opened only when changing absorption cells or gratings. The grating is mounted on a ball-bearing shaft and is turned slowly by a motor and worm gear arrangement. A counter attached to the drive trips a special pen on the recorder and thus puts a wave-length scale on the chart. A vacuum thermocouple on which the final slit image is focussed causes a high-sensitivity Leeds & Northrup galvanometer to deflect a beam of light across two photo-cells. The differential output of these cells is amplified by a d.c. amplifier described by Bell, Noble, and Nielsen.[1] The final amplified signal is reproduced on charts by either a Bristol recording milliammeter, or Leeds & Northrup Speedomax Type G. Slides illustrating the details of the instrument and its performance will be shown.

[1] E. E. Bell, R. H. Noble, H. H. Nielsen, Rev. Sci. Inst. 18, 48 (1947).

2. Mechanism of Luminescence of Infra-Red-Sensitive Phosphors. FERD E. WILLIAMS, *University of North Carolina.*—The model of potential energy *versus* configuration coordinate proposed by Williams and Eyring[1] to correlate diverse properties of luminescent solids has been found applicable to infrared-sensitive phosphors. An explanation of the complex afterglow of the rare earth-activated strontium sulfoselenides is that electron traps of various depths are active. Calculations from the model indicate that at high temperatures only the deepest traps are active, therefore, assuming a predominantly monomolecular rate-determining process, the afterglow should be exponential. This is verified by an analysis of the data of Shrader[2] for SrS:Sm, Eu, and the thermal trap depths are found to be related to the optical depths as expected. As also predicted from the model, pronounced temperature-dependence of luminescent efficiency is encountered and can be precisely reproduced assuming an activated step in the luminescent process competing with the radiationless recombination of the excited electron and center. The frequency factors of the specific rate constants are small, indicating changes in multiplicity. The contributions of first- and second-order rate processes and the probable trap distribution are computed from buildup, afterglow,[2] and stimulation[3] data.

[1] F. E. Williams and H. Eyring, Phys. Rev. 69, 257 (1946).
[2] R. E. Shrader, Paper 15 at Am. Opt. Soc. Mtg. in Cleveland (March 1946).
[3] R. T. Ellickson and W. L. Parker, Phys. Rev. 70, 290 (1946).

3. The Evaporation of Gallium. S. K. HAYNES, *Clinton Laboratories and Vanderbilt University.*—A thin β-ray source was made by evaporating gallium onto a thin sheet of polystyrene. Since gallium was not among the metals for which evaporation procedures were given by Olsen, Smith, and Crittenden[1] an investigation was made to find the best procedure. A modification of the procedure for aluminum[1,2] was finally used. The gallium was warmed just above its melting point and "buttered" onto a cooler clean open helix of 30 mil tungsten wire, drop by drop, until the tungsten was almost covered. When the tungsten was flashed to a dull red in vacuum, a fraction of the gallium reacted with it, while the remainder dropped off. The tungsten retained all the gallium ready for the final evaporation after a second "buttering" and flashing. Several other methods were tried with less success, including a close wound conical helix of tungsten and a tantalum crucible heated by a filament.

[1] J. App. Phys. 16, 425 (1945).
[2] J. Strong, Proc. in Exp. Phys. (Prentice Hall), p. 168.

4. A Mechanism for Ductile Failure in a Notched Steel Bar.* PAUL E. SHEARIN, *University of North Carolina.*—A mild-steel bend bar, $0.75''\times0.75''\times4.6''$, having four 15 percent Izod notches undergoes a mode of failure in the slow-bend test in which the head of the advancing crack remains sensibly parallel to the rootline of the initiating notch, when failing in a ductile manner.[1] In such a test the work associated with the fracturing of a unit-cross-sectional area (unit work) is to a first-order approximation a linear function of the distance to the neutral axis, $(a-x)/2$, where x represents the distance the crack has traveled and a is the original retained depth of the specimen at the roots of the notches. This is so since, as the crack opens, a wedge of material between the crack front and the neutral axis is undergoing plastic deformation. As the crack progresses the height of this wedge decreases. Integration of $f[(a-x)/2]$ yields the result that unit work is proportional to the mean distance of the area from the final crack terminus. Experimental results indicate the essential correctness of this result.

* Work done under contract ONR, NRL, N6ori-227.
[1] C. Zener and J. H. Holloman, J. App. Phys. 17, 69 (1946).

5. Voltaic Effects in Waterglass. E. SCOTT BARR, *Tulane University.*—Sodium silicate in the waterglass form shows two voltaic effects which make it a complicating factor when used as a binder in cements which come into contact with electrical measuring leads. It has been found that during the drying period of the material there are voltage differences between different portions of the material sufficient to produce appreciable indications on a sensitive galvanometer. Furthermore, during the drying period, and apparently to some extent after drying, waterglass polarizes very noticeably. This latter effect precludes accurate potentiometer measurements of developed e.m.f., and measurements of resistance with a Wheatstone bridge or ohmmeter.

In the work now in progress, two identical wire windings, of copper or nickel, are put at the ends of a glass plate which is then coated with a thin layer of waterglass. It has been found that the winding in the more moist portion of the film is positive. Voltages up to 50 millivolts and more have been observed between the windings. These effects and the decay of voltage after the film has been polarized by an external voltage source are to be discussed.

6. Conductivity of Sodium-Ammonia Solutions. MELVIN EISNER AND JOSEPH W. STRALEY, *The University of North Carolina.*—Ogg[1] and Hodgins[2] have reported the existence of persistent currents in dilute solutions of Na in ammonia at liquid air temperatures. Boorse[3] and others have been unable to confirm these observations. An attempt is being made to reproduce these experiments. The apparatus consists of a search coil of 1010 turns wound on a Bakelite spool whose inside diameter is 1 cm. This coil is capable of detecting the magnetic field due to a current change in a neighboring circuit of 0.4 ampere-turns. Two types of cells have been used, the first consisting of slide covers separated by a mica spacer as described by Ogg, the second being a glass toroid of 2 cm diameter. Of seventy-five tests forty have shown negative results. Although slight deflections were thought to be observed in the remaining tests, they were not large enough to be distinguished with certainty from the random motions of the galvanometer. Work is being continued.

[1] Phys. Rev. 70, 93 (1946).
[2] Phys. Rev. 70, 568 (1946).
[3] Phys. Rev. 70, 92 (1946).

7. Diffuse Reflection from Dielectrics. WM. A. RENSE, *Louisiana State University.*—When light strikes an unpolished surface of a dielectric, some of it will be absorbed or transmitted and the rest will be sent back into the original medium in many or all directions. Diffuse reflection is said to occur. Previous theories of diffuse reflection either have been of a semi-empirical nature, or have limited the reflecting mechanism to that of elementary regular mirrors oriented in various ways on the illuminated surface.

A new theory is here developed which treats the diffusely reflected light as being made up of three parts: (1) light regularly reflected from elementary mirrors, (2) light scattered from edges and points on the surface, (3) light which, after entering the surface and suffering absorption, has been deflected back into the incident medium in some manner. Fresnel's equations from Maxwell's electromagnetic theory and classical equations for the scattering of light by an anisotropic molecule permit explicit expression of (1) and (2). Simplifying assumptions allow (3) to be estimated. The final expressions contain formulae for finding the total intensity and the intensities of the polarized components in terms of six parameters related directly to the roughness of the surface and to the refractive index and absorption properties of the dielectric.

8. Positive Grid Characteristics of a Triode. GEORGE W. WOOD, *Louisiana State University.*—Theory concerning the triode is meager. However, a recent treatment of the diode by Jaffé, wherein the electrons are assumed to have uniform initial velocities, provides a means of extending our knowledge of the triode. By operating the grid of a

triode at a positive potential, it becomes a virtual cathode discharging electrons with uniform initial velocity and thus the theory becomes applicable. The positive grid characteristics of a number of radio receiving triodes are determined and matched with those determined from the theory. An agreement, satisfactory under given conditions, is found in the region of low plate voltages.

Departure of the empirical curves from the theoretical ones is appreciable because the practical tubes tested do not, by any means, correspond to the ideal conditions of the theory: the electrodes are not plane; the electrostatic field is not homogeneous; secondary emission from the grid is present; contact potentials exist; and there is always a velocity distribution among the electrons. While the investigations described cannot be taken as conclusive, they point the way towards a better theory of the triode.

9. Effect of Scattering on Experimental Determinations of *XR* for High Energy Particles. F. T. ROGERS, JR., *The University of North Carolina.*—In certain apparatuses for determining XR for a high energy particle (R is the radius of curvature which the path would have if the particle were to traverse a suitable electrostatic field X perpendicularly to the X-vector), X may be available in a convenient non-ideal configuration, R may be calculated from the particle's deflection (s) in this X, and uncertainties[1] may be introduced into the measured deflection by a thin scattering medium in the particle's path before entering X. Thus if the proper X-value can be extracted from the available configuration, then the uncertainty in XR is

$$\epsilon_N=\theta_{AV}L/s+\Delta s/s, \qquad (1)$$

where θ_{AV} is a suitable measure of scattering,[2] L is a dimension, and Δs is a measure of errors of "triangulation," both terms being essentially Gaussian. A discussion will be presented of the estimated lower limit to which ϵ_N might be reducible.

[1] The author is indebted to Dr. J. C. Street for having pointed out the importance of the θ_{AV}-contribution to ϵ_N.
[2] E. J. Williams, Phys. Rev. 58, 292 (1940).

10. Two Non-Linear Springs. G. W. CRAWFORD, *North Carolina State College of Agriculture and Engineering,* AND F. T. ROGERS, JR., *The University of North Carolina.*—The equation

$$T=t+\delta(L-l)+\Delta(L-l)^2, \qquad (1)$$

where t, δ, and Δ are constants and where $(L-l)$ is the extension beyond a minimum length (l), has been proposed[1] for the tension of strings (about 0.0004-in. diameter) in certain commercial string-galvanometers. To exhibit this concept on a large scale, two plane springs of 0.13 cm diameter phosphor-bronze wire were made in grid form; nine grid elements were used, each 0.75″×1.5″; they were rectangular in one, not in the other. The constants t, δ, and Δ were found to be, respectively,

$$0,\ 1.82\times10^5 \text{ dynes/cm},\ -0.0586\times10^5 \text{ dynes/cm}^2, \qquad (2a)$$
$$0,\ 6.1\times10^5 \text{ dynes/cm},\ 1.68\times10^5 \text{ dynes/cm}^2, \qquad (2b)$$

and represented the non-linearities to within *A.D.*'s of 2×10^4 and 6×10^4 dynes, respectively; these representations are valid for $(L-l)$ up to 10 cm and 4 cm, respectively, which extensions approached the elastic limits of the two springs.

[1] F. T. Rogers, Jr., Rev. Sci. Inst. 12, 351 (1941).

11. A Redetermination of the Nuclear Magnetic Moment of Sodium by the Polarization of Resonance Radiation. MARGUERITE M. ROGERS, *The University of North Carolina.*—A redetermination of the nuclear magnetic moment of sodium was made by measuring the degree of polarization in the resonance radiation from sodium vapor subjected to various magnetic fields. This effect is well known and has been previously measured by Larrick[1] and by Ellett and Heydenburg.[2] In the present experiment, great care was exercised to reduce the self-reversal in the sodium source by means of a specially designed discharge tube.

The variation of the degree of polarization with field strength was compared with theoretical values from computation of the Paschen-Back intensities of the hyperfine structure based on a spin of $\frac{3}{2}$. The values of the Landé g-factor and nuclear magnetic moment resulting from fitting the observed curve to the theoretical one gave good agreement, within the accuracy of the experiment, to the accepted, precise values of Millman and Kusch of 1.4765 and 2.215

[1] Larrick, Phys. Rev. 46, 581 (1934).
[2] Ellett and Heydenburg, Phys. Rev. 46, 583 (1934).

12. Quantum Mechanics of Vibrating String. NATHAN ROSEN, *The University of North Carolina.*—As a simple example of the quantization of a continuous medium, the transverse oscillations of a perfectly flexible string stretched under tension between two fixed supports are treated by means of wave mechanics. The energy levels and wave functions of the stationary states are determined. One obtains the well-known infinite zero-point energy, which would have to be discarded to give finite values for the energy of the string. The degree of degeneracy of the system is considered.

13. Problem of Homogeneous Incompressible Fluid Sphere in General Relativity. BROWNIE NEWMAN AND NATHAN ROSEN, *University of North Carolina.*—The Schwarzschild and related solutions of the gravitational field equations for the problem of the homogeneous sphere impose the conditions $T_1^1=T_2^2=T_3^3=-p$ and $T_4^4=\rho$ =constant. Eddington[1] pointed out that for an incompressible homogeneous fluid the last condition should be replaced by T_α^α=constant. An attempt has been made to solve the problem for this case. Starting with a line element of the Schwarzschild form, one obtains a set of field equations which can be reduced to a single equation with one unknown. This equation is, however, of a rather complicated nature, and thus far it has not been possible to find its general solution in closed form. Two particular solutions for the interior of the sphere can be obtained, but they are not satisfactory from the physical standpoint. It may be that the problem will have to be solved by numerical integration of the differential equation.

[1] A. S. Eddington, Mathematical Theory of Relativity (Cambridge, 1923), p. 170.

14. The Limits of Visibility and the Maximum Brightness of Continuous Spectra at Various Color Temperatures. OTTO STUHLMAN, JR., *University of North Carolina.*—Preliminary data on the visibility of radiation at low intensities and low color temperatures indicate that the sensibility to threshold brightness conforms to the results of Weaver and Hussing (J. O. S. A. 16, 29, 1939). At higher color temperatures the visibility departs from the above results. The maximum brightness wave-length parallels the blue end of the spectrum.

15. Preliminary Experiment on Convection Currents in a Porous Medium. H. L. MORRISON, *North Carolina State College of Agriculture and Engineering,* AND F. T. ROGERS, JR., *The University of North Carolina.*—To assess a theory recently advanced[1] for the minimum temperature gradient necessary to cause convection of a liquid in a porous medium, an experiment has been initiated using glycerol in a sand having a permeability of about 95 darcys. The mixture was placed in a beaker to a depth of 10 cm; thermocouples were used to observe temperatures; heat was applied from below; and microscopic observations were made of suspended impurities. When the particles of impurity moved, the temperature gradient was about 80°C locally, but varied widely throughout the depth of the mixture. The theory clearly calls for a gradient of excess of 200°C/cm *if uniform* and if boundary conditions such as those in the experiment are negligible (there is apparently no information on the viscosity of glycerol above 30°C, so that logarithmic extrapolation is being used to higher temperatures until suitable measurements can be completed). Weighing all these uncertain factors together, it can only be concluded at present that the theory predicts excessive minimum gradients, a conclusion which was anticipated in the presentation of the theory.

[1] C. W. Horton and F. T. Rogers, Jr., J. App. Phys. 16, 367 (1945).

16. Alternative Basic Theories for the Carbon-Pile Type of Voltage-Regulator. CHARLES W. DUBS AND F. T. ROGERS, JR., *The University of North Carolina.*—A second theory for the carbon-pile type of voltage-regulator,[1] developed on the assumption of coulombic friction, predicts one or more half-cycles of cosine waves in the output-voltage for a step-function change of input-voltage; this is in disagreement with the apparently exponential waveform which is observed[2] and which the first theory[2] predicts. A third theory, based on coulombic friction and neglecting armature inertia as compared with inductive reactance, leads to an exponential character in the output-voltage in which the time-constant suddenly decreases (recovers, sharply) when the armature begins to move. All three theories have been compared to a minimum of experimental data: for a 16 percent step applied to a certain model of regulator, they predict 1.9 percent, zero to 16 percent, and 1.9 percent to 16 percent changes (after transients) in output-voltage, while the measured change is 3.6 percent. All three theories appear in their present forms to predict response-times at least an order of magnitude smaller than the 30 milliseconds observed for this model.

[1] W. G. Neild, Trans. AIEE, 63, 839 (1944).
[2] F. T. Rogers, Jr., Instruments 19, 256 and 381 (1946).

17. Measurement of the Ionization Potential of Gases in Photoelectric Cells. ARTHUR WALTNER, *The University of North Carolina.*—When an alternating e.m.f. is applied across a gas-filled photoelectric cell the current wave form passes through three distinct phases as the voltage is increased: (1) For very low voltages (2 or 3 volts) a half-wave rectified pattern is observed; (2) as saturation sets in a rather close approximation of a square wave appears; (3) when the voltage is sufficiently great to produce ions by collision an "ionization hump" appears at the top of the square wave. By observing the voltage at which this hump first appears, it is possible to approximate the ionization potential of the gas. A more accurate determination can be made by photographing the wave form and measuring the phase angle at which the hump begins and ends. Corrections must be made for the finite velocity of the electrons as they leave the cathode. This correction is made by potentiometric measurement. Values which are correct to within 5 percent of the accepted values have been obtained.

18. Magnetic Facilities Provided by the Kensington Magnetic Laboratory. B. P. RAMSAY AND F. L. YOST, *Naval Ordnance Laboratory.*—During the war, the Carnegie Institution of Washington operated for the Naval Ordnance Laboratory special facilities which were known as the Kensington Magnetic Laboratory. The facilities included coil systems of unusual size, design, and construction. These were employed to generate in the laboratory magnetic conditions and signals which are useful in the development of Naval Ordnance. Generically, these coil systems have been called magnetic generators. Solenoids, Helmholtz coils, and gradhelms* were specific types of generators in use. The largest solenoid was 3 ft.×4 ft. ×40 ft. Several helmholtzes were framed in 20-ft. cubes; and gradhelms were comparable in size. In various applications, signals from several types of magnetic generators were superimposed. The signals were controlled in contour, amplitude, period, and phase by simulators of various types. The periods of the signals which were generally employed fell in the range from 1 sec. to 1000 sec. Matters of general technical interest regarding construction, accuracy, and interaction will be discussed.

* G. H. Shortley and A. May, J. May, J. App. Phys. 16, 841-843 (1945).

19. A Photoelectric Nephelometer. N. UNDERWOOD AND A. H. DOERMANN, *Vanderbilt University.*—A nephelometer is described that does not require a precision optical system or an electronic amplifier. It is sensitive enough to measure the growth of *B. coli* from a starting concentration of approximately 2×10^6 bacteria per ml. The readings are reliable from 10^7 to 10^9 bacteria per ml. A graph of the photo-current due to the scattered light *versus* the number of *B. coli* per ml is given. The *B. coli* culture is a saturated 24 hr. nutrient broth culture in the

lag phase. In this range of bacterial concentrations the scattered light is proportional to the number of scattering centers. The instrument is well adapted to the study of growth curves of bacterial cultures and the lysis phenomena that occur when the organisms are attacked by bacteriophages.

A horizontal beam of light passes through the vertical test tube containing the specimen. The light scattered downward is measured with a barrier layer photo-cell. The horizontal incident light produces a photo-current of 2.4×10^{-3} amperes. The light scattered by a specimen whose titer is 1.6×10^{8} *B. coli* per ml produces a photo-current of 1.2×10^{-5} amperes. In this case the scattered light is 1/200 of the incident light.

20. Mass Measurement with a Single Field Mass Spectrometer. E. P. NEY AND A. K. MANN, *University of Virginia.*—An improved Nier type 60 degree mass spectrometer has been used in the measurement of the mass ratio H_2^{1+}/H_e^{4++}. Measurements of this type have previously been made with "double focussing" or "velocity selecting" mass spectrographs.[1] The value of the H_e^4/H_1^1 ratio was computed from the measured H_2^{1++}/H_e^{4++} ratio and compared with Aston's value.[2] The agreement was well within the accuracy of the measurement. This is significant because it indicates that precision mass measurements as well as relative abundance measurements can be made with a single field mass spectrometer of sufficiently high resolving power. The primary advantage of this method lies in the comparatively short time required for the experiment. The fifty-six observations of the double separation of $H_2^{1+}-H_e^{4++}$ were made in approximately 15 hours. Data and a mass spectrum will be shown.

[1] K. T. Bainbridge and E. B. Jordan, Phys. Rev. 50, 282 (1936).
[2] F. W. Aston, Nature 137, 357 (1936).

21. The Production of Constant High Rotational Speed. J. W. BEAMS AND J. L. YOUNG, III, *University of Virginia.*—A steel rotor is supported in a vacuum (less than 2×10^{-6} mm Hg) by an electro-magnetic suspension and is spun by a magnetic field rotating at a fixed constant speed. The rotating magnetic field is produced by two pairs of coils in which the phase of the current differs by 90 degrees. The two pairs of coils are placed symmetrically around the rotor and at right angles to each other. The frequency of the current in the coils is controlled by a piezoelectric crystal circuit. The induced currents in the rotor start it spinning. Because of the very small rotor drag, the rotor continues to accelerate up to the frequency of the rotating field where it "locks in" and spins at the same frequency as the field, i.e., it operates as an armature of an induction motor until it reaches full speed and then operates as a synchronous motor. Rotor hunting is found to damp out quickly so that the rotor speed is as constant as the frequency of the piezoelectric crystal circuit. With a 1.59 mm. rotor spinning at 10^5 r.p.s. the temperature rise was less than 6°C. The arrangement makes possible a very constant high rotational speed mirror.

22. Neutron-Proton Interaction. H. M. MOSELEY AND NATHAN ROSEN, *University of North Carolina.*—The potential energy of interaction between a neutron and proton in the triplet state is taken to be of the form $-B/(e^{r/a}-1)$. The Schrödinger equation with this potential energy is solved exactly for the ground state of the deuteron, giving a relation between B and a to account for the observed binding energy. The problem of neutron-proton scattering is then treated on the basis of a combination of ^3S and ^1S scattering. For the singlet state the interaction potential is taken to have the same form as for the triplet but with a different coefficient B'. The latter is fitted to the scattering data at low energies. It is found that taking $a=1\times10^{-13}$ cm, $B=60$ Mev, and $B'=38$ Mev (corresponding to an energy of about 60,000 ev for the virtual singlet state) gives satisfactory agreement with experiment. Further work using spin-dependent forces is planned.

23. Neutron-Proton Scattering. MELVIN EISNER AND NATHAN ROSEN, *The University of North Carolina.*—Since the exact law of interaction between a neutron and a proton is not yet known, it is of interest to consider various possible interactions and compare predictions based on them with experiment. In the present case it is assumed that the interaction potential energy is of the form $V=-V_0\,\mathrm{sech}^2(r/a)$, where V_0 has different values for the triplet and singlet states. The constants were chosen to give the correct binding energy for the ground state of the deuteron and to give a total neutron-proton scattering cross section of 19.7×10^{-24} cm² at $E=0.01$ Mev. It is found that for $a=1\times10^{-13}$ cm agreement with scattering data is obtained. For the triplet state V_0 is about 112 Mev, for the singlet, about 77 Mev, corresponding to a virtual singlet level of about 70,000 ev.

24. Tolerance Concentrations of Radioactive Substances. KARL Z. MORGAN, *Clinton Laboratories.*—A series of equations is developed in a form convenient for use in determining the tolerance amount of radioactive material that can be permitted safely in the human body. The body organ that sustains the maximum damage from a given radioactive material determines the body tolerance. It is assumed that this body organ rids itself of the radioactive isotope according to a simple exponential function such that the effective half-life, T, is given by the equation: $T=TeTr/Te+Tr$, in which Te is the body elimination half-life and Tr is the radioactive decay half-life. When a parent substance is taken into the body and later disintegrates into a daughter radioactive substance, the disinregration rate of the parent is equal to the disintegration rate of the daughter when the disintegration rate of the daughter is a maximum. Graphs are given comparing these particle disintegration rate curves with the energy dissipation rate curves. These equations are used in determining the tolerance concentration in air and in water, for external and internal exposure to a number of radioisotopes. The calculated concentrations check rather closely with the experimental values that have been established. The maximum permissible radiation dose is assumed to be 0.1 roentgen per day for gamma radiation and 0.01 equivalent physical roentgens per day for internal exposure to alpha rays. The general safe tolerance concen-

trations determined for beta or gamma radioisotopes is $10^{-7}\mu$ curies per cc in air or $5\times10^{-4}\ \mu$ curies per cc in water and for alpha emitters it is $10^{-10}\mu$ curies per cc in air or $10^{-6}\mu$ curies per cc in water (1μ curie taken as 3.7×10^{4} dis/sec.).

25. A Portable Instrument for the Detection of Fast Neutrons in the Presence of Gamma Radiation. PAUL W. REINHARDT, *Clinton Laboratories.*—The instrument consists of two ionization chambers mounted on a yoke assembly and connected so that the unbalance ionization current can be read on a Lindemann electrometer. One of the chambers is paraffin-coated inside and filled with butane at 30 pounds pressure. The other is filled with argon at about 35 pounds pressure. The pressures in the two chambers are so adjusted that their gamma ray ionization currents balance. Recoil protons ejected from the paraffin and butane by fast neutrons produce a differential ionization current which is read on the electrometer. A fast neutron flux of about 5 neutrons per cm² per second can easily be detected.

The electrometer circuit provides for 5 fixed electrometer sensitivities, and an adjustable sensitivity control for maintaining constant sensitivity over a long period of time. The collecting voltage is supplied from a 450-volt battery pack. Except for the ionization chambers, the entire assembly is housed in an aluminum box $3\frac{5}{8}''\times4\frac{3}{8}''\times8\frac{5}{8}''$.

26. Preliminary Evaluation of "Special Fine Grain Particle Film" for Use in Neutron Monitoring. J. S. CHEKA, *Clinton Laboratories.*—Eastman's Special Fine Grain Particle Safety Film is used at Clinton Laboratories to monitor personnel for neutron exposure. A portion of the film is shielded by cadmium, which stops thermal neutrons, and a part of it is exposed without a shield, intercepting both thermal and fast neutrons.

Calibrations were made to determine the sensitivity of the emulsion for both thermal and fast neutrons in terms of proton tracks observable in a dark field under a microscope of 970× magnification. The ratio $3.01\times10^{5}\ n_{th}$/observed track was noted for the $N^{14}(n,p)C^{14}$ reaction, and the ratio, $2.05\times10^{4}\ n_f$/observed track was noted for proton recoils. Evaluating expected track densities, based on N-atom density for n_{th} and H-atom density for n_f, the first process was found to be about 53 percent effective and the latter 46 percent effective in producing recognizable tracks of three grains or more in this emulsion.

Based on tolerance values of 4700 n_{th}/(cm² sec.) and 266 n_f/(cm² sec.), one week's tolerance doses are indicted by 20 tracks/50 fields for n_{th}, and 17 tracks/50 fields for n_f. However, since different batches of this film were found to differ in sensitivity, a calibration must be made on each batch before use.

To be Read by Title

27. Integrating $\sin^2x/x$. S. M. CHRISTIAN, *Agnes Scott College.*—

$$\int_0^x \frac{\sin^2 t}{t}dt=\tfrac{1}{2}[\gamma+\log_e(2x)-\mathrm{Ci}(2x)].$$

$\gamma=0.577,215,7$ and $\mathrm{Ci}(z)$ is the cosine integral. W. F. Brown, M. S. Corrington, Tolminson Fort, J. K. Mackenzie and others suggest that this formula gives quicker and more reliable results than the series previously used.[1]

x	Integral	x	Integral	x	Integral
0.1	0.004,992	1	0.423,691	11	1.833,309
.2	.019,867	2	1.052,246	12	1.896,801
.3	.044,330	3	1.218,516	13	1.903,509
.4	.077,897	4	1.267,117	14	1.949,275
.5	.119,906	5	1.462,629	15	2.005,723
.6	.169,539	6	1.555,951	16	2.013,281
.7	.225,841	7	1.573,438	17	2.043,656
.8	.287,743	8	1.682,002	18	2.094,072
.9	.354,096	9	1.755,531	19	2.103,836
		10	1.764,264	20	2.123,538

[1] S. M. Christian, Phys. Rev. **69**, 546 (1946).

28. Differential Equation for the Over-All Behavior of a Servo-Operated Recording Potentiometer. F. T. ROGERS, JR., AND MARGUERITE M. ROGERS, *The University of North Carolina.*—A type of recording potentiometer which is widely used industrially, contains a continually running motor which slowly actuates the recording pen at regular intervals (~2 sec) through a galvanometer-controlled clutch. At the instant of clutch-engagement, the galvanometer indicates the difference between the input-terminal emf (V) and the recorder emf (v), and so assures that a predetermined fraction (k) of $V-v$ is transmitted by the clutch in the time interval (Δt) as a Δv. That is, the over-all "smoothed" behavior of the instrument follows the differential equations

$$\left.\begin{aligned} dv/dt&=k(V-v),\ -M\leqslant V-v\leqslant M,\\ dv/dt&=kM\ \mathrm{sgn}(V-v),\ |V-v|\geqslant M.\end{aligned}\right\}\qquad(1)$$

The second of these equations indicates the predetermined limit of response of the galvanometer. For a typical instrument of this type, with $0\leqslant v\leqslant 10$ mv, the quantities M and k have been measured so as to allow the use of Eq. (1) in correcting v-records for instrumental lags: $M=3$ mv, and $k=0.0005$ sec.$^{-1}$ for low circuit-resistances.

29. The Rational Design of the Computor for a Certain Class of Mechanical System Containing Feedback-Control.—F. T. ROGERS, JR., *The University of North Carolina.*—Consider a mechanical system in which a motor (constant speed ω_M) operates a load at speed ω, through first a speed-controller (delivering speed $\omega=F(\theta)\cdot\omega_M$, where $F(\theta)$ is specified or known) and then a "take-off" unit; here θ, an input to the controller, essentially governs the ratio ω/ω_M. If some fraction (f) of ω be withdrawn through the take-off unit from $t=0$, and $\phi=\int f\omega dt$ be converted to θ through a computor, $\theta=G(\phi)$, the problem is so to design this computor (or function G) that ω behaves in the predetermined way, $\omega=\Omega(t)$. Clearly, the computor-design equation results from the elimination of t between

$$\phi=f\int_0^t \Omega(x)dx \qquad(1)$$

and

$$F(\theta)=\Omega(t)/\omega_M. \qquad(2)$$

An interesting simple case is that in which $\Omega(t)$ is to be exponential in time; here Eqs. (1)–(2) yield G linear in ϕ for F linear in θ.

30. Statistical Significance of Some Measurements on the Permeabilities of Unconsolidated Sands. H. L. MORRISON, *North Carolina State College of Agriculture and Engineering*, AND F. T. ROGERS, JR., *The University of North Carolina*.—The permeabilities (k) of some sands have been repeatedly measured by the method of Terzaghi,[1] using the vertical percolation of water through 90-cm columns of the sands; the pressure head was carefully measured as a function of time in each case, but no other particular precautions were taken. The k-values for a local red sand of 40–45 mesh had a mean value of 63 darcys and a standard deviation of 7.5. Mean k-values for the clean natural sand from White Lake (Bladen Co.), N. C., were 90.3 darcys for the 40–50 mesh component, 105.5 for the unscreened sand, and 125.1 for the (remaining) 30–40 mesh component; standard deviations in each case were between 1 percent and 2 percent. All these measurements were made with columns of 1.34 cm diameter; doubling the diameter in the case of the 30–40 mesh white sand changed the mean k-value by about 2 percent. The above information clearly allows estimates to be made of the significance of a mean k-value for such sands as found by a severely restricted series of measurements of low precision.

[1] M. Muskat, *Flow of Homogeneous Fluids Through Porous Media* (McGraw-Hill, 1937), p. 84.

31. On the Reduction of Data Which Are Values of a Definite Integral. F. T. ROGERS, JR., *The University of North Carolina*.—Data which represent physical observations may, for example in measuring the work done by a force of varying magnitude, of necessity be in the form[1]

$$kW=\int_y^z e(x)b(x)dx. \tag{1}$$

Here $e(x)$ would be a sought-for "unit-work function"; the constant k and the function $b(x)$ would be known; and y and z would be available as variables. Clearly the function $e(x)$ can be obtained from the data by differentiation with respect to the limit x or y,

$$e(y)=-k(\partial W/\partial y)/b(y), \quad e(z)=k(\partial W/\partial z)/b(z), \tag{2}$$

if the experiment is properly designed.

[1] See, for example, Phys. Rev. 61, 728 (1942).